Low Temperature Growth of Carbon Nanotubes by Remote-Plasma CVD and their Application to LSI Interconnection

リモートプラズマ CVD によるカーボンナノチューブの低温合成および LSI 配線応用に関する研究

Takayuki Iwasaki

Waseda University

Major in Nano Science and Nano Engineering

School of Science and Engineering

February, 2008

Low Temperature Growth of Carbon Nanotubes by Remote-Plasma CVD and their Application to LSI Interconnection

Takayuki Iwasaki

February, 2008

Contents

Chapter 1

Introduction

1.1 Background and overview of the thesis

Carbon nanotubes (CNTs) were discovered by Iijima in 1991 [1]. A CNT can be thought of as a stripe cut from a single graphite plane (a so-called graphene) and rolled up to form a hollow seamless cylinder. As in graphite, the C atoms form a hexagonal network. While there is a pure sp^2 hybridization in graphene, some small contributions of sp^3 are mixed in, due to the curvature of the network in the case of CNTs. Besides single-walled carbon nanotubes (SWNTs), which consist of a single graphite layer (Fig. 1.1(a)), multi-walled carbon nanotubes (MWNTs) have also been prepared, which consist of numerous cylinders nested inside each other (5 cylinders in Fig. 1.1(c)). In the case of two cylinders, the structure is called a double-walled carbon nanotube (DWNT) as shown in Fig. 1.1(b).

CNTs have the potential for use in many applications such as field-effect transistors (FETs) [2] and interconnections [3, 4] in large scale integration (LSI) circuits, field emitters [5, 6] for displays, and electric double-layer capacitors (EDLCs) [7] for energy storage due to their high electrical conductivity, ballistic transport, large surface area, high aspect ratio, and structural stability. In pioneering works, the excellent properties of CNT devices were demonstrated. However, from the viewpoint of the growth methods of CNTs, particularly for SWNTs, there are many issues that should be addressed to ensure the reliable fabrication of the devices. For the synthesis of CNTs, the conventional methods are laser ablation [8], arc discharge [9], and thermal chemical vapor deposition (CVD) [10-14]. These methods have the following issues: (1) high growth temperatures in the range of 800–1200°C are required, (2) CNTs are not aligned,

(3) a number of impurities such as catalyst particles and other carbon phases are formed, (4) CNTs cannot be directly grown on a substrate, (5) short SWNT lengths are obtained using catalysts with short lifetimes, and (6) highly selective growth of SWNTs, DWNTs, and MWNTs is not achieved. There have been no growth methods that can address all these issues. The ability to control the structure, position, length, orientation, and density of CNTs at low temperatures is a prerequisite to realizing many practical applications.

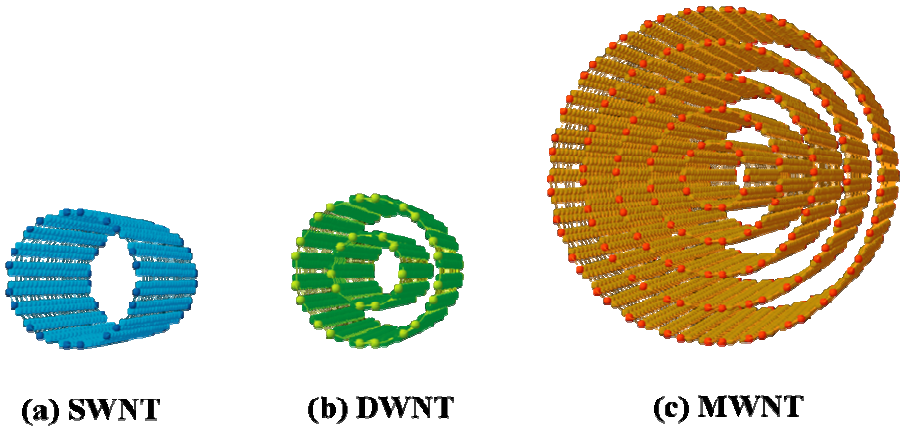

Figure 1.1 CNT family.

In this thesis, a growth method of SWNTs that can overcome the above problems is investigated and developed. Millimeter-long vertically aligned SWNTs are synthesized at a low temperature of 600°C by remote-plasma CVD using catalysts with an ultralong lifetime. Highly dense oriented SWNTs are formed directly on a substrate and their growth position is controlled by catalyst patterning. Since the synthesized SWNTs are almost impurity-free, they can be used without further purification. As a basis for future microelectronics, SWNT vias are fabricated using the proposed growth method. In addition, vertically aligned DWNTs are synthesized with high selectivity and are applied for EDLCs. For LSI interconnection, MWNTs with metallic properties are synthesized below 400°C and their electrical properties are demonstrated. This study focuses on the vertical array growth of CNTs because it is appropriate for the fabrication of practical applications. A brief overview of the chapters is as follows.

In Chapter 2, the remote-plasma CVD apparatus used for the growth of CNTs is described and the low-temperature (600°C) growth of vertically aligned and dense SWNTs is demonstrated using the apparatus. As a catalyst, a sandwich-like structure of

Al_2O_3 / Fe / Al_2O_3 is used, and it is confirmed that this structure plays an important role in the growth of vertically aligned SWNTs. The diffusion-limited growth of vertically aligned SWNTs is demonstrated using patterned catalysts, and 5-mm-long SWNTs are obtained. Moreover, by optimizing the growth temperature, 7.4-mm-long SWNTs are synthesized on nonpatterned catalysts.

In Chapter 3, the root growth mode of vertically aligned SWNTs is clarified by a new method, marker growth. SWNT stacks are formed by interrupting the growth, causing an interface to be formed between the stacks. By using the interface as a 'marker', the growth mode is clarified. The interface structure and growth mechanism of layered SWNTs are investigated by separating the layers.

In Chapter 4, vertically aligned DWNTs with a selectivity of 90% are synthesized, which is the highest reported value for vertically aligned DWNTs, by a controlled heating method without any purification. Their EDLC characteristics are evaluated and a specific capacitance of 83 F/g is obtained, which is one of the largest reported values for vertically aligned CNTs in a nonaqueous solution. DWNTs are promising candidates for practical capacitors because of their superior characteristics, such as their structural robustness and less bundled growth.

In Chapter 5, the fabrication processes and electrical properties of CNT-based LSI interconnection are developed. In Section 5.2, the author discusses the successful growth and the electric properties of uniform vertically aligned MWNTs fabricated by remote-plasma CVD at 390°C, which is below the allowable process temperature in a Si LSI. The resistances of CNTs planarized by chemical mechanical polishing (CMP) are lower than those of CNTs without CMP, due to the increase in the number of carrier paths using the inner graphite shells of MWNTs. In Section 5.3, the synthesis of SWNT arrays in SiO_2 holes 100–550 nm in diameter is described. It is shown that the growth rate of SWNTs in the holes decreases as the hole size becomes smaller. The author demonstrates that ion implantation can be used for the preparation of catalyst particles, as discussed in Section 5.4. On the SiO_2 surface, Ni catalyst particles with a density of 10^{11}–10^{12} cm^{-2} are formed. The catalyst size and density can be controlled by post-implantation annealing, and vertically aligned CNTs are synthesized from particles annealed at 700°C.

Finally, the contents of the thesis are summarized in Chapter 6.

Further research background and an introduction to each topic are described at the beginning of sections or chapters.

1.2 Geometrical and electronic structures of CNTs

Geometrical structure

A SWNT is defined by a cylindrical graphene sheet. The structure of SWNTs is described by the **chiral vector $\mathbf{C_h}$**, which represents the full circumference of the SWNT, defined by

$$\mathbf{C_h} = n\mathbf{a_1} + m\mathbf{a_2} \qquad (1.1)$$

where $\mathbf{a_1}$ and $\mathbf{a_2}$ are the unit vectors in the hexagonal lattice, and n and m are integers ($0 \le m \le n$), (Figure 1.2). A SWNT is constructed by rolling up the sheet such that the two end-points of the vector $\mathbf{C_h}$ are superimposed. This tube is denoted as (n,m) tube with diameter given by

$$d = \frac{|C_h|}{\pi} = \frac{a\sqrt{n^2 + m^2 + nm}}{\pi} \qquad (1.2)$$

where $a = |a_1| = |a_2|$ is lattice constant of graphite. Furthermore, $\mathbf{C_h}$ settles the so-called chiral angle which is the angle between $\mathbf{C_h}$ and $\mathbf{a_1}$. If m is zero, the chiral angle is 0° and the structure is called *zigzag*. If n = m, the chiral angle is 30° the structure is called *armchair* (Fig. 1.3). All other nanotubes show chiral angles between 0° and 30°. They are known as *chiral* nanotubes because they produce a mirror image of their structure upon an exchange of n and m.
The chiral angle is defined as,

$$\cos\theta = \frac{2n + m}{2\sqrt{n^2 + m^2 + nm}} \qquad (1.3)$$

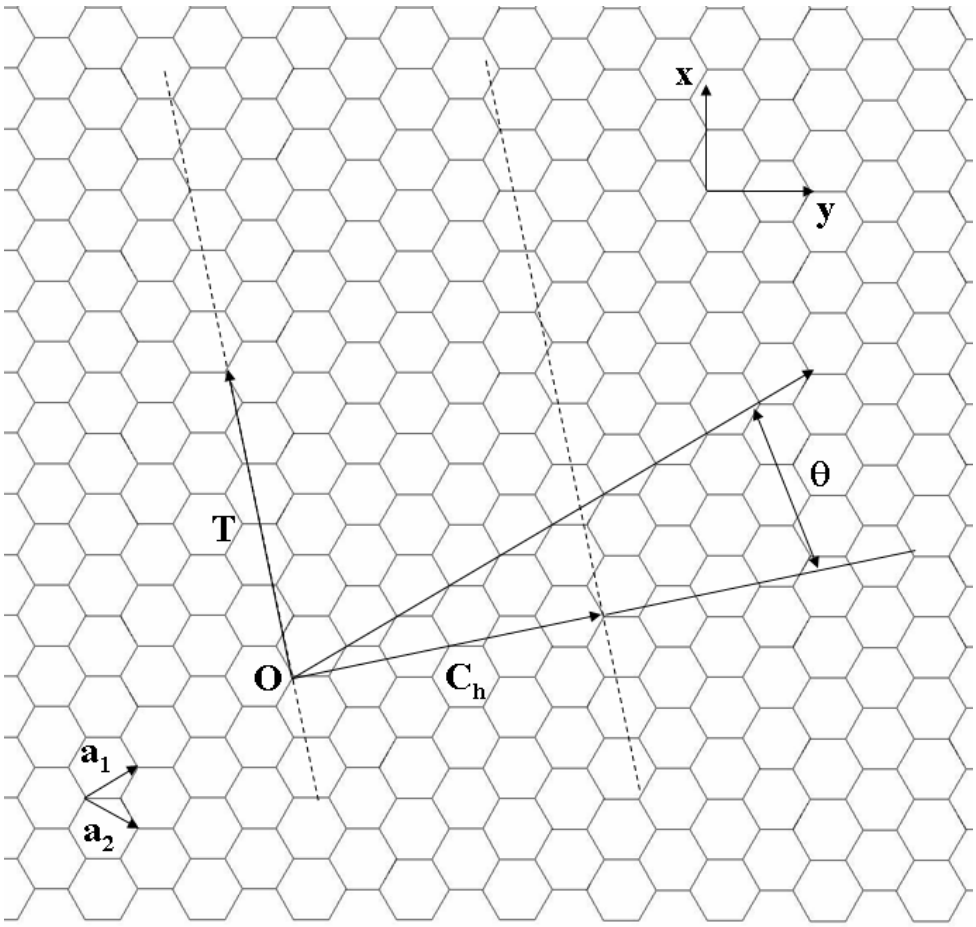

Figure 1.2 The unrolled honeycomb lattice of a nanotube, graphene. This figure corresponds to **Ch** = (4, 2).

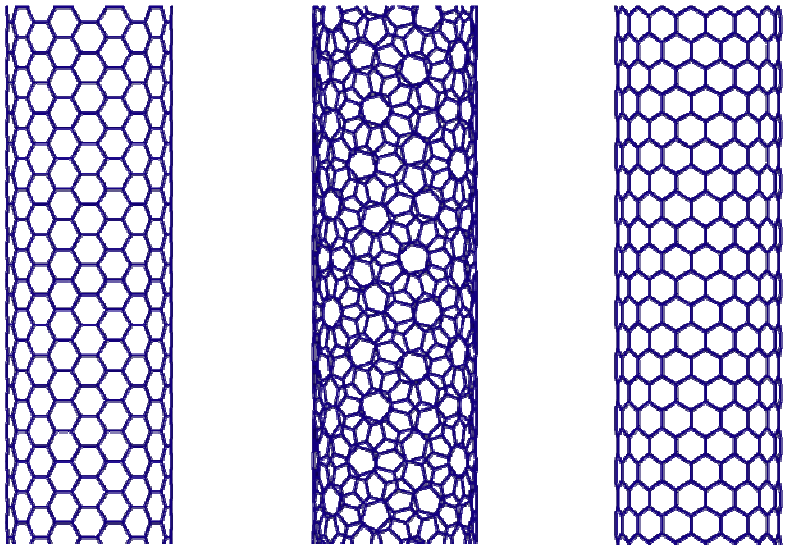

Figure 1.3 Armchair, chiral, and zigzag type. The three SWNTs have almost the same diameter, ~ 1.3 nm.

Electronic structure

The discussion of the electronic structure of SWNTs starts again with graphene. Wallace [15] derived an expression for the 2-D energy states, W_{2D}, of the π-electrons in the graphene plane as a function of the wave vectors k_x and k_y,

$$W_{2D}(k_x,k_y) = \pm\gamma_0\left[1+4\cos\left(\frac{\sqrt{3}k_x a}{2}\right)\cos\left(\frac{k_y a}{2}\right)+4\cos^2\left(\frac{k_y a}{2}\right)\right]^{1/2} \qquad (1.4)$$

where γ_0 denotes the nearest-neighbor overlap integral and a = 0.246 nm is the in-plane lattice constant. The two different signs in Eq. (1.4) represent the π- and π*-band. The calculations show that the π- and π*-band just

touch each other at the corners of the 2-D Brillouin zone. (Figure 1.4) In the vicinity of the Γ point, the dispersion relation is parabolically shaped, while towards the corners (K points) it shows a linear dependence. At T = 0 K, the π- band is completely filled with electrons and the π*-band is empty. Because the bands only touch at the K points, integration over the Fermi surface results in a vanishing density of states.

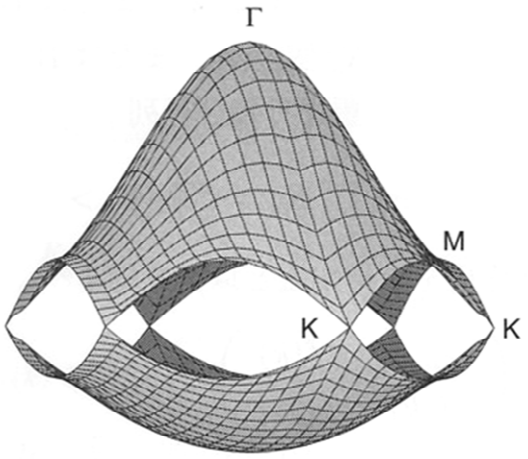

Figure 1.4 Brillouin zone of graphene

For the description of the band structure of graphene, it has been assumed that the graphene plane is infinite in two dimensions. SWNTs have a structure which is macroscopic along the tube axis, but the circumference is in atomic dimensions. Thus, while the density of allowed quantum mechanical states in axial direction will be high, the number of states in the circumferential direction will be very limited. More precisely, the roll-up by the chiral vector $\mathbf{C_h}$ leads to periodic boundary conditions in the circumferential direction. Quantum mechanically, these boundary conditions define allowed modes (1-D states) along the tube axis according to,

$$C_h \cdot k = 2\pi j \qquad \text{with} \quad |j| = 0, 1\ 2, \ldots \qquad (1.5)$$

In the case of armchair tubes, the periodic boundary condition yield allowed values for the wave vector in circumferential direction according to,

$$k_{y,j} = \frac{j}{q_y}\frac{2\pi}{\sqrt{3}a} \qquad (1.6)$$

where $q_y = n = m$. For the armchair geometry, the tube axis is identical to the x-direction and the circumference represents the y-direction. As an example of an armchair tube, Figure 1.5 shows the dispersion relation, the projection of the allowed 1-D states onto the first Brillouin zone of graphene for a (3, 3) tube. Due to the periodic boundary conditions, i. e. by inserting Eq. (1.6) into Eq. (1.4), the allowed states condense into lines (parallel lines in Fig. 1.5(a)). Here, there are $q_y = 3$ lines on either side of the center of the Brillouin zone and an additional line going through the center. In case of a (3, 3) tube, the allowed states include the K points. Therefore, the (3, 3) tube, and armchair tubes in general, show a metallic behavior.

As an example of a chiral tube, Figure 1.5(b) shows the dispersion relation, the projection of the allowed 1-D states onto the first Brillouin zone of graphene for a (4, 2) tube. The electronic properties of this (4, 2) tube is very different from the (3, 3) tube despite their very similar diameters. Again, due to the periodic boundary conditions, the allowed states condense into lines (parallel lines in Fig. 1.5(b)). In contrast to the (3, 3) tube, the $\mathbf{C_h}$ vector is not parallel to the y-direction and, hence, leads to a mixed quantization of k_x and k_y. The propagation of an electron along the tube axis is described by a combination of k_x- and k_y-components. The band structure of (4, 2) tubes is determined by the fact that there are no modes which include the K points of the Brillouin zone of graphene (Figure 1.5(b)). Therefore, this type of tube is a semiconductor. The band gap is approximately inversely proportional to the tube diameter. According to the tight-binding description of the electronic structure, the band gap, E_{gap} is given by,

$$E_{gap} = \frac{2\gamma a}{\sqrt{3}d} \qquad (1.7)$$

where γ is the hopping matrix element [16-18]. This equation indicates that CNTs with large diameters have very small band gaps, resulting in nearly metallic behavior.

In general, the semiconducting or metallic behavior of SWNTs is controlled by the $\mathbf{C_h}$ vector and, hence, by the relation of n and m. Metallic behavior occurs for

$$n - m = 3q \qquad (1.8)$$

where q is an integer. As a consequence, one-third of all SWNT types are metallic for a statistic distribution of chiralities including all armchair types.

The periodic boundary conditions for zigzag tubes, (n, 0) tubes, results in allowed wave vectors according to,

$$k_{x,j} = \frac{j}{q_x}\frac{2\pi}{a} \qquad (1.9)$$

The condition for metallic tubes, Eq. (1.8), is fulfilled for one-third of the zigzag tubes, i.e. if n is multiple of three.

The discussion so far has been restricted to isolated SWNTs. Theoretical and experimental studies have shown that the intertube coupling within MWNTs and bundles of SWNTs [19, 20] have a relatively small effect on the band structure of a tube [16]. As a consequence, semiconducting and metallic tubes retain their character if they are a part of MWNTs or bundles. By statistical probability, most of the MWNTs and bundles show an overall metallic behavior, because one single metallic tube is sufficient to short-circuit all semiconducting tubes.

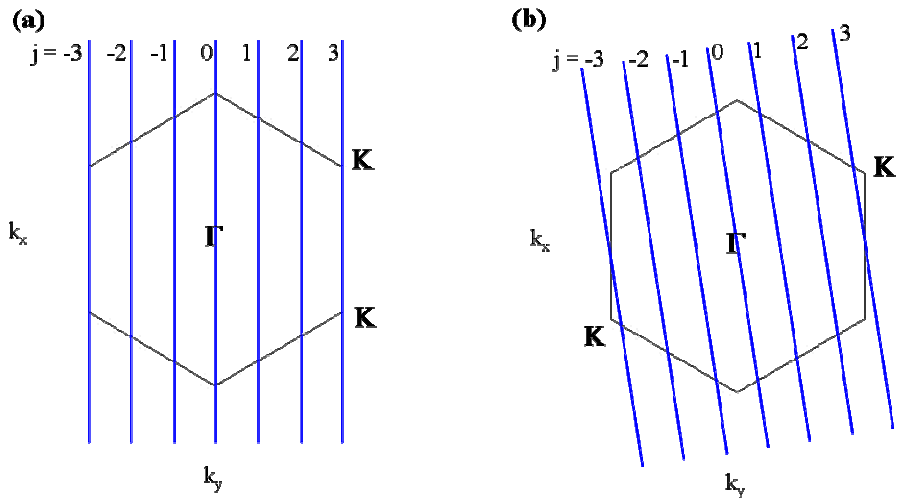

Figure 1.5 Dispersion relation of SWNTs. Projection of the allowed states onto the first Brillouin zone of graphene. (a) (3, 3) tube. (b) (4, 2) tube.

References

[1] S. Iijima, Nature 354, 56 (1991).

[2] A. Javey, J. Guo, D. B. Farmer, Q. Wang, D. Wang, R. G. Gordon, M. Lundstrom, H. Dai, Nano. Lett. 4, 447 (2004).

[3] M. Nihei, M. Haribe, A. Kawabata, Y. Awano, Jpn. J. Appl. Phys. 43, 1856 (2004).

[4] G. S. Duesberg, A. P. Graham, F. Kreupl, M. Liebau, R. Seidel, E. Unger, W. Hoenlein, Diam. Relat. Mater. 13, 354 (2004).

[5] L. Nilsson, O. Groening, C. Emmenegger, O. Kuettel, E. Schaller, L. Schiapbach, H. Kind, J-M. Bonard, K. Kern, Appl. Phys. Lett. 76, 7071 (2000).

[6] J. S. Suh, J. Seok, J. S. Lee, Appl. Phys. Lett. 80, 2392 (2002).

[7] J. Li, A. Cassell, L. Delzeit, J. Han, M. J. Meyyappan, Phys. Chem. B 106, 9299 (2002).

[8] A. Thess, R. Lee, P. Nikolaev, H. Dai, P. Petit, J. Robert, C. Xu, Y. H. Lee, S. G. Kim, A. G. Rinzler, D. T. Colbert, G. E. Scuseria, D. Toma´nek, J. E. Fischer and R. E. Smalley, Science 273, 483 (1996).

[9] C. Journet, W. K. Maser, P. Bernier, A. Loiseau, M. Lamy De La Chapelle, S. Lefrant, P. Deniard, R. Lee and J. E. Fischer, Nature 388, 756 (1997).

[10] J. Kong, H. T. Soh, A. M. Cassell, C. F. Quate and H. Dai, Nature 395, 878(1998).

[11] A. M. Cassell, J. A. Raymakers, J. Kong and H. Dai: J. Phys. Chem. B 103, 6484 (1999).

[12] J.-F. Colomer, C. Stephan, S. Lefrant, G. Van Tendeloo, I. Willems, Z. Ko´nya, A. Fonseca, C. Laurent and J. B. Nagy, Chem. Phys. Lett. 317, 83 (2000).

[13] M. Su, B. Zheng and J. Liu, Chem. Phys. Lett. 322, 321 (2000).

[14] H. Hongo, M. Yudasaka, T. Ichihashi, F. Nihey and S. Iijima: Chem. Phys. Lett. 361, 349 (2002).

[15] P. R. Wallace, Phy. Rev. 71. 622 (1947).

[16] *Carbon Nanotubes*, M. Dresselhaus, G. Dresselhaus, and Ph. Abouris, Eds., Springer-Verlag (Berline, 2001).

[17] M. S. Dresselhaus, G. Dresselhaus, R. Saito, Phys. Rev. B 45, 6234 (1992).

[18] J. W. Mintmire, B. I. Dunlap, and C. T. White, Phys. Rev. Lett. 68 631 (1992).

[19] A. A. Maarouf, C. L. Kane, and E. J. Mele, Phys. Rev. B 61, 11156 (2000).

[20] H. Stahl, J. Appenzeller, R. Martel, Ph. Avouris and B. Lengeler, Phys. Rev. Lett. 85, 5186 (2000)

Chapter 2

Low Temperature Synthesis of Vertically Aligned SWNTs by Remote-Plasma CVD

Parts of this chapter are discussed based on the following papers:

- 岩崎孝之, 鐘国倣, 川原田洋, プラズマ・核融合学会誌, 81, 665 (2005).
  T. Iwasaki, G. Zhong, H. Kawarada, Journal of Plasma and Fusion Research, 81, 665 (2005).
- T. Iwasaki, G. Zhong, H. Kawarada, New. Diam. Front. C. Tec, 16, 177 (2006).
- G. Zhong, T. Iwasaki, K. Honda, Y. Furukawa, I. Ohdomari, H. Kawarada, Jpn. J. Appl. Phys, 44, 1558 (2005).
- G. Zhong, T. Iwasaki, J. Robertson, H. Kawarada, J. Phys. Chem. B, 111, 1907 (2007).

2.1. Introduction

Controlling the growth direction of single-walled carbon nanotubes (SWNTs) on a substrate is important for the fabrication of SWNT-based applications, such as field effect transistors (FETs) [1-4] and interconnects for ULSI [5]. Chemical vapor deposition (CVD) is reliable for the controlling the growth of SWNTs as an alternative to arc discharge [6] and laser ablation [7]. SWNTs were laterally oriented on a substrate by applying a bias voltage between lithographic patterned electrodes with catalysts [8] or by the direction of gas flow during CVD [9]. Although recent progress has made it possible to directly grow vertically aligned SWNTs by thermal CVD [10, 11], thermal CVD methods require high temperatures of 750 – 1000˚C for pyrolysis of feedstock gases, which limits the application of SWNTs. In addition, the maximum height of vertically aligned SWNTs obtained with good reproducibility is 2-3 mm for thermal CVD methods [11, 12]. Plasma-assisted CVD is effective for controlling the growth of multi-walled carbon nanotubes (MWNTs) at low temperatures. However, it rarely succeeded in controlling the growth of SWNTs. This chapter reports very high yield growth of vertically aligned SWNTs at a low temperature of 600°C on Si substrates coated with a sandwich-like structure of Al_2O_3/Fe/Al_2O_3 using a remote-plasma CVD apparatus. Furthermore, our ultra-long lifetime catalysts have led to growth of 5 mm long SWNTs at 600°C and 7.4 mm at 690°C.

2.2. Remote-plasma CVD apparatus

Vertically aligned SWNTs were synthesized using the remote-plasma CVD apparatus shown in Fig. 2.1. This apparatus has an antenna in the chamber and 2.45-GHz microwaves are transmitted to the antenna. A spherical plasma is generated at the edge of the antenna and the plasma is fixed there. Therefore, the system can be operated at a low power of 60 W and substrates with catalysts can be placed far from the plasma. In this study, the substrates were placed on a molybdenum holder that was 50 mm from the plasma ball such that no ions reached the substrates. No ion current was measured when a bias voltage was applied between the antenna and the substrate holder at a 50 mm distance, as show in Fig. 2.2. As a result, only carbon radicals, not ions, act as activated sources for CNT growth. Therefore, there is no ion etching of the catalyst and growing CNTs. In addition, CNTs can be synthesized at low temperatures by remote-plasma CVD because the growth temperature is almost independent of the plasma in this system and high temperatures are not required unlike thermal CVD. In conventional microwave plasma systems, the temperature can be increased readily to several hundred degrees because the plasma is fixed on the substrate holder. The antenna-type remote-plasma CVD is suitable for low temperature and damage-free growth of CNTs.

A high-frequency induction heater is installed near the substrate holder. This heater can increase the temperature very rapidly, so small catalyst particles, suitable for SWNTs, can be formed from a thin film. If the substrate temperature is raised slowly, catalyst atoms and clusters diffuse and aggregate into large particles, resulting in the growth of low-density and large-diameter CNTs. The maximum size of the substrate that can be installed on the substrate holder is 16 mm x 16 mm. The induction heater limits the size since the heater cannot rapidly increase the temperature of a larger holder.

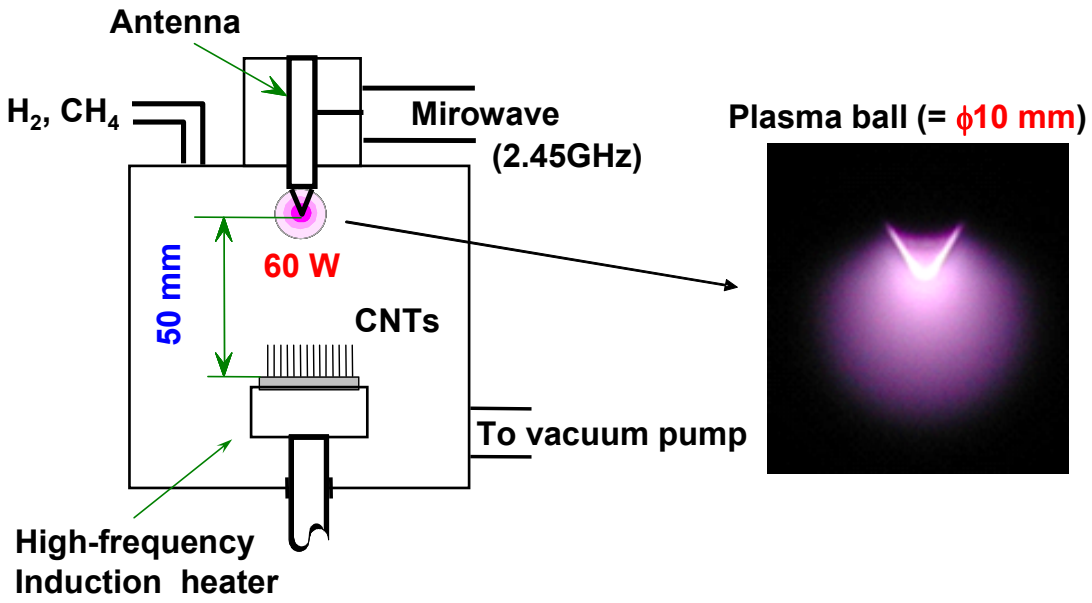

Figure 2.1 Schematic of the remote-plasma CVD apparatus.

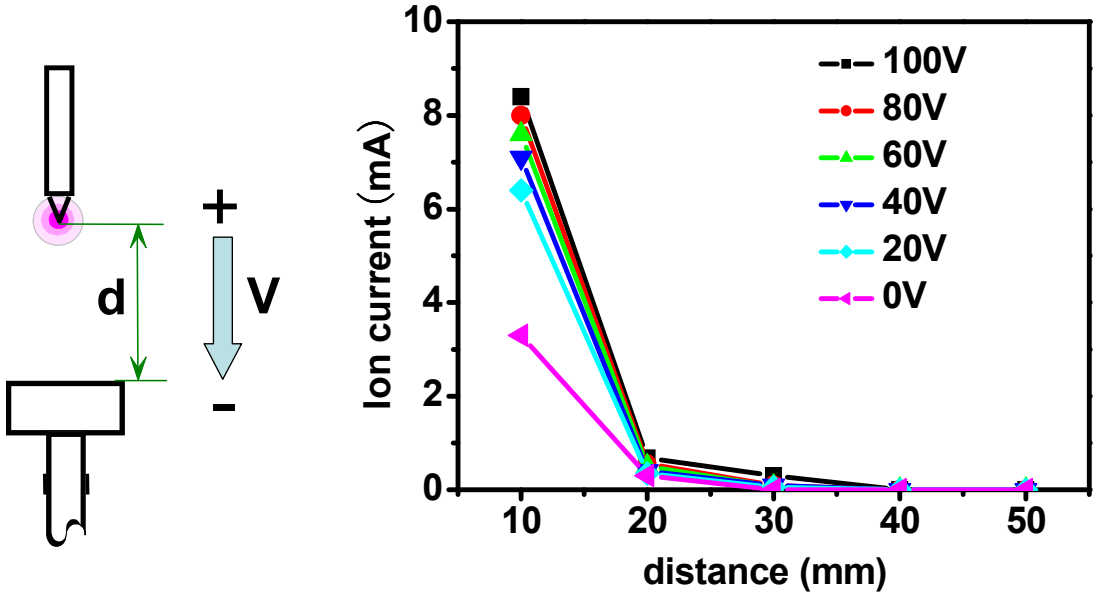

Figure 2.2 Dependence of ion current at the substrate holder on the distance between the plasma and the holder.

Large-area deposition of CNTs is essential for mass production and LSI processes which require uniformity over the entire substrate of 300 mm diameter. In the current system, only an antenna is equipped in the chamber. It is expected that the edges of large substrates will have shorter CNTs because of the longer diffusion path lengths of carbon radicals generated at the antenna. There is a concept of a multi-antenna system to overcome this problem, as shown in Fig. 2.3. This system has several antennas placed some distance apart in the chamber. With an optimized distance between antennas, uniform CNT arrays should be obtained on large substrates of, in principle, infinite area.

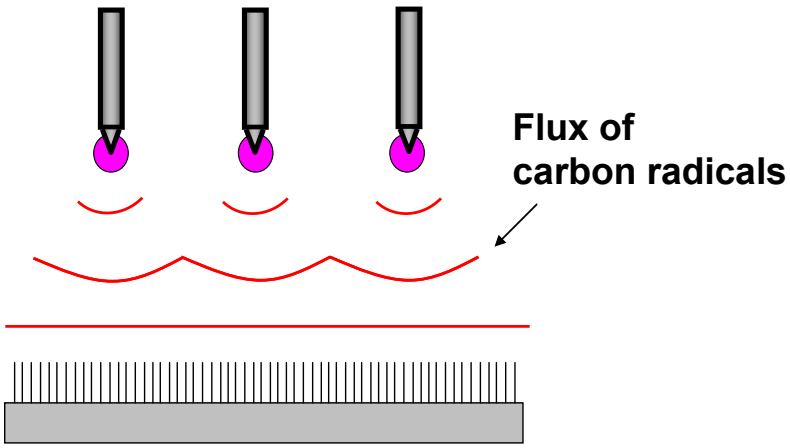

Figure 2.3 Concept of large-area deposition of CNTs in the multi-antenna system.

2.3. Low temperature synthesis of vertically aligned SWNTs

2.3.1. Experimental conditions: catalyst and CVD conditions

As a catalyst, a sandwich-like structure of Al_2O_3 (0.5 nm) / Fe (0.5 nm) / Al_2O_3 (> 5 nm) was deposited on Si wafers. The catalyst preparation is illustrated in Fig. 2.4. To prepare this structure, first, the Al layer (> 5 nm) was coated using a radio-frequency (RF) magnetron sputtering system on a Si wafer and the layer was oxidized in air for a week to form an Al_2O_3 layer. Then, thin Fe (0.5 nm) and Al (0.5 nm) layers were coated on the Al_2O_3 layer. The top Al layer was also oxidized in air for a week. Since the Fe layer was covered by the top Al layer, it is speculated that the Fe layer was less oxidized. Although the Fe layer is also oxidized, the oxidized Fe is reduced during preheating in hydrogen atmosphere and the Fe particles act as catalysts. The function of the two Al_2O_3 layers is discussed in Section 2.3.5.

For growth of SWNTs, substrates with the catalyst were installed in the CVD chamber. After vacuum reached to 3.0 x 10^{-5} Torr, the substrates were heated rapidly at 600°C for 5min to form catalytic nanoparticles, and then plasma was turned on in a gas mixture of H_2 (45 sccm) and CH_4 (5 sccm) for the growth of SWNTs. The microwave power and total gas pressure were 60 W and 20 Torr, respectively. After the growth, the plasma and heater were stopped and the substrate was cooled.

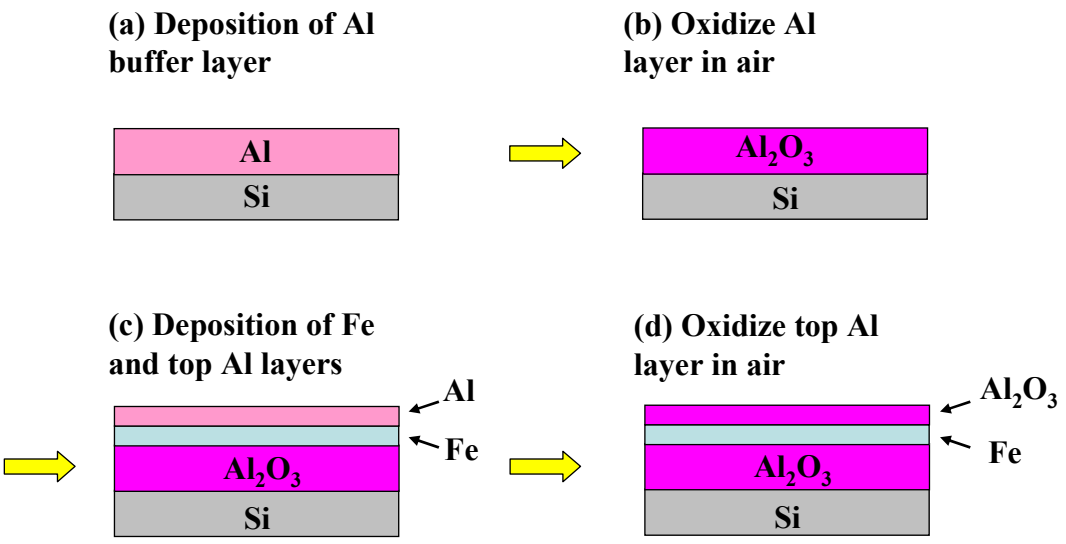

Figure 2.4 Preparation process of the sandwich-like structure of catalysts.

2.3.2. Morphology of vertically aligned SWNTs observed by SEM and TEM

Figure 2.5(a) shows an SEM image of SWNTs grown for 3 min. All SWNTs are vertically aligned on the substrate and have a very high density. Magnified images of the top surface and cross section are shown in Fig. 2.5(b, c). Although SWNTs are vertically aligned, they are bent and curved at the top surface (Fig. 2.5(b)), probably because of the small diameters and low density of SWNTs in the initial growth stage. The cross-sectional view shows aligned SWNT bundles. A bundle consists of several SWNTs that attract one another via van der Waals' forces.

Interestingly, cracks were observed in a longer sample, as shown in Fig. 2.6. Figure 2.6(b) shows a top view of weblike cracks formed randomly in a vertically aligned SWNT mat. The cracks have been observed only in SWNT samples, and there are no cracks in MWNTs grown on thick (> 1 nm) catalyst films. It is speculated that the samples are stressed by van der Waals' attractive forces among neighboring SWNTs during the CVD process and that the cracks are formed when the stress becomes stronger for longer SWNTs. MWNTs have lower van der Waals' attractive forces and the density is lower than that of SWNTs, resulting in no cracks in the samples.

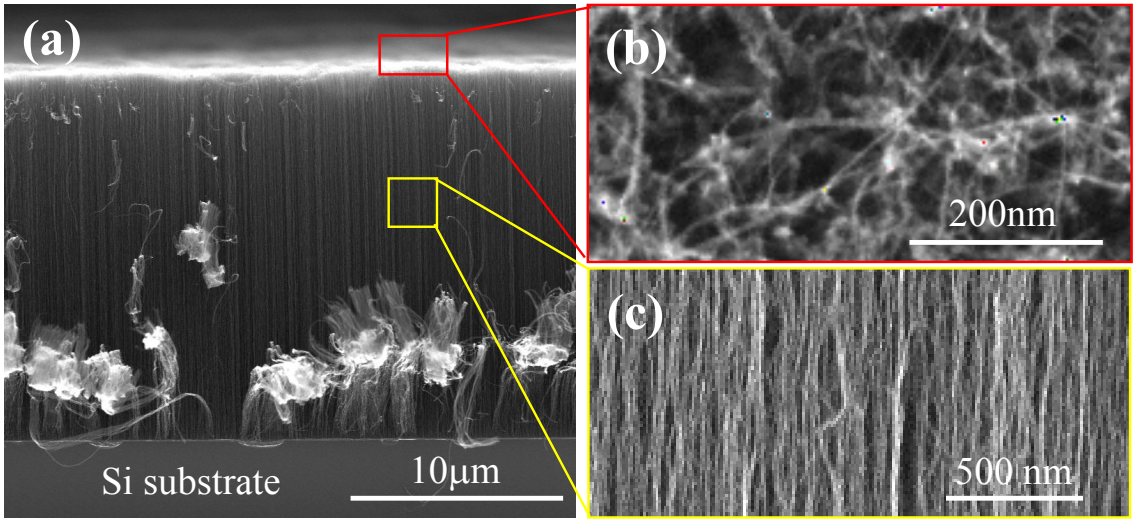

Figure 2.5 SEM images of vertically aligned SWNTs.

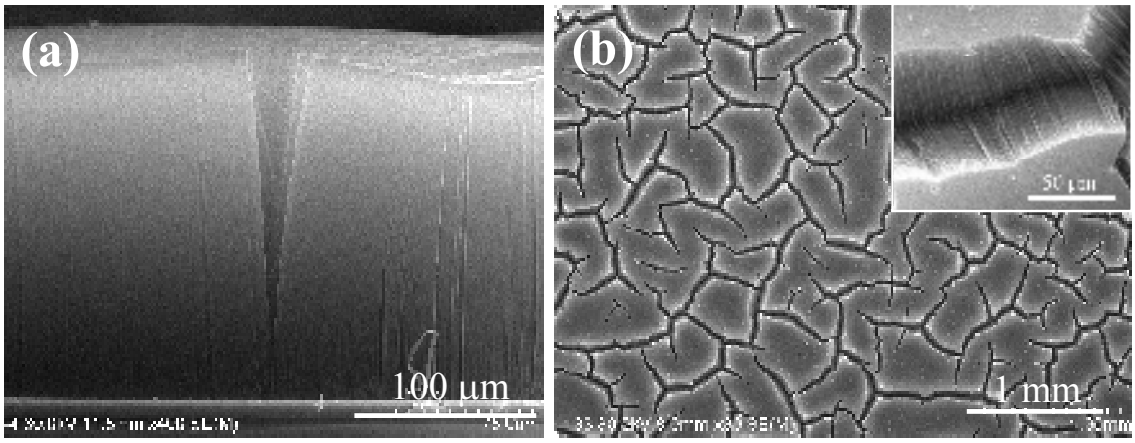

Figure 2.6 Crack formation in vertically aligned SWNT film.

The synthesized CNTs were characterized by TEM. Vertically aligned CNTs were dispersed in alcohol with ultrasonication and drops containing CNTs were put on microgrids. The low-magnification image in Fig. 2.7(a) shows bundles of SWNTs. Despite long ultrasonic treatment, it was difficult to disperse SWNTs perfectly due to their strong van der Waals' attractive forces, as described above. In contrast, a mixture of SWNTs and MWNTs grown using a 1-nm-thick Fe catalyst film can be easily separated by an ultrasonic method because larger-diameter SWNTs and MWNTs have weaker attractive forces. Isolated SWNTs are shown in Fig. 2.7(b, c). Examination of many SWNTs revealed that almost all components were single-walled although there were a few DWNTs. Figure 2.8 shows the diameter distribution of vertically aligned SWNTs, estimated from TEM images. The diameter ranges from 1.4 to 4.0 nm and the mean diameter is 3.1 nm. Note that there might be small-diameter SWNTs (< 1 nm) in the sample. However, they were difficult to be found during observations since they were not well dispersed during ultrasonication.

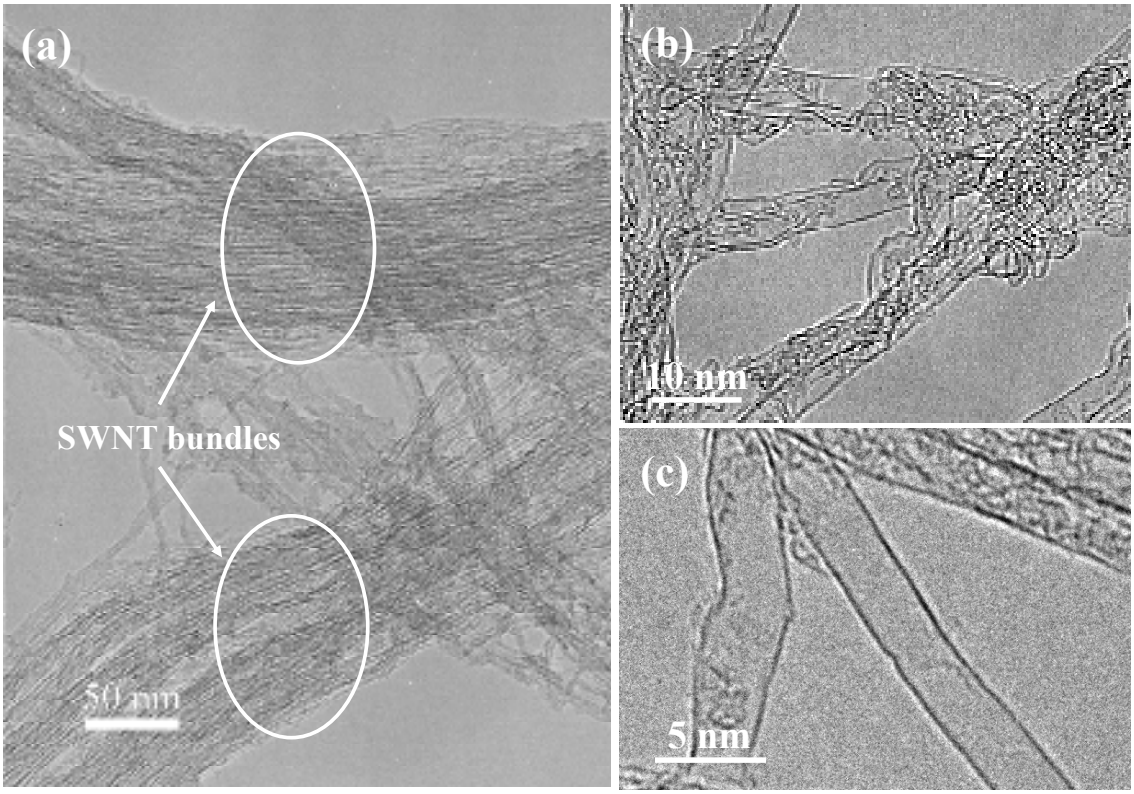

Figure 2.7 TEM images of SWNTs. (a) Low magnification showing SWNT bundles. (b, c) High magnification showing isolated SWNTs.

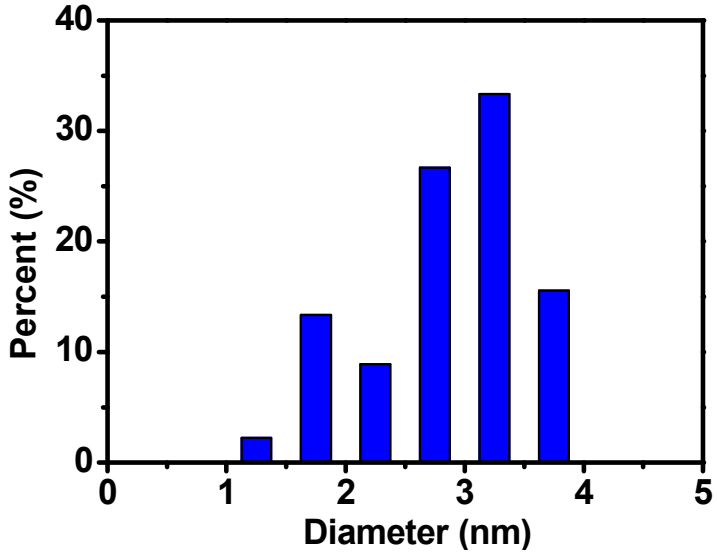

Figure 2.8 Diameter distribution of vertically aligned SWNTs, estimated by TEM.

2.3.3. Raman scattering measurements

Raman spectroscopy of as-grown vertically aligned SWNTs measured using a laser of 514 nm is shown in Fig. 2.9(a). Two peaks at 1589 cm^{-1} and 1333 cm^{-1} are identified as G-peak and D-peak, respectively. The G-peak arises from the graphite structure and the D-peak is induced by graphite disorders. A shoulder of the G peak at 1570 cm^{-1} and the radial breathing mode (RBM) in the low-frequency region (< 400 cm^{-1}) are the fingerprints of SWNTs. While the G-peak at 1589 cm^{-1} is associated with carbon atom vibrations along the nanotube axis, the split of the G-peak at 1570 cm^{-1} is associated with vibrations of carbon atoms along the circumferential direction of the SWNT. The RBM peak is a bond-stretching out-of-plane phonon mode for which all the carbon atoms move coherently in the radial direction. Figure 2.9(b) shows a magnified graph of RBM peaks. A RBM peak corresponds to a diameter and a chirality of a SWNT. The diameter was estimated from the RBM peaks using the correlation, $d = 248/\nu$ [13], where d is the diameter of SWNTs in nm and ν is the Raman shift in cm^{-1}. Diameters calculated using the correlation are shown in the superior axis of Fig. 2.9(b) showing that SWNTs have diameters of 0.9 – 3.5 nm, which is similar with the TEM result. Larger diameters are below the range of normal RBM peaks because the low frequencies below < 80 cm^{-1} are filtered. A high G- to D-peak ratio indicates the high quality of as-grown SWNTs despite low-temperature synthesis.

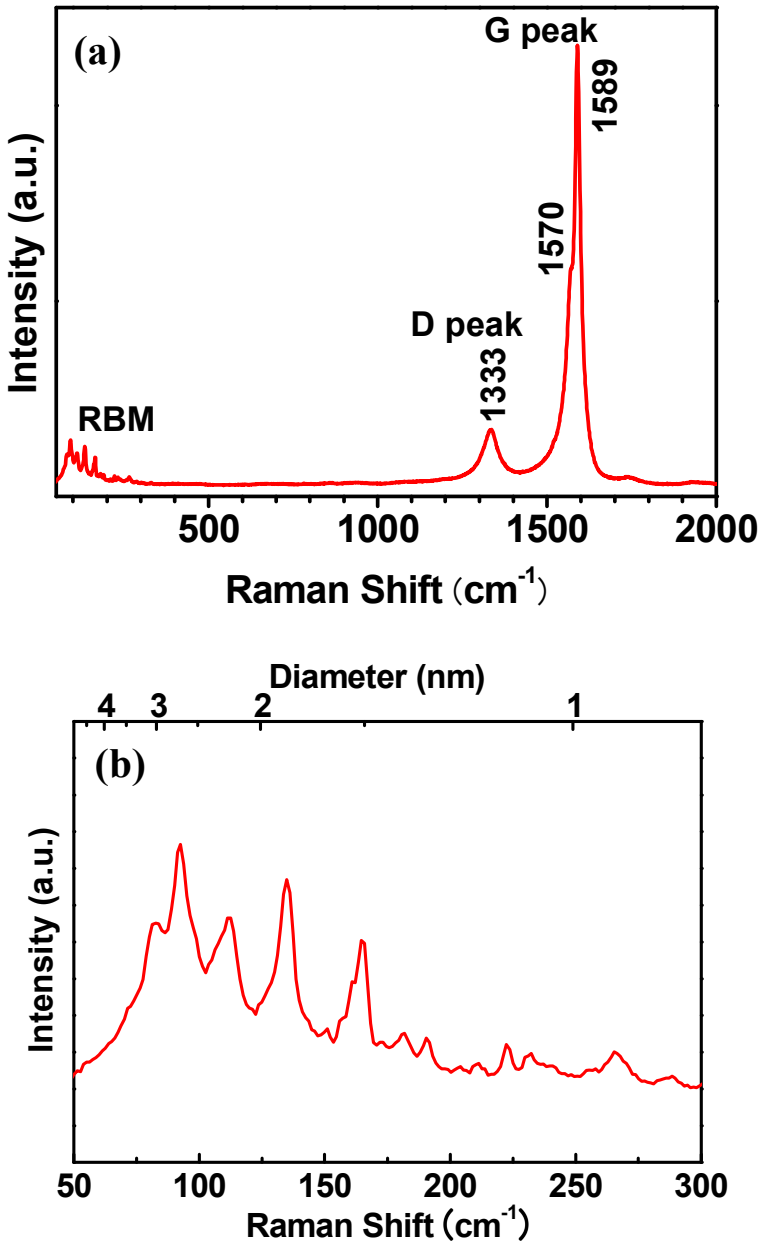

Figure 2.9 Raman spectroscopy of as-grown vertically aligned SWNTs. (a) Large range showing G, D, and RBM peaks. (b) RBM peaks at the low frequency region.

2.3.4. Patterned growth of vertically aligned SWNTs

The position and the shape control of vertically aligned SWNTs are very important techniques for SWNT-based applications. The position and the shape can be easily controlled by selective deposition of catalyst films. Figure 2.10 shows vertically aligned SWNTs with various shapes. SWNTs in Fig. 2.10(a) were grown on a catalyst deposited using a metal mask during sputtering. Since SWNTs do not grow without catalyst particles, SWNTs can be obtained only where the catalyst was deposited. The metal mask allows catalyst deposition with large sizes (> 100 μm). Thus, for smaller shapes, electron beam lithography was used, which made it possible to synthesize SWNTs less than 100 μm in width (Fig. 2.10(b-d)).

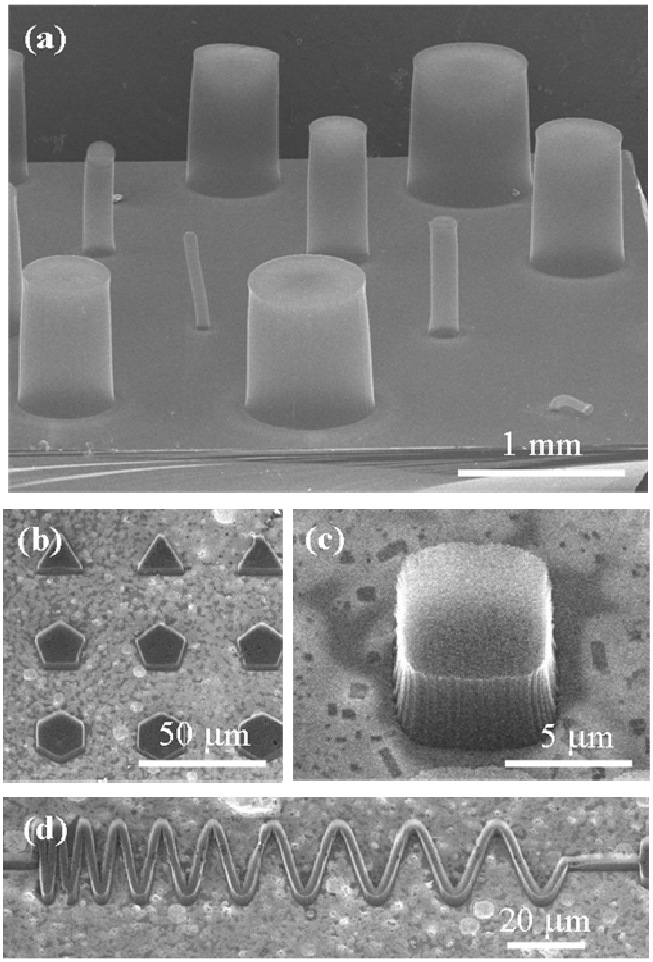

Figure 2.10 Vertically aligned SWNTs patterned with various shapes.

2.3.5. Effects of sandwich-like catalyst structure

One SWNT with length on the order of micrometers cannot be free standing because a SWNT has an extremely small diameter (< 4 nm). To achieve vertically aligned SWNTs, they should be dense and must support one another with van der Waals' attractions. Therefore, it is essential to prepare a high density of catalytic nanoparticles. Moreover, for the SWNT growth, the size of catalyst particles must be very small less than 4 nm because larger particles result in the growth of CNTs with larger wall numbers, such as DWNTs and triple-walled CNTs.

First, a structure of Fe (0.5 nm) / Al_2O_3 (> 5 nm) on Si wafers was prepared (Fig. 2.11(a)). The Fe film acts as a catalyst and the Al_2O_3 layer between the Fe film and the Si substrate acts as a buffer layer to prevent Si and Fe from reacting during preheating and CNT growth periods. CNTs grown on this substrate were a mixture of SWNTs and MWNTs, and they are random and not oriented (Fig. 2.11(e)). It is speculated that Fe particles aggregated easily into larger particles and their density would be low, resulting in the mixture of MWNTs and random growth.

Second, a sandwich-like structure of Al_2O_3 (0.5 nm) / Fe (0.5 nm) / Al_2O_3 (> 5 nm) on Si wafers was used (Fig. 2.11(b)). Dense and vertically aligned SWNTs were synthesized using the sandwich-like structure, indicating that the top Al_2O_3 layer above the Fe film plays a key role in the synthesis of vertically aligned SWNTs (Fig. 2.11(f)). The particle density with the top Al_2O_3 layer was about 1.4 times higher than that without the top layer. During preheating, the thin top Al_2O_3 layer become into pieces around the Fe clusters, which increases the surface diffusion barrier of Fe catalytic atoms markedly so that the aggregation of Fe atoms can be suppressed during the preheating period (Fig. 2.11(d)). As a result, a high density of small Fe particles was obtained. Without the top Al_2O_3 layer, Fe particles moved on the substrate and became larger particles because of aggregation (Fig. 2.11(c)). Thus, the necessary density for the growth of vertically aligned SWNTs was not achieved.

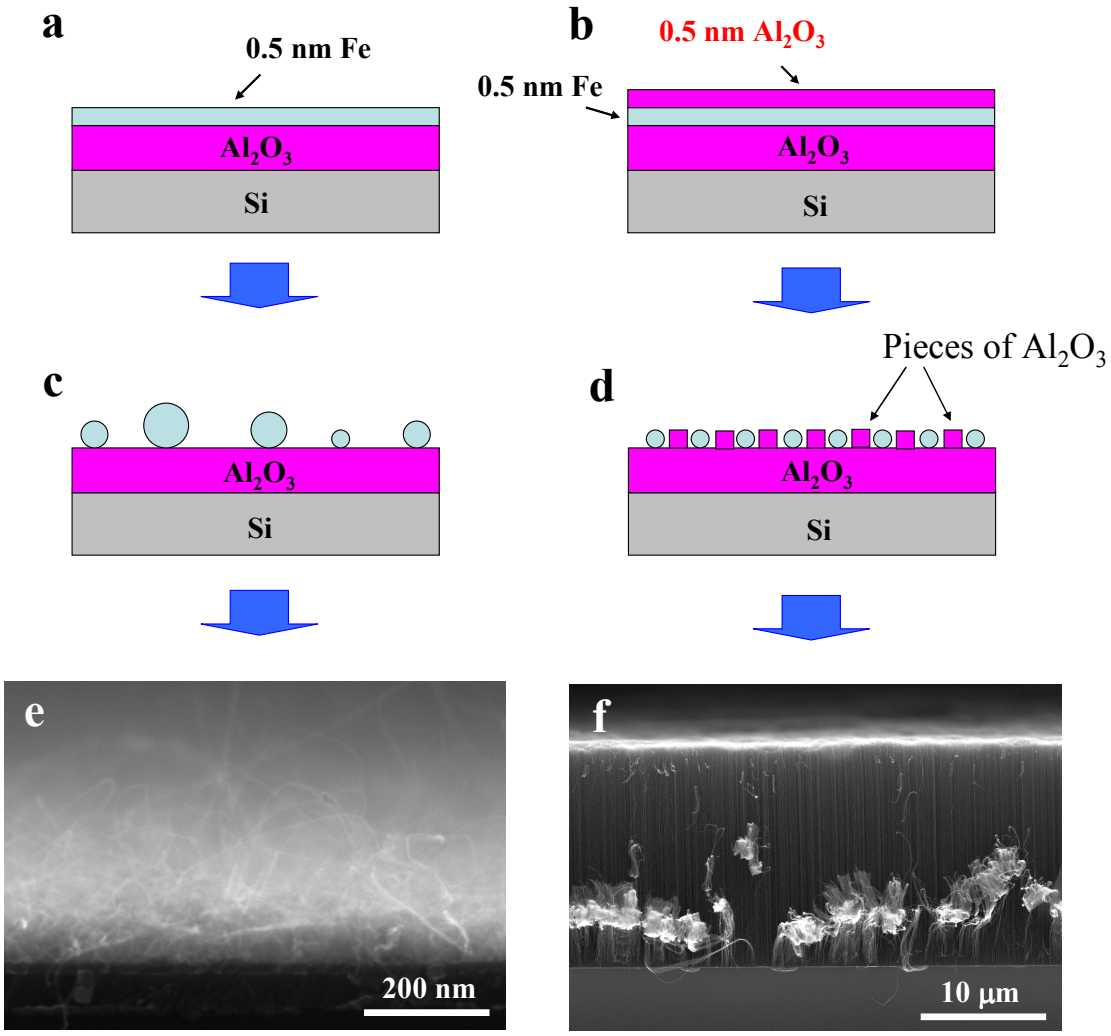

Figure 2.11 Effects of catalyst structure on alignment of SWNTs.

2.3.6. Variation in growth rate with microwave power and gas pressure

The effects of microwave power and gas pressure on the growth rate of SWNTs were investigated. The growth rate of SWNTs was 200-300 μm/h under the conditions of 60 W and 20 Torr. Figure 2.12 shows the variation in the growth rate with microwave power and pressure, and SEM images of SWNTs grown under various power and pressure conditions. The higher the power and the pressure were, the higher the growth rate was. Increasing both the microwave power and the gas pressure is effective for obtaining higher growth rates rather than increasing only one parameter. It is thought

that a larger amount of carbon radicals is generated under higher power and pressure. Although higher growth rates were obtained, the quality of the sample became worse. As shown in Fig. 2.13(b), the G/D ratio decreased and a broad band was observed between G and D peaks. Also, RBM peaks disappeared for SWNTs grown under 120 W/60 Torr and 180 W/80 Torr, as shown in Fig. 2.13(a). These were probably caused by the formation of defects as a result of higher growth rates and the deposition of amorphous carbon around SWNTs owing to the large amount of carbon radicals. To obtain a high growth rate and good quality at the same time, the introduction of oxygen-containing gas such as O_2 and H_2O would be effective [11]. Note that, in this study, the microwave power was set to below 200 W because a higher power could cause melting of the antenna and O-ring near the antenna.

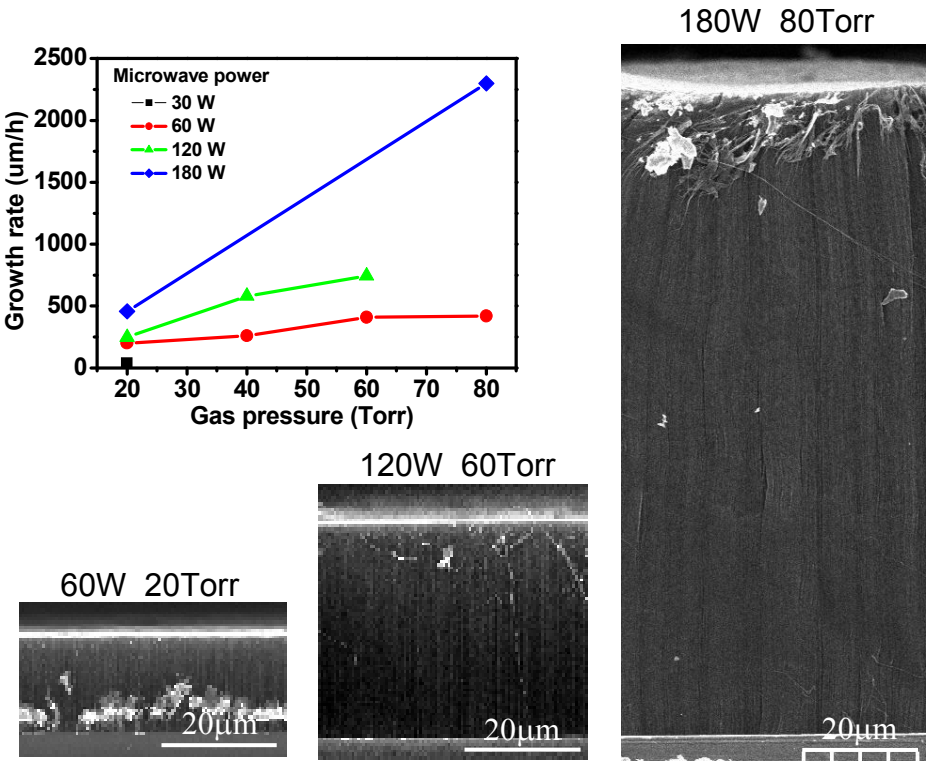

Figure 2.12 Variation in growth rate with microwave power and gas pressure. The growth time was 3 min.

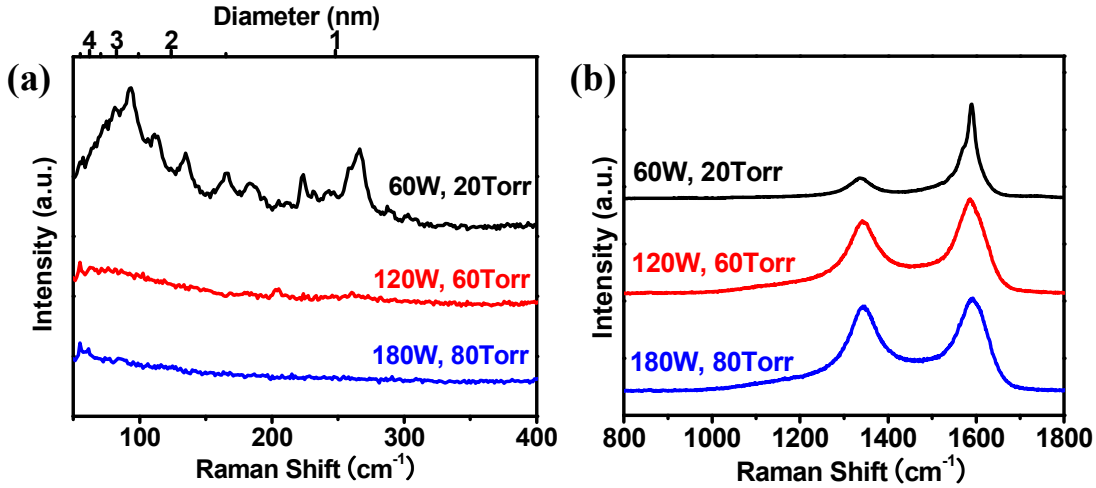

Figure 2.13 Raman spectra of SWNTs grown under various microwave power and gas pressure conditions, measured with a 514 nm laser. (a) RBM peaks. (b) G- and D-peaks.

2.3.7. Evaluation of SWNT density

The SWNT density is an important factor for applications such as EDLCs and LSI interconnection. The mass of densely-packed SWNTs can be obtained by measuring mass gain after CVD, so the volume density can be calculated to estimate the density of SWNTs. A volume density of about 70 kg/m^3 was achieved, which is the highest value for vertically aligned SWNTs. The areal density can be also calculated from the volume density. An areal density of 10^{16} /m^2 was obtained and this value corresponds to 1/10 of the closed-packed density.

The volume and areal densities were estimated as follows.

Volume density

The volume density (ρ_v) of vertically aligned SWNTs can be calculated by

$$\rho_v = \frac{\Delta M}{SL} \qquad (2.1)$$

where ΔM is a mass gain of SWNTs, obtained by measuring the substrate weight before and after CVD, S and L are the growth area and length of SWNTs, respectively. For

example, the mass gain was 4.8 mg from 730 μm-long SWNTs on a 10.0 x 10.0 mm^2 substrate. The volume density is 66 kg/m^3 for this sample. Figure 2.14 shows variation in the volume density of SWNTs with their length. The volume density has almost constant value (66-72 kg/m^3) for the four samples regardless of the length, meaning that all catalyst particles were active and SWNTs continued to grow during the CVD process.

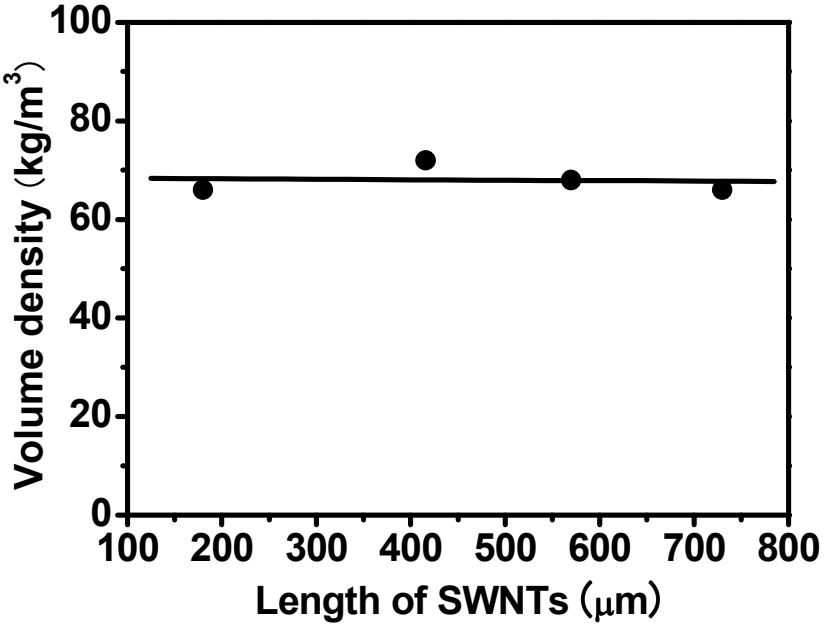

Figure 2.14 Volume density of SWNTs as a function of the length.

Areal density

For vertically aligned SWNTs, it would be more effective to use areal density, instead of volume density, to represent how dense SWNTs are. Due to the bundling nature of SWNTs, direct measurement of the areal density (ρ_s) of vertically aligned SWNTs by electron microscopy techniques is almost impossible, but it can be estimated from the volume density by

$$\rho_s = \frac{\rho_v}{m_u} = \frac{3\sqrt{3}\, a^2_{c-c}}{4\pi m_c} \cdot \frac{\rho_v}{d} \qquad (2.2)$$

where m_u is the mass of a SWNT of unit length with an average diameter of d; m_C is the mass of one carbon atom (1.993 x 10^{-26} kg); and a_{C-C} is the C–C bond length in a nanotube (0.144 nm). As the SWNT diameters distribute from 0.9 to 4 nm from the Raman and TEM observations, the areal density is thus on the order of 10^{16} /m^2, corresponding to one-tenth of the close-packed density.

2.3.8. Field emission properties of vertically aligned SWNTs

CNTs are expected to be good field emitters because of their high aspect ratio and structural stability. Field emission properties of as-grown vertically aligned SWNTs were measured. Two samples of different surface morphologies were used. As shown in Fig. 2.15(a, b), sample 2 has many cracks in the film because SWNTs are longer than those in sample 1. Emission currents were measured in a high vacuum of 5.3 x 10^{-7} Pa. The distance between the anode and the sample surface was fixed at 0.3 mm. The measured area was 2 mm in diameter. Figure 2.15(c, d) shows emission currents and F-N plots of the two samples. It is clearly seen that emission from sample 2 began at a lower voltage than that from sample 1. The CNT density of the two samples is the same, so the difference in the threshold voltage should be related to the surface morphology. In principle, field emission easily occurs at a sharp structure, where an electric filed is enhanced. Although the two samples have the same CNT density, sample 2 has a larger space around each CNT block, resulting in a strong electric field at the edge of the cracks. Therefore, the low threshold voltage was obtained for sample 2.

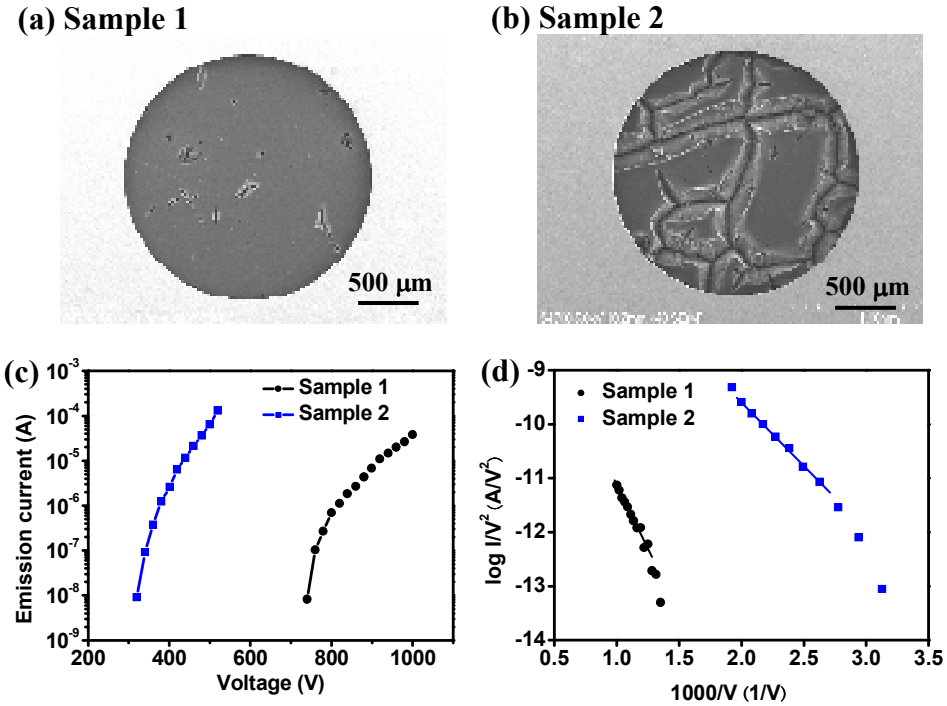

Figure 2.15 Field emission properties of vertically aligned SWNTs. (a, b) SEM images of top surfaces of SWNT arrays. The samples have different morphology. (c) Emission currents. (d) F-N plots.

2.4. Growth kinetics of millimeter-long vertically aligned SWNTs

2.4.1. Millimeter-long vertically aligned SWNTs and their Raman spectra

The massive growth of vertically aligned SWNTs is an important technology for the mass production of SWNTs, the fundamental experiments for SWNT evaluation, and the applications such as EDLCs and LSI global interconnections. Because SWNTs have very small diameters, they cannot be handled by hand or with a machine. However, making a large quantity of SWNTs grow very long, such as on the millimeter order, we or a machine can pick up SWNTs directly and put them on a substrate at the desired positions and orientations. As a result, physical characteristics, such as thermal conductivity and tensile strength, of SWNTs are expected to be measured precisely. For EDLCs, long SWNTs are of interest for increasing the capacitance.

Millimeter-long vertically aligned SWNTs have been successfully synthesized by long-time deposition. The heights of SWNTs grown for 10 h and 20 h were 1.5 mm and 1.9 mm , respectively, as shown in Fig. 2.16(a, b). The Fe catalytic particles remained active for more than 30 hours. Figure 2.16(c) shows the time evolution of the length of SWNTs. The growth rate of SWNTs decreases as the growth time increases and SWNTs grow longer. In general, there are two reasons for the decrease in the growth rate of CNTs: catalyst lifetime and the diffusion-limited mechanism. Catalyst particles become inactive when they are covered by amorphous carbon or graphite, or are oxidized by gas including oxygen, such as alcohol [10] and water [11]. When the catalysts are fully covered by other carbon phases, the growth of SWNTs stops and the length of SWNTs is saturated. In our case, however, growth rate decreases gradually but is not completely saturated, as shown in Fig. 2.16(c). Considering the diffusion-limited mechanism, it is important to reveal the growth mode of SWNTs. Our SWNTs grow through the root growth mode, as described in Section 3.2, so carbon radicals generated at the antenna must diffuse to the catalysts at the bottom of vertically aligned SWNT forests, indicating that the diffusion pass length of carbon radicals becomes longer and longer while SWNTs continue to grow. Carbon precursors collide with SWNTs before reaching catalytic particles on the substrate, because of the high density of long SWNTs, resulting in the decrease in growth rate.

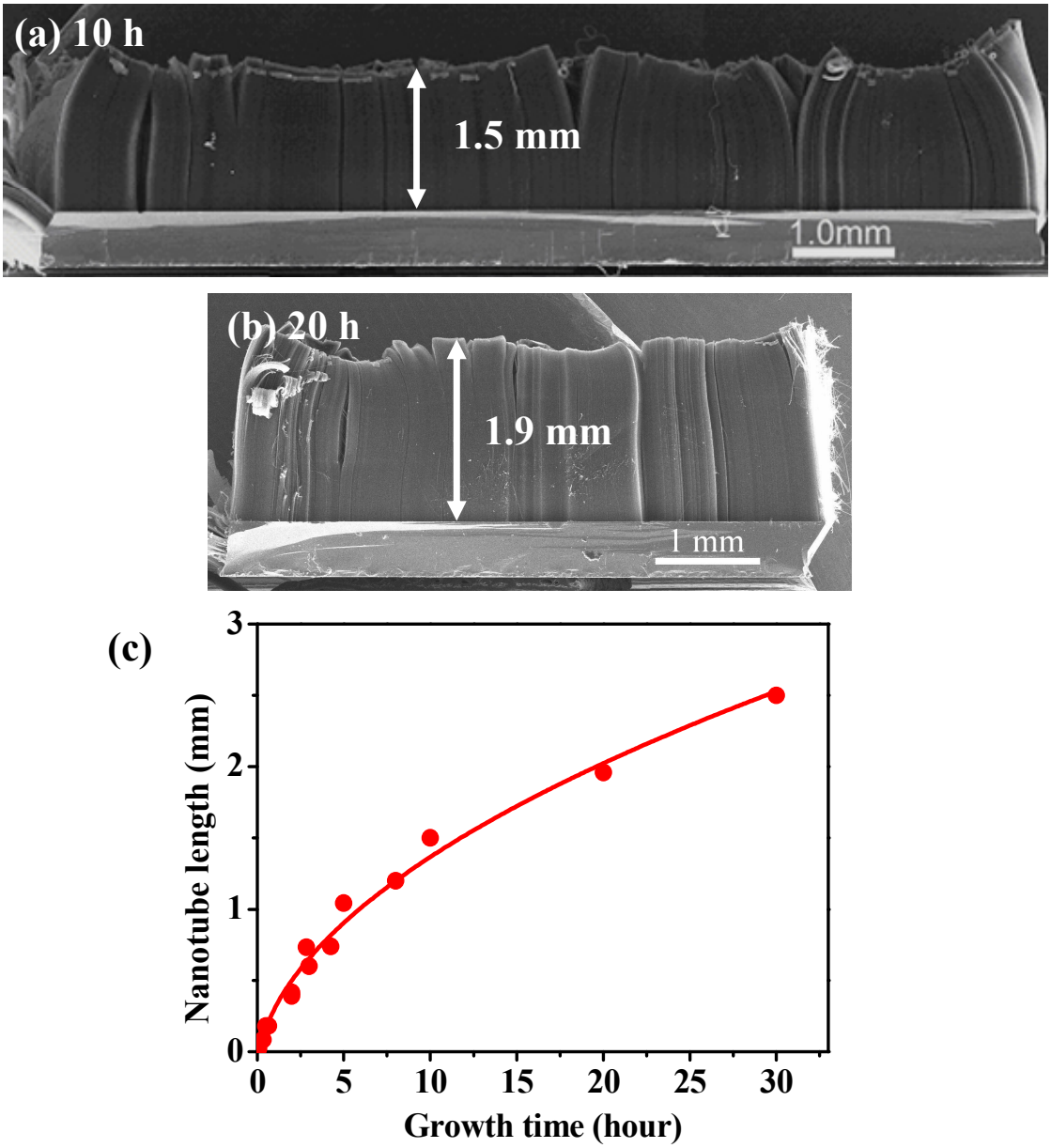

Figure 2.16 Millimeter-long vertically aligned SWNTs. SEM images of SWNTs grown for (a) 10 h and (b) 20 h. (c) Time evolution.

Figure 2.17 shows a series of Raman spectra measured along the length of the SWNT mat using the 633 nm excitation wavelength. Except for a few Raman spectra from the SWNT tip portion, the RBMs span from about 70 to 400 cm^{-1}, and all of the profiles of RBMs and the high-frequency tangential mode bands (G bands at 1590 cm^{-1}) remain almost unchanged along the length. This suggests that the long vertically aligned SWNTs have a range of diameters from 0.6 to 3.0 nm, and also retain their distributions along the length. However, it was found that the intensity of disorder-induced bands (D bands at 1314 cm^{-1}) increases slightly from root to tip, which implies some degradation of vertically aligned SWNTs in quality. The high overall intensity ratios of G bands to D bands in Fig. 2.17 suggest that 2 mm-long SWNTs are still fairly high quality.

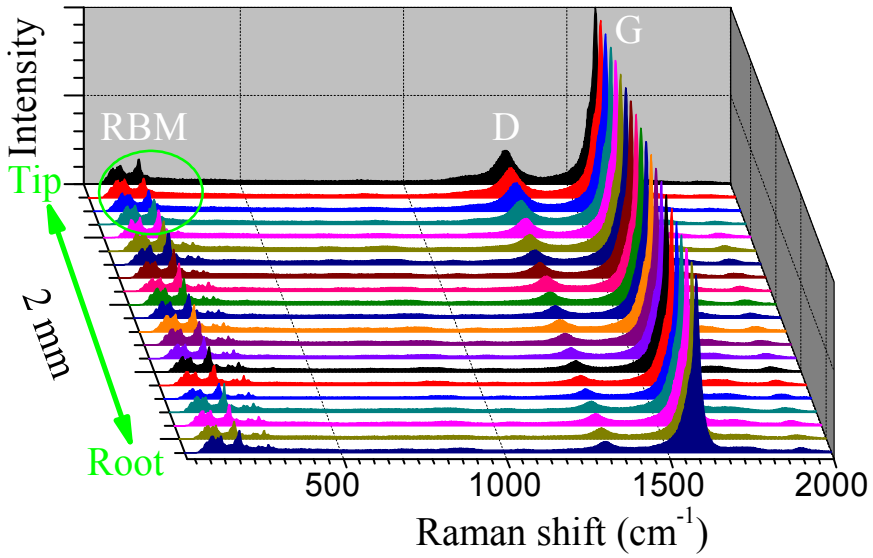

Figure 2.17 Series of Raman spectra measured at a constant increment from tip to root of a 2 mm-long vertically aligned SWNT sample. The excitation laser is 633 nm.

2.4.2. Diffusion-limited model of vertically aligned SWNTs

Fick's law is the starting point for elucidating the relationship between the SWNT height and growth time. Figure 2.18 shows a schematic of the concentration of carbon radicals in a SWNT mat. The amounts of carbon radicals flowing in and out from (absorbed by catalysts) the SWNT mat (area: S) in a unit time are given by

$$\frac{\Delta J_{in}}{\Delta t} = SD\frac{C_0 - C_1}{H} \qquad (2.3)$$

$$\frac{\Delta J_{out}}{\Delta t} = \beta S C_1 \qquad (2.4)$$

where ΔJ_{in} and ΔJ_{out} are the amounts of carbon radicals flowing in and out during Δt, respectively. J_{out} indicates carbon radicals absorbed by catalysts on a substrate and carbon radicals do not really flow out from the SWNT mat. H is the SWNT height, D is the diffusion coefficient of carbon radicals in the SWNT mat, and β is the possibility that a carbon radical on the substrate surface is absorbed by a catalyst in a unit time. In the steady state, ΔJ_{out} is equivalent to ΔJ_{in}. From Eqs (2.3), (2.4), the concentration of carbon radicals at the substrate surface is obtained as

$$C_1 = \frac{D}{D + \beta H} C_0 \qquad (2.5)$$

This relation indicates that the concentration of carbon radicals at the surface decreases with increasing SWNT height.

Next, ΔH is considered, which is the amount of SWNT height increase during Δt. Because the absorbed carbon radicals precipitate to SWNTs, ΔH is proportional to ΔJ_{out},

$$\Delta J_{out} = N\Delta H \cdot \sigma S = N\sigma S\Delta H \qquad (2.6)$$

where N is the number of carbon atoms in a unit length of one SWNT, and σ is the area density of SWNTs. From Eqs (2.4)-(2.6), we get

$$\frac{\Delta H}{\Delta t} = \frac{C_o}{N\sigma}\frac{D}{H + \frac{D}{\beta}} \qquad (2.7)$$

Finally, the relationship between the SWNT height and the growth time is obtained as

$$H^2 + AH = B(t - \tau) \qquad (2.8)$$

where $A = 2D/\beta$, $B = 2DC_0/N\sigma$, and τ is the incubation time, during which carbon radicals are absorbed until catalyst particles become supersaturated. Therefore, the growth rate of SWNTs decreases with growth time because the diffusion path lengths increase with longer SWNTs.

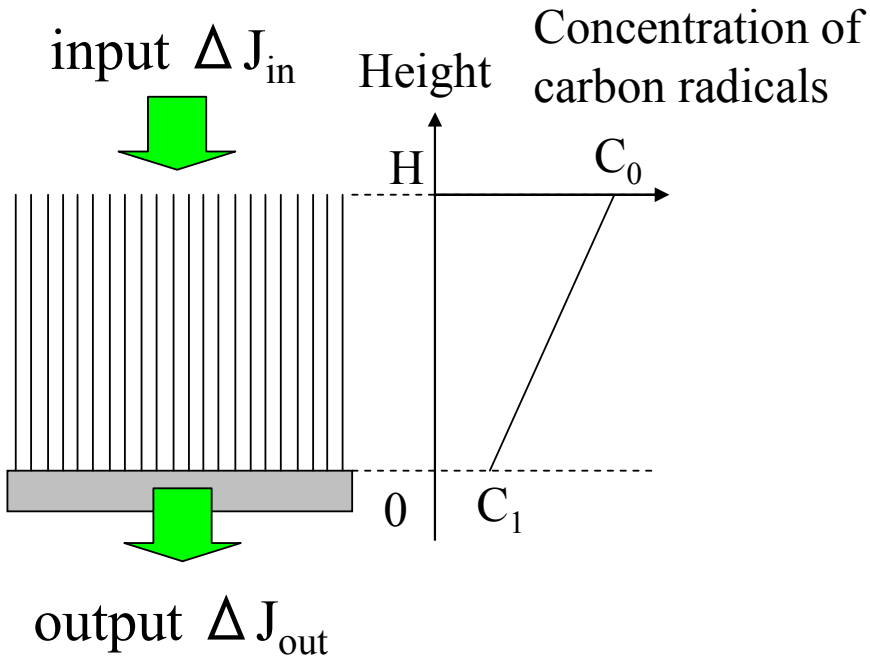

Figure 2.18 Concentration of carbon radicals in a SWNT mat. ΔJ_{in} and ΔJ_{out} are the amounts of carbon radicals flowing in the SWNT mat and absorbed by catalysts on a substrate during Δt, respectively.

2.4.3. 5 mm-long SWNTs by patterned growth

To confirm diffusion-limited growth of SWNTs, experiments with three types of patterned-catalyst substrates were performed. Type I: substrates are Si wafers fully coated without patterning. Type II: substrates are type I substrates onto which an array of 0.7 mm diameter gold dots has been evaporated, leaving a honeycomb pattern of exposed catalyst. Type III: substrates are Si wafers directly patterned with dots or lines of the sandwich catalyst, for growing rod arrays or wall-shaped SWNTs.

Figure 2.19(a, b) shows vertically aligned SWNTs on Type I and III substrates, respectively. Although the two samples were grown for the same growth time, 10 h, the rod-patterned sample in Fig. 2.19(b) were taller than the homogeneous grown SWNTs. Because there are large space around SWNT rods for patterned growth, carbon radicals can diffuse from side walls of the patterned SWNTs where the diffusion path lengths of carbon radicals can be shorten. This and the root growth suggest that growth of vertically aligned SWNT mats is limited by diffusion of growth species through the porous mat to the growth site.

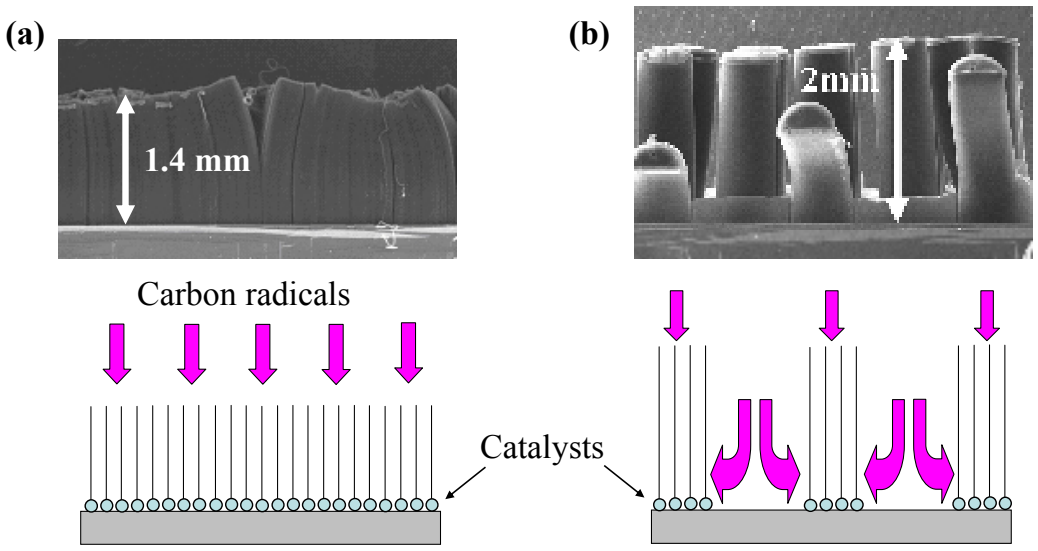

Figure 2.19 Comparison with homogeneous and patterned growth of SWNTs.

Figure 2.20 shows digital and SEM images of half centimeter-long vertically aligned SWNT samples of a honeycomb mat and an individual thin wall which grow from patterned substrates. Figure 2.21 displays the time evolution of the heights of

vertically aligned SWNTs for unpatterned (type I) and patterned (type III) substrates. These produce SWNT mats 2 mm and 5 mm high, respectively, for 20 h. Figure 2.21 illustrates a linear growth trend of the wall-shaped pattern. The continuous increase of SWNT length with time shows that the catalyst activity is highly durable. The growth rate of non-patterned SWNTs does decrease with time, but it does not show the sharp, exponential saturation due to catalyst poisoning (termination of catalyst lifetime) found in other reports [14, 15]. For the wall-pattern, gas has access to both sides of wall mats. Therefore, their growth is limited by $\beta C_1/N\sigma$ obtained from Eqs (2.4), (2.6). β is the reaction rate of catalysts and C_1 is associated with surface diffusion of carbon radicals on the substrate. Note that C_1 is independent of time for the patterned growth.

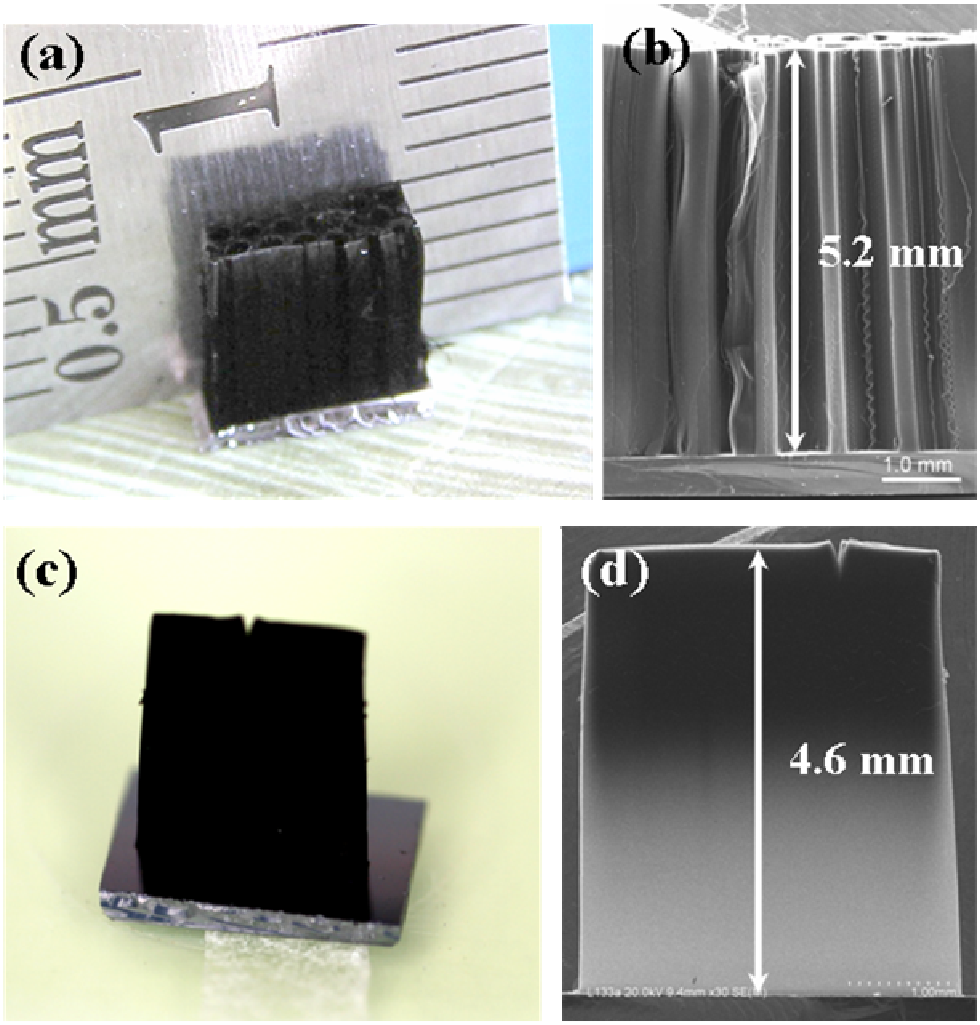

Figure 2.20 Digital (a, c) and SEM (b, d) images of 5 mm-long vertically aligned SWNT samples grown on type II and III substrates: (a, b) a honeycomb mat (pitch size, 900 μm; hole diameter, 700 μm), and (c, d) an individual thin wall (300 μm x 4 mm).

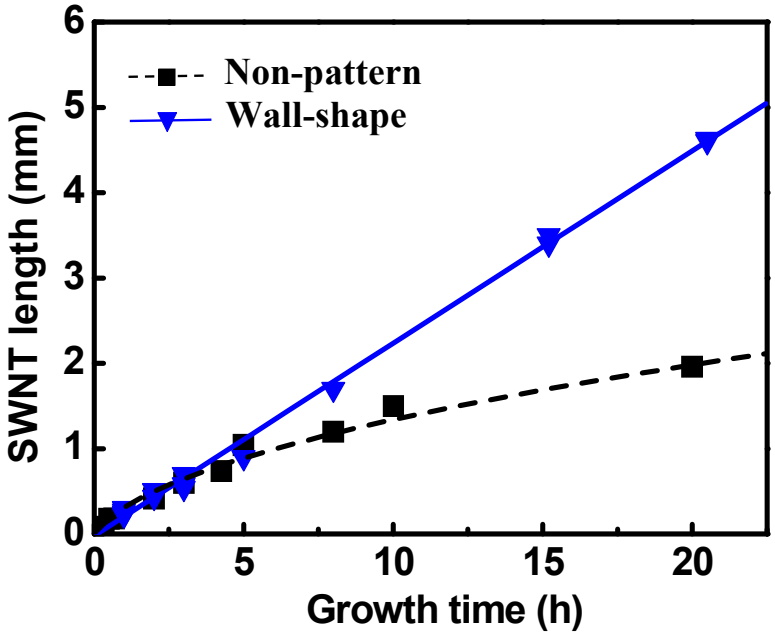

Figure 2.21 Time evolution of the growth of vertically aligned SWNTs on different types of substrates: non-pattern (Type I) and thin SWNT walls (Type III).

Why is the catalyst highly durable against poisoning? Here, CH_4 was used, which is a high-purity and an endothermic source of carbon, unlike acetylene. It is less likely to coat catalytic nanoparticles by pyrolitic amorphous carbon. Second, remote-plasma CVD has some advantages over other methods for controlling carbon activity at the catalyst surface, and balancing deposition and etching. The carbon radical concentration at the substrate can be controlled below a critical level not to form amorphous carbon on the catalyst by the gas ratio of CH_4 to H_2, the microwave power, the chamber pressure, and the distance between the microwave plasma and the substrate. Third, once SWNTs start to grow, the diffusion-limited kinetics further lowers the carbon radical concentration at the SWNT/substrate interface, a negative feedback to inhibit catalyst poisoning. In contrast, Futaba suggests [14] that water vapor may act as a gentle etchant, limiting the overgrowth of carbon on the catalyst, but eventually a strong poisoning effect is seen in their growth kinetics. Dai notes [16] that O will balance the concentrations of C and H radicals.

2.4.4. TEM and TGA measurements of 5mm SWNTs

TEM and thermogravimetric analysis (TGA) were used to evaluate the purity of the free standing millimeter-high SWNT mats. Figure 2.22(a) shows a typical TEM image of a SWNT sample. Many TEM images confirm that the nanotubes are no doubt SWNTs in bundles and free from catalytic nanoparticles. The individual SWNTs usually show relatively large average diameters around 3 nm.

The TGA spectrum of the 5 mm-long SWNT mat is shown in Fig. 2.22(b). The combustion of SWNTs was observed from 550 to 750°C. The slight weight loss up to 550°C indicates there is a small percentage of amorphous carbon co-deposited with SWNTs. There is no measurable residue remaining after heating above 800°C, which agrees with the extremely high production yield, suggesting that the vertically aligned SWNT mats are essentially catalyst-free unlike samples produced by arc-discharge and CO decomposition methods. The purity (over 90 wt %) of our millimeter-high SWNT mats is thus very close to purified SWNTs produced by different methods [17, 18].

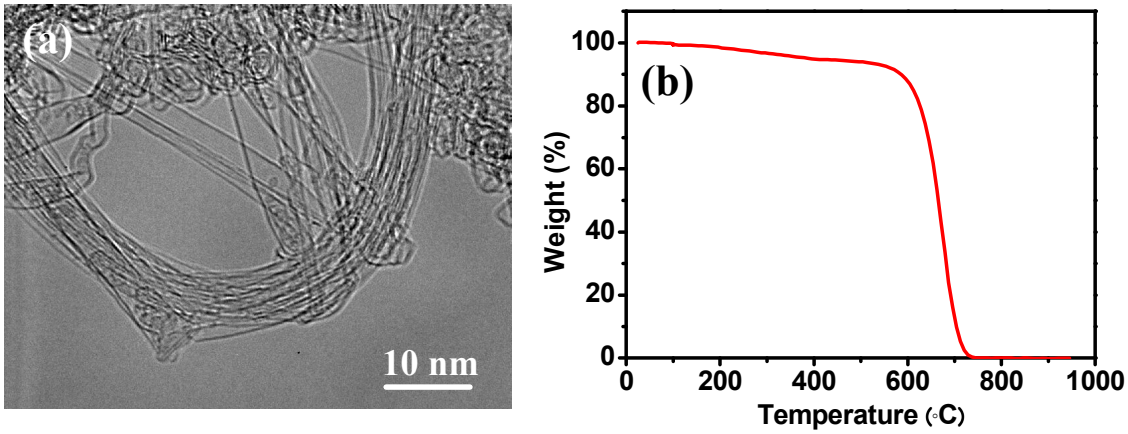

Figure 2.22 Characterization of 5 mm long vertically aligned SWNTs (a) TEM image of clean SWNT bundles; (b) TGA result of the raw SWNT mats (ramping rate at 5 °C /min under fluxing air).

2.5. Optimization of remote-plasma CVD conditions for long SWNT growth

2.5.1. Variation in growth rate with temperature, CH_4 concentration, and gas flow rate

From the point of view of the mass production of SWNTs, patterned growth is undesirable. Here, growth conditions of the temperature, the CH_4 concentration, and the gas flow rate were optimized to achieve long SWNTs (> 5 mm) on nonpatterned substrates. Figure 2.23 shows the variation in the growth rate with growth temperature. The highest growth rate (~ 850 μm/h) was obtained at 680-690°C, probably as a result of the higher catalyst activity than that at 600°C. The growth rate decreased markedly above 700°C. It is speculated that the alloy state of the Fe catalyst and the Al buffer layer changed, resulting in low activities of Fe catalyst particles.

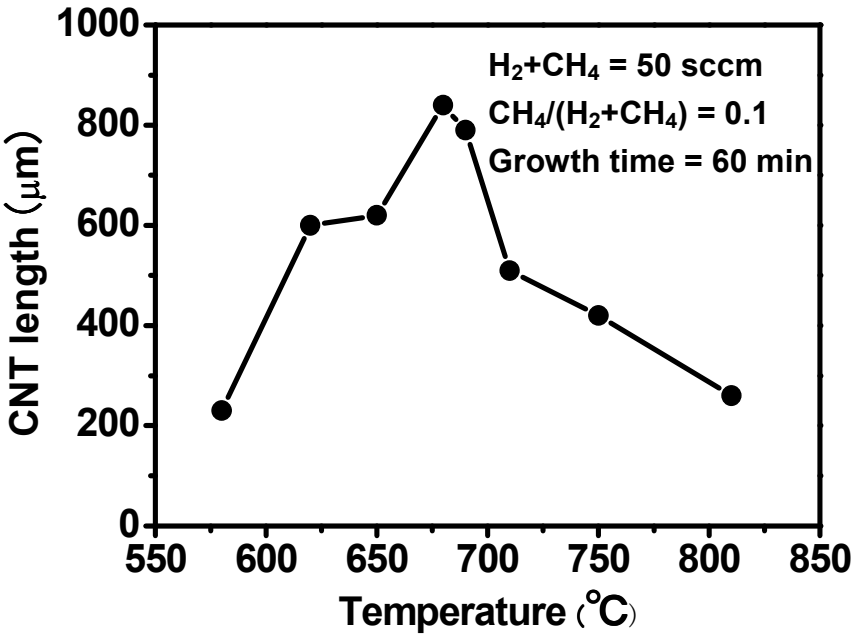

Figure 2.23 Variation in growth rate with growth temperature.

Figure 2.24(a, b) shows the variation in the growth rate with CH_4 concentration and total gas flow rate, respectively. Although higher growth rates were obtained at a CH_4 concentration of 15% and a total gas flow rate of 25 sccm compared with the conventional conditions (CH_4 concentration: 10%; total gas flow rate: 50 sccm), a problem occurred under these conditions. After long deposition time under these conditions, carbon impurities were deposited at the edge of the antenna in the chamber because of the high carbon concentration. This would cause plasma instability and imbalance between SWNT deposition and impurity etching by hydrogen, so the conventional CH_4 concentration and the total gas flow rate were used in the following experiments.

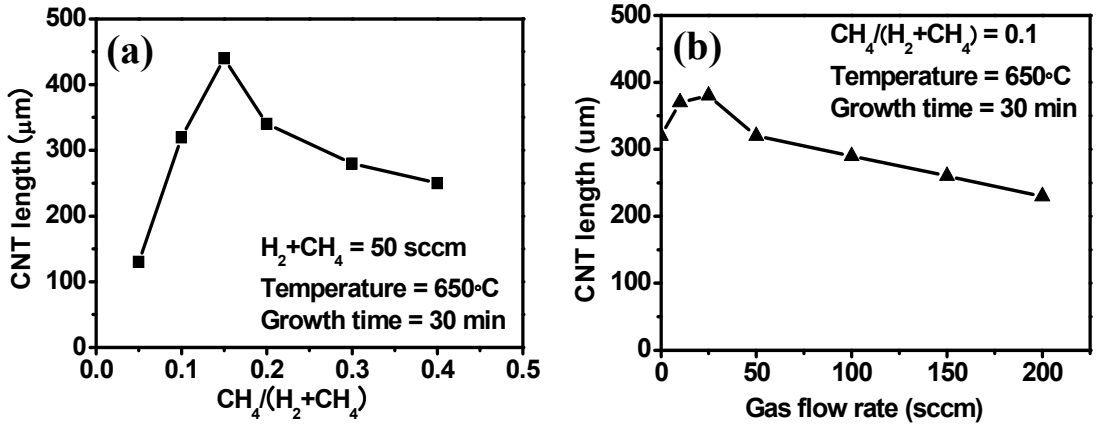

Figure 2.24 Variations in growth rate with CH_4 concentration and gas flow rate.

2.5.2. Superlong SWNTs grown under optimized conditions

Growth at the optimized temperature (690°C) was performed without catalyst patterning. As shown in Fig. 2.25, even for homogeneous growth, 7.4-mm-long vertically aligned SWNTs were obtained, which is longer than the patterned SWNTs described in Section 2.4.3. Figure 2.26 shows the time evolution of SWNT lengths grown at 600°C and 690°C; the lengths of SWNTs grown at 690°C were much longer than those grown at 600°C for 30 h. However, the growth rate at 690°C also decreased with increasing growth time. It is speculated that the growth at 690°C was also diffusion-limited because the growth was not completely saturated in a similar way with that at 600°C.

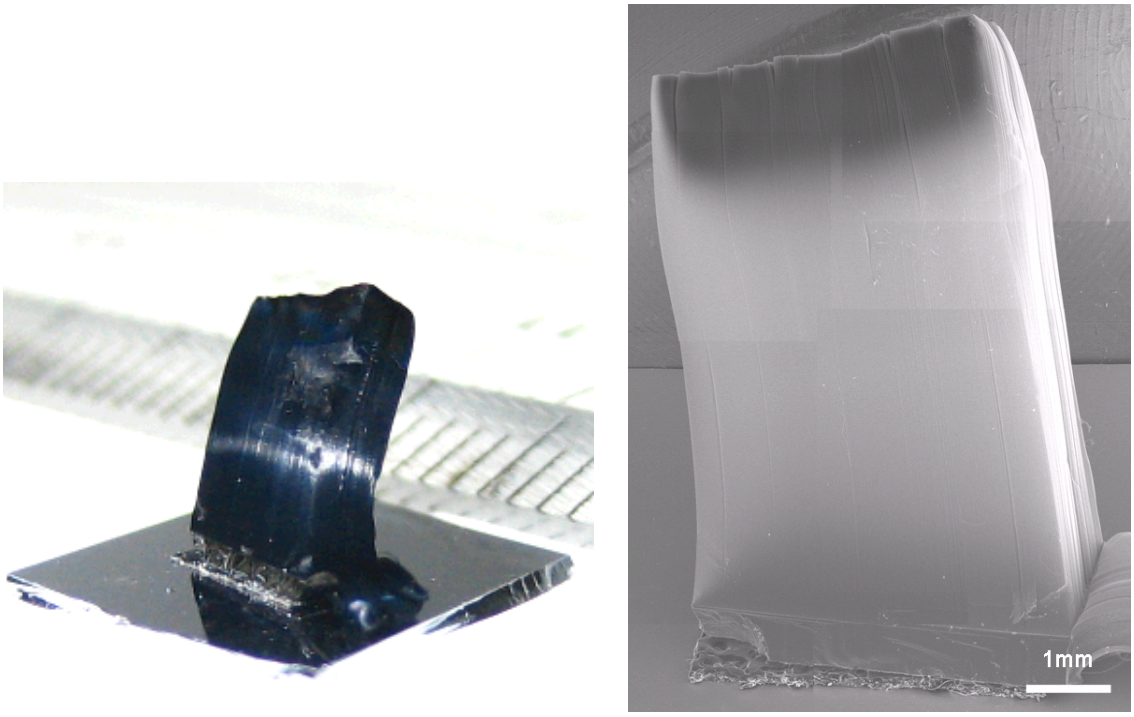

Figure 2.25 Digital-camera and SEM images of 7.4-mm-long vertically aligned SWNTs.

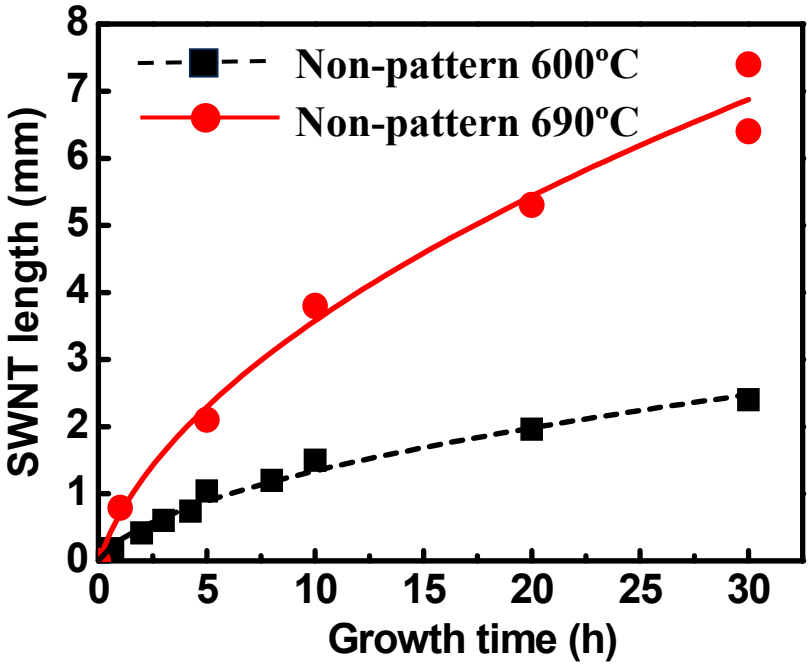

Figure 2.26 Time evolution of length of vertically aligned SWNTs at different growth temperatures: 600°C and 690°C.

2.6. Summary

Dense and vertically aligned SWNTs were successfully synthesized at a low temperature of 600°C by remote-plasma CVD. We found that a high density of catalytic nanoparticles by the sandwich-like structure of Al_2O_3 (0.5 nm) / Fe (0.5 nm) / Al_2O_3 (> 5 nm) was necessary to achieve vertically aligned SWNTs. Without the top Al_2O_3 layer, only randomly entangled SWNTs were synthesized. The SWNTs can grow on the order of millimeters for a long-time deposition, and the volume and areal density were 70 kg/m^3 and 10^{16} $/m^2$, respectively, which correspond to 1/10 of the close-packed density. Diffusion-limited growth was proposed for non-patterned vertically aligned SWNTs, and it was proven by the patterned growth. Patterned SWNTs showed higher growth rates than homogeneous growth and 5 mm-long SWNTs were synthesized. For line catalyst patterns, wall-shaped SWNTs continued to grow linearly with the growth time. By increasing the growth temperature to 690°C, 7.4 mm-long vertically aligned SWNTs were obtained even for non-patterned catalysts.

References

[1] S. J. Tans, A. R. M. Verschueren and C. Dekker, Nature 393, 49 (1998).

[2] S. J. Wind, J. Appenzeller, R. Martel, V. Derycke and P. Avouris, Appl.Phys.Lett. 80, 3817 (2002).

[3] A. Javey, Q. Wang, A. Ural, Y. Li and H. Dai, Nano Lett. 2, 929 (2002).

[4] A. P. Graham, G. S. Duesberg, R. Seidel, M. Liebau, E. Unger, F. Kreupl and W. Hönlein, Diam. and Relat. Mater. 13, 1296 (2004).

[5] M. Nihei, M. Haribe, A. Kawabata and Y. Awano, Jpn. J. Appl. Phys. 43, 1856 (2004).

[6] C. Journet, W.K. Maser, P. Bernier, A. Loiseau, M. Lamy de la Chapelle, S. Lefrant, P. Deniard and R. Lee. Fischer, Nature 388, 756 (1997).

[7] A. Thess, R. Lee, P. Nikolaev, H. Dai, P. Petit, J. Robert, C. Xu, Y.H. Lee, S.G. Kim, A.G. Rinzler, D.T. Colbert; G.E. Scuseria, D. Tomanek, J.E. Fischer and R.E. Smalley, Science 273, 483 (1996).

[8] Y. G. Zhang, A. L. Chang, J. Cao, Q. Wang, W. Kim, Y. M. Li, N. Morris, E. Yenilmez, J. Kong and H. J. Dai, Appl. Phys. Lett. 79, 3155 (2001).

[9] S. M. Huang, X. Y. Cai and J. Liu, J. Ame. Chem. Soc. 125, 5636 (2003).

[10] Y. Murakami, S. Chiashi, Y. Miyauchi, H. Minghui, M. Ogura, T. Okubo and S. Maruyama, Chem. Phys. Lett, 385, 298 (2004).

[11] K. Hata, D. N. Futaba, K. Mizuno, T. Namai, M. Yumura and S. Iijima, Science, 19, 1362 (2004)

[12] S. Noda, K. Hasegawa, H. Sugime, K. Kakehi, Z. Zhang, S. Maruyama and Y. Yamaguchi, J. Jpn. Appl. Phys. 46, L399 (2007).

[13] A. Jorio, R. Saito, J. H. Hafner, C. M. Lieber, M. Hunter, T. McClure, G. Dresselhaus, M. S. Dresselhaus. Phys. Rev. Lett. 86, 1118 (2001).

[14] D. N. Futaba, K. Hata, T. Yamada, K. Mizuno, M. Yumura, S. Iijima, Phys. Rev. Lett. 95, 056104 (2005).

[15] A. A. Puretzky, D. B. Geohegan, S. Jesse, I. N. Ivanov, G. Eres, Appl. Phys., A 81, 223 (2005).

[16] G. Y. Zhang, D. Mann, L. Zhang, A. Javey, Y. M. Li, E. Yenilmez, Q. Wang, J. P. McVittie, Y. Nishi, J. Gibbons, H. Dai, J. Proc. Natl.Acad. Sci. U.S.A. 102, 16141 (2005).

[17] A. C. Dillon, T. Gennett, K. M. Jones, J. L. Alleman, P. A. Parilla, M. J. Heben, Adv. Mater. 11, 1354 (1999).

[18] K. Tohji, T. Goto, H. Takahashi, Y. Shinoda, N. Shimizu, B. Jeyadevan, I. Matsuoka, Y. Saito, A. Kasuya, T. Ohsuna, H. Hiraga, Y. Nishina, Nature 383, 679 (1996).

Chapter 3

Layered Growth of Vertically Aligned SWNTs for Clarifying Growth Mode

Parts of this chapter are discussed based on the following papers:

- T. Iwasaki**,** G. Zhong, T. Aikawa, T. Yoshida, H. Kawarada, J. Phys. Chem. B, 109, 19556 (2005).
- T. Iwasaki, J. Robertson, H. Kawarada, Nano Lett, in press (2008).

3.1. Introduction

Nanotubes are known to grow by one of two growth mechanisms, root- or tip-growth, depending on whether the nanotube grows from the catalyst at its root or tip as shown in Fig. 3.1. Although the root growth mode of our vertically aligned SWNTs was suggested from the patterned growth experiments in Chapter 2, it is important to develop a method with versatility to clarify the growth mode because the growth mode strongly depends on CVD conditions and combination of substrates and catalysts. MWNTs can grow by either the root growth mode or the tip growth mode according to the residing positions of catalytic nanoparticles, which can be observed easily by scanning electron microscopy (SEM) and transmission electron microscopy (TEM) [1-5]. However, due to the small size and high production yield of our as-grown SWNTs, catalytic particles can hardly be confirmed by SEM and TEM. In the present study, a novel experimental method called marker growth was developed to determine the growth mode of vertically aligned SWNTs.

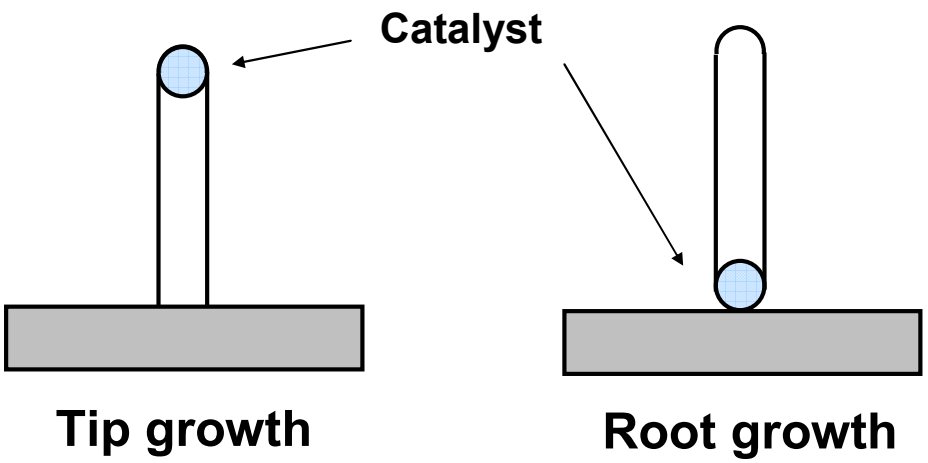

Figure 3.1 Growth mode of CNT

3.2. Direct evidence for root growth mode of vertically aligned SWNTs by a layered growth method

3.2.1. Design of layered growth for clarifying growth mode

To confirm the growth mode of vertically aligned SWNTs, a new method was designed, marker or layered growth. The plasma and heater are stopped after growth of SWNTs (the 1st layer, referred to as '1st' in Fig. 3.2(a, b)). Then, when the plasma and heater are turned on again, SWNTs grow again on the same substrate (the 2nd layer, referred to as '2nd' in Fig. 3.2(c, d)). It can be expected that there is an irregular part at the interface between the two layers, yellow part in Fig 3.2(c, d). Our SWNTs grow at a constant growth rate in a few hours and the top surface is very flat. Therefore, by changing the growth time for the 2nd layer (shorter time case shown in Fig. 3.2), the 1st and 2nd layers could be identified using the interface as a marker and determine the growth mode of vertically aligned SWNTs.

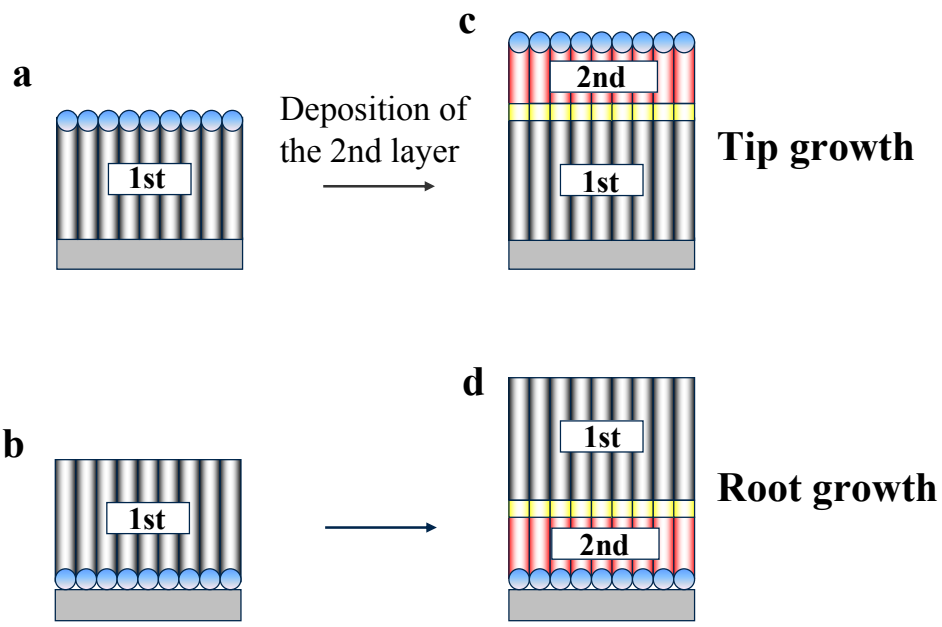

Figure 3.2 Model for determining the growth mode of vertically aligned SWNTs. (a) (b) The 1st layer grown through the tip and the root growth mode, respectively. (c) (d) Deposition of the 2nd layer in a shorter growth time than the 1st layer. Short yellow part shows an interface between the 1st and the 2nd layers.

3.2.2. Proof of root growth mode by layered growth

Vertically aligned SWNTs were grown intermittently as follows. The substrate was heated at 600°C for 5 min for pre-heating, and a microwave power of 60W was applied in a mixture of H_2 and CH_4 gases (H_2/CH_4 = 9/1, total pressure = 20 Torr) in 40 min for growth of the 1st layer. Then, the plasma and heater were switched off, and the sample was cooled for 30 min, after which the substrate was heated at 600°C and the plasma was turned on again for 20 min to allow the growth of the 2nd layer. Then, the system was cooled.

Figure 3.3(a) shows a cross-sectional FE-SEM image of a synthesized film in which a line can be seen marked with yellow arrows. Figure 3.3(b) shows a higher magnification view of the marker. A different appearance was observed perpendicular to the orientation of SWNTs, but details of the structure will be clarified in Section 3.3. Compared with the illustrations in Fig. 3.2, the growth mode of vertically aligned SWNTs can be revealed as root growth. The marker was formed in all SWNT samples and confirmed the root growth mode of a large number of SWNTs. This is the first direct observation of the root growth mode of vertically alinged SWNTs. Since the marker growth does not require complicated and time-consuming experiments, this method can overcome the quantitative limitation of TEM observation.

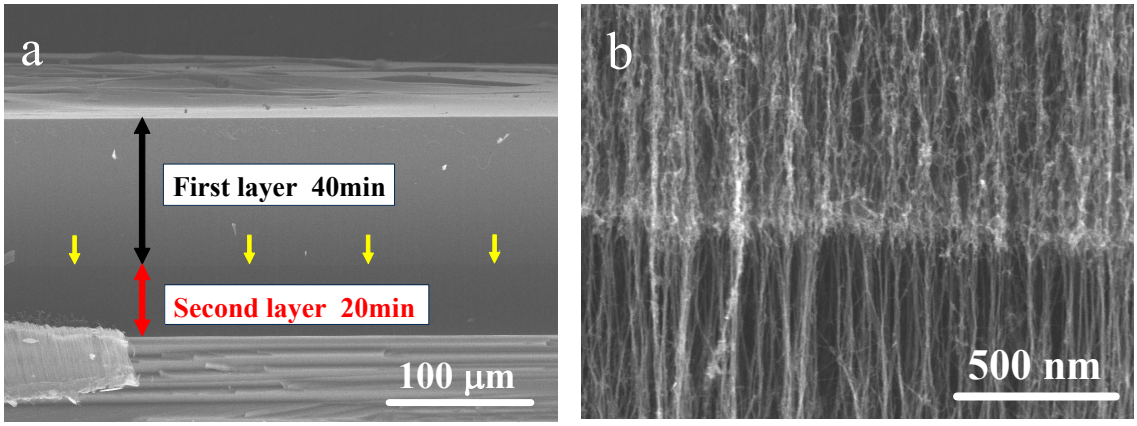

Figure 3.3 Cross-sectional SEM images of vertically aligned SWNTs grown intermittently. (a) A sample composed of two layers. Yellow arrows indicate a marker. (b) Magnified image of the marker.

3.2.3. Raman spectra of two SWNT layers

Characterization of the 1st and 2nd layers was performed by micro-Raman spectroscopy. Cross-sections of SWNT layers were also used for Raman measurement. Two excitation lasers with wavelengths of 514 nm and 633 nm were used to evaluate the diameters of SWNTs over a wide range. Radial breathing mode (RBM) peaks of SWNTs can be seen clearly in Fig. 3.4(a). The diameter was estimated using the correlation, $d = 232/(\nu-6.5)$, where d is the diameter of SWNT in nm and ν is the Raman shift in cm^{-1} [6]. The 1st and 2nd layers showed almost the same radial breathing mode peaks. No large shift was seen in the diameter distribution after deposition of the 2nd layer. From this result, it is expected that SWNTs of the 2nd layer grew using the same catalyst particles the sizes of which were kept constant during growth of the 1st layer and the cooling period. Note that the measurements were performed at the center of each layer and the resolution of the lateral direction of the micro-Raman apparatus is a few micrometers with a 50× objective lens, so all of the Raman signal arose from each layer.

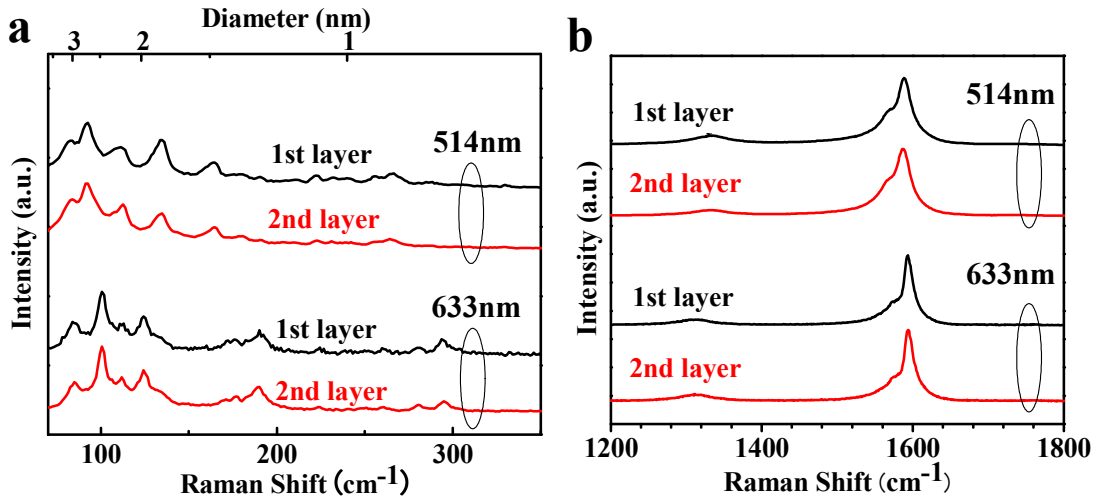

Figure 3.4 Raman spectra of the two SWNT layers grown intermittently, measured using 514 nm and 633 nm lasers. (a) Raman data for RBM of two layers. (b) Large-range Raman data including the G- and D-bands.

3.2.4. Peel-off of layers at interfaces

Interestingly, the marker growth can be performed many times, *e.g.*, Figure 3.5(a) shows a sample composed of three layers grown by marker growth. When the substrate was cut for FE-SEM observation, the 2nd and 3rd layers were peeled off from the 1st. Figure 3.5(b) also shows the layer below the marker peeled off from that above the marker, indicating that SWNTs of the layers did not connect completely. It is speculated that a layer below the marker connected weakly with the marker.

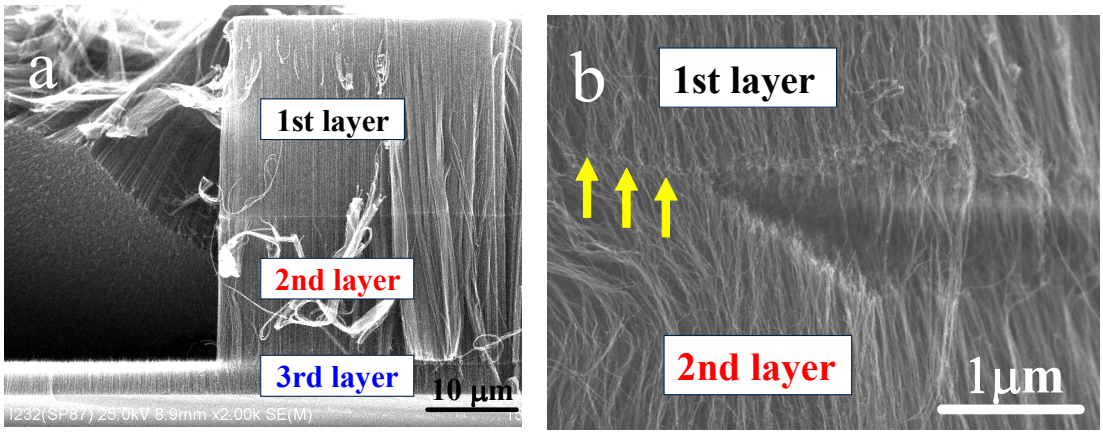

Figure 3.5 SEM image of peel-off at interfaces. (a). (b) Magnified image of peel-off at a corner. Yellow arrows show the uncut marker. The peeling was caused by cutting the substrate for the cross sectional SEM observation.

3.2.5. Layered growth at various CVD conditions

The examination of marker growth is not limited to the set of conditions outlined above, and experiments under various CVD conditions for deposition of each layer were performed. Figure 3.6(a) shows three layers grown under different microwave powers: 60 W for the 1st layer, 120 W for the 2nd, and 180 W for the 3rd. Growth time was 5 min for all three layers, and other conditions were also the same. Normally, higher microwave power is associated with faster SWNT growth rate because the amount of carbon precursors increases at higher microwave powers as discussed in Section 2.3.6. Therefore, the growth mode of the sample in Fig. 3.6(a) is the root growth.

Moreover, the growth temperature can also be changed for each layer deposition (Fig. 3.6(b)). Raman spectra measured with an excitation wavelength of 633 nm showed different profiles (Fig. 3.6(c, d)). High temperatures should result in better crystallinity of SWNTs and a higher ratio of G to D peaks, indicating the root growth mode of the sample in Fig. 3.6(b). As the temperature increased, predominant peaks of RBM shifted to the lower frequency region. SWNTs with larger diameters were synthesized at higher growth temperatures. Although the peaks at 294 cm^{-1} and 190 cm^{-1} were prominent at 600°C, the peak at 294 cm^{-1} was decreased markedly at 680°C and 760°C. In contrast, the peak at 101 cm^{-1} increased at 680°C and 760°C. Maruyama *et al.* [7] also reported that high growth temperatures resulted in synthesis of SWNTs with larger diameters using alcohol CVD. It is speculated that catalytic particles were strongly anchored with the substrate and they became slightly flatter in shape under high temperatures, or catalytic particles have expanded slightly at the high temperature. As a result, the diameter distribution of SWNTs shifted to the large region at the deposition of the 2nd and the 3rd layers.

Although we have succeeded in synthesizing SWNTs with lengths in the order of millimeters, the growth rate of SWNTs decreases gradually as the length of SWNTs increases as discussed in Section 2.4. Carbon precursors are blocked to diffuse to catalytic particles on the substrate by a high density of long SWNTs. When SWNTs grow by the tip growth mode, carbon precursors can arrive at the catalysts at the tips of SWNTs without interruption of diffusion by SWNTs [8]. However, for the tip growth mode, a different problem related to temperature should be considered. The temperature of the SWNT film surface decreases as the height of SWNTs increases, which could cause a decrease in the growth rate of SWNTs. Precise temperature control is necessary for the unlimited synthesis of SWNTs. For MWNTs, different materials for the buffer layer lead to both tip and root growth modes [3]. Investigations using combinations of different catalysts and buffer layers, and various CVD conditions are required for the tip growth of SWNTs. The marker method would be useful to investigate the tip growth mode of vertically aligned SWNTs.

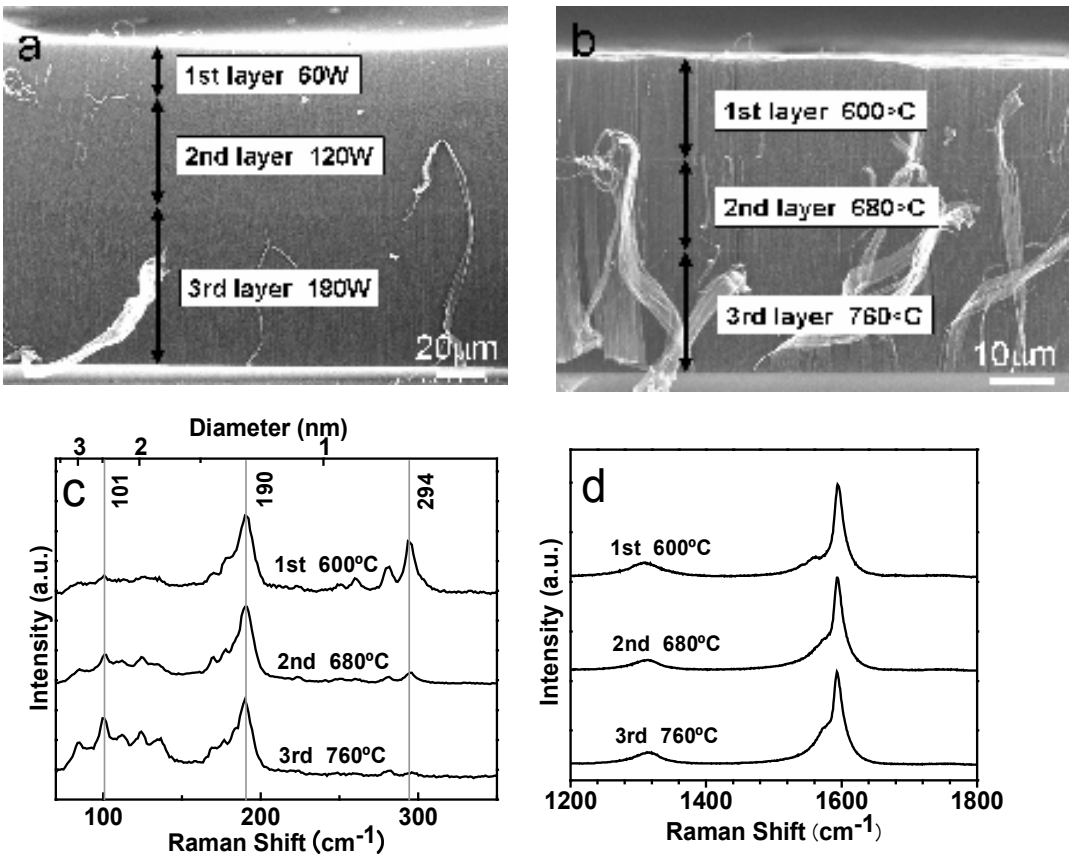

Figure 3.6 Marker growth performed under various CVD conditions. (a) SEM image of three layers grown at 60 W, 120 W and 180 W. (b) SEM image of three layers grown at 600°C, 680°C and 760°C. (c) Raman data for RBM of (b), measured using a 633 nm laser. (d) Large-range Raman data of (b) including the G- and D-bands.

3.3. Mechanism analysis of layered growth of SWNT arrays

3.3.1. Introduction

The marker growth experiment raises the question, how does growth restart? It was found possible to separate the layers at the interface formed by interrupted growth by cutting by a razor blade. This indicates a weak adhesion between the layers. This exposed the top surface of the second layer, and then the tip structure was characterized. The top surface of the lower layer was found to possess caps, showing that it re-grew just like a fresh layer. And many selected area Raman spectra show that the chirality distribution of the two layers is same across the interface, despite new caps being formed.

Smalley et. al [8, 9] suggested that a way to produce a nanotube mat of single chirality is by 'cloning'; to form a mat of previously separated nanotubes, and to continue the growth of the nanotubes by tip growth after 'docking' catalyst atoms on their tips. This section demonstrates another means to produce continued growth while retaining chirality distribution, but in the root growth mechanism, which is the prevalent growth mechanism of SWNT mats. In addition, this section shows that this growth method may prove a degree of chirality selection of SWNTs.

3.3.2. Cutting layers by a razor blade

The layers were separated by applying a lateral force by a razor blade lightly and slowly to the upper layer as shown in Fig. 3.7(a). The samples were stuck on glass slides or Si substrates with double-sided tape. The upper layer would peel off easily, indicating that adhesion at the interface is surprisingly weak. This means that the nanotubes may not be continuous across the interface. Fig. 3.7(d, e) shows the sample after cutting the layer 1. Only the layer 2 was left on the substrate. Hand cutting is possible because the upper layers are quite thick, ~1 mm [10]. The cutting process could be optimized; applying a slicing action from opposite sides produced a better separation.

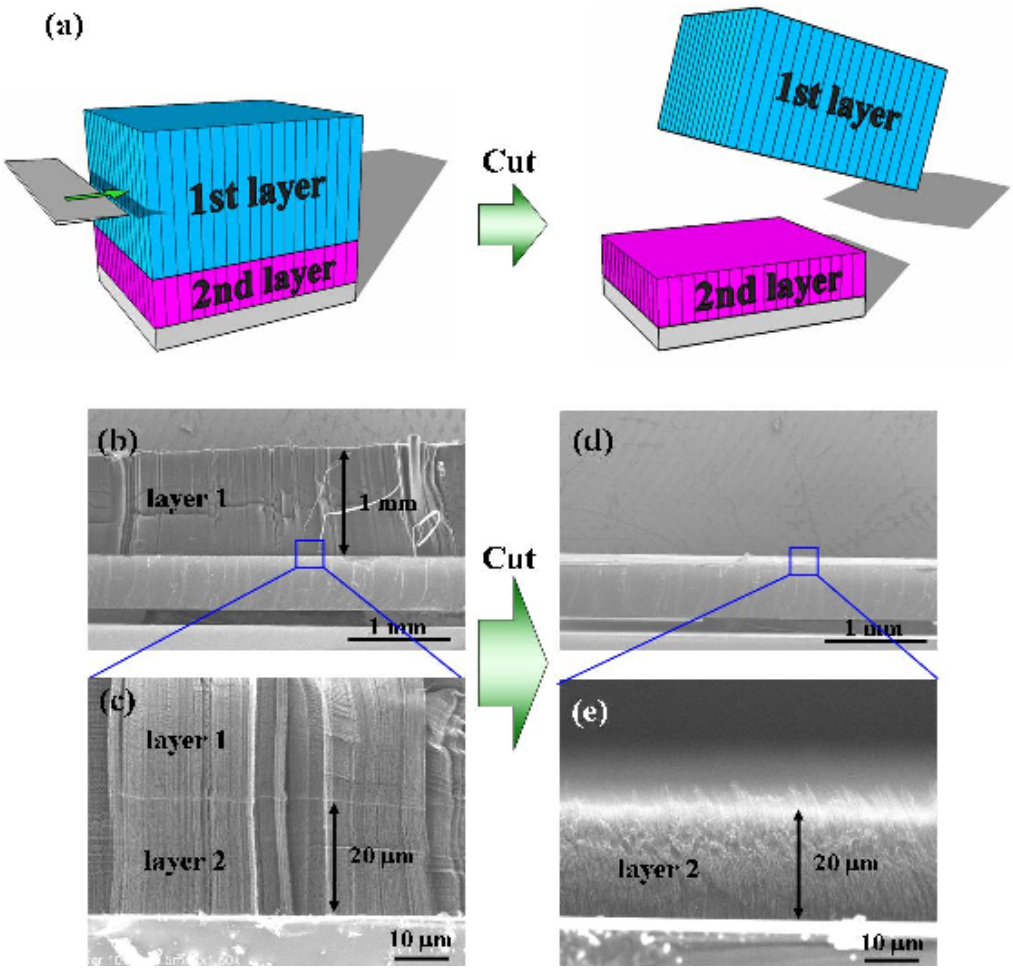

Figure 3.7 Cutting of layered SWNTs. (a) Schematic of the cutting procedure using a razor blade. (b, c) Double-layered vertically aligned SWNTs before cutting. Length of the layer 1 was in the order of millimeter to make cutting easy. (d, e) The sample after cutting. Only the layer 2 was left on the substrate.

3.3.3. Growth mechanism of layered SWNTs

The nanotube tips of each layer were examined by TEM. Figure 3.8(a, b) show tips of a SWNT and a DWNT in the top layer. Both tips have a cap and no catalyst particles were observed. This is typical for root growth [11, 12]. Figure 3.8(c, d) show that tips of a SWNT and a DWNT in layer 2 also have caps. This is a key observation, as it shows that re-growth of the layer 2 started with new caps, not by continuing the previous tubes. To make DWNTs in Fig. 3.8(b, d), the preheating temperature was raised to 640°C to obtain the appropriate particle size. The other conditions were same as SWNT growth. The growth of DWNTs is described in detail in chapter 4.

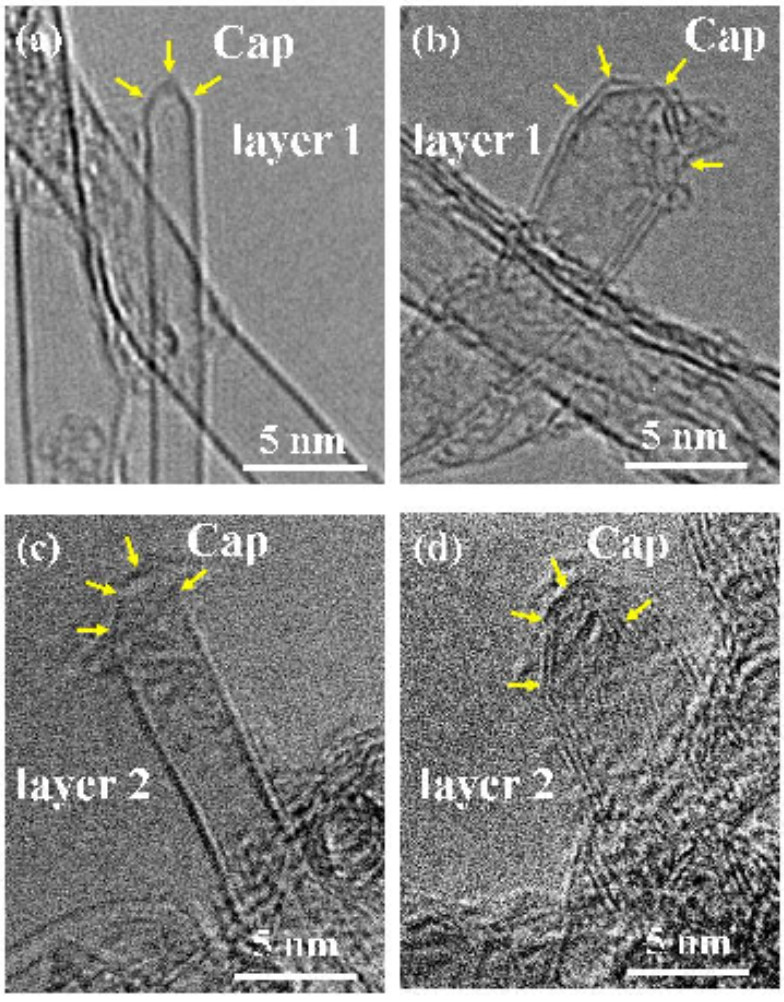

Figure 3.8 TEM images of tip structures of (a) 1st SWNT, (b) 1st DWNT, (c) 2nd SWNT and (d) 2nd DWNT.

Raman measurements were used to measure the diameter and chirality distribution of the SWNTs in each layer. Figure 3.9 shows the low frequency RBMs of layer 1 and 2 for two samples that were grown in different CVD runs. The RBM wavenumber is inversely proportional to the nanotube diameter. The Raman spectra of layers 1 and 2 for each sample show almost the same RBM peaks (peak position and relative intensity), while the detailed peak distribution is different in each sample.

RBMs of particular nanotube chiralities have a high intensity when their sub-band gaps are resonant with the excitation wavelength. This allows the nanotube chiralities to be indexed from their RBM peaks [13, 14]. Nanotubes in layers 1 and 2 show almost the same peaks in their RBM peaks in Fig 3.9. Although the two samples show different RBM peaks, especially for 633 nm excitation, the relative intensities in each sample are preserved after growth of layer 2. This suggests that the two SWNT layers in each sample have the same diameter and chirality distribution.

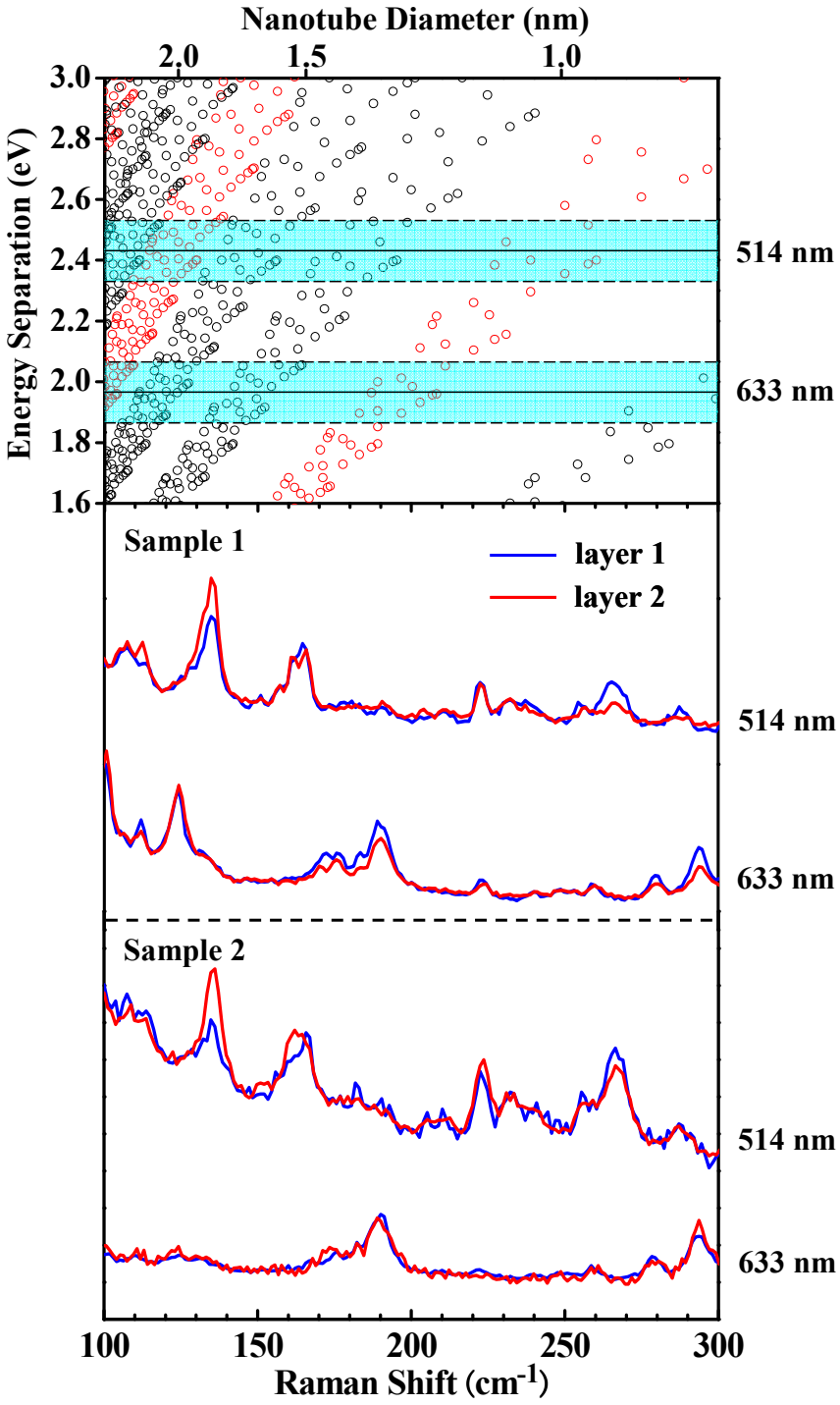

Figure 3.9 RBM peaks in Raman spectra of layer 1 and layer 2. Raman spectra were measured using 514 nm and 633 nm excitation lasers. The sample 1 and 2 were grown in different CVD runs. The top graph shows a Kataura plot as a function of nanotube diameter and wavenumber. Black and red circles indicate semiconducting and metallic nanotubes, respectively.

There are three observations; (1) there is weak adhesion across the interface, (2) new tips occur when growth restarts, and (3) the diameter and chirality distribution appears to be continuous across the interface. A possible growth mechanism to account for these factors is shown in Fig. 3.10. The catalyst exists as a series of nano-particles on the support. First, a carbon cap nucleates on each catalyst nano-particle surface, perhaps anchored at its step edges. This cap then grows into a SWNT in layer 1. When layer 1 growth is interrupted, growth restarts by forming a new cap, which then grows into a tube of layer 2. Because the new cap grows from the same catalyst nano-particle, which is solid, it can have the same diameter as the first cap. The interface adhesion between the new cap and the old tube is not so strong, and may be bound by van der Waals' forces. This accounts for the rather weak adhesion across the interface.

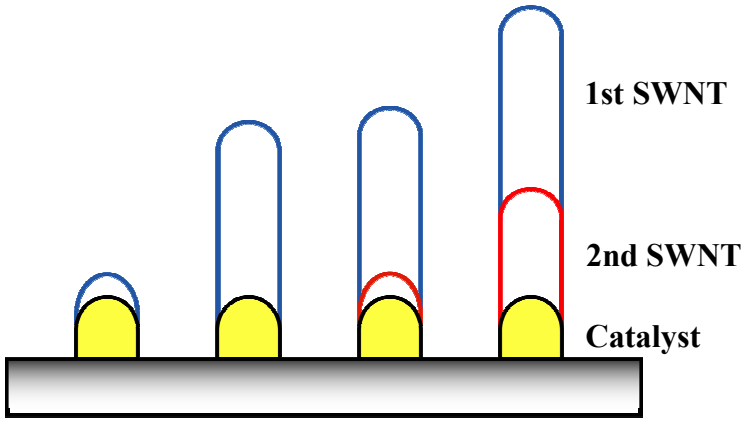

Figure 3.10 Schematic of the growth mechanism of layered SWNTs.

On restarting growth, why do new carbon atoms form a new cap, instead of simply continuing the growth of the previous nanotube? The answer is that cooling the system causes a carbon super-saturation within the catalyst nano-particle. On re-heating, this carbon rapidly emerges from the catalyst and precipitates as a new cap [15-17]. SWNTs can only form when there is a moderate, continuous supply of carbon, not an over-supply.

At an atomic level, a new cap forms if a graphitic cap is forced to form by rapid precipitation of carbon. This breaks the normal C-Fe bonds anchoring the cap to the catalyst surface. If the temperature is not reduced, the C-Fe bonds are retained, and new C atoms can be continuously added to the root of the growing nanotube, without

forming a new cap. The new cap is somewhat analogous to the bamboo structure which can form in MWNTs [18, 19].

To show the importance of the cooling on formation of layer 2, interrupting growth by switching off the plasma, but without cooling was tried. (Note that a plasma is needed for growth in our system under normal conditions, because the source gas is methane). Several CVD runs using many substrates were performed, and no interface was observed for any samples as shown in Fig. 3.11. During the interval, a catalyst remains saturated with carbon but not over-saturated. In this case it is assumed that new carbon atoms of layer 2 precipitate directly on the edge of the existing SWNTs and continuous SWNTs are grown.

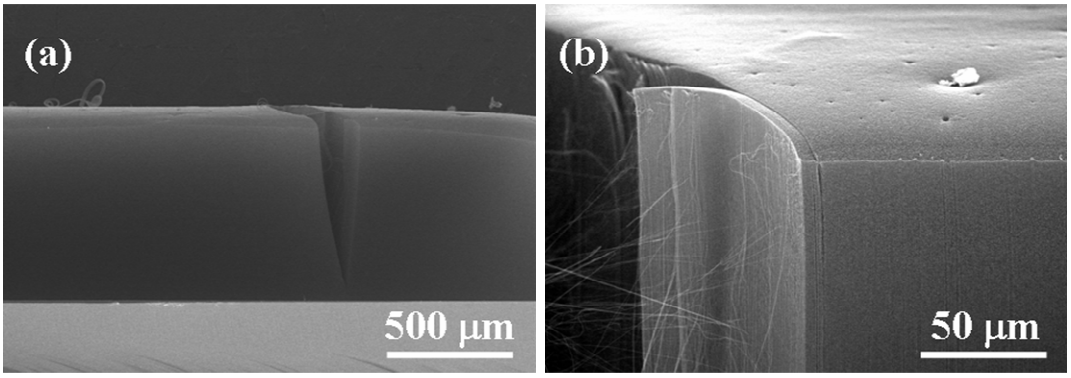

Figure 3.11 Typical cross-sectional SEM images of a SWNT sample grown without cooling after the 1st growth. (a) A sample grown for 5 min in the 1st and 2 h in the 2nd growth. (b) Magnified image near the surface. The length is about 750 μm, indicating that the sample continued to grow for 2 h because, taking into account the growth rate, the SWNT length grown for 5 min should be about 30-50 μm. No interface was observed in the film. Therefore, SWNTs grown without cooling become fully continuous.

The effects of rapid temperature changes on the cluster shape can be considered. For in-situ heating up to 700°C and cooling of a catalyst with an as-grown SWNT, Zhu et. al [11] found that the catalyst shape and crystallinity were retained. Thus, the heating for the second growth stage will not affect the catalyst shape on the condition that the same temperature was used. As a result, the second SWNT has the same diameter as the first one, even though they are not continuous. Repeating cooling, heating, cap formation and SWNT growth should not change the catalyst cluster shape and crystal phase, and SWNTs with the same diameter can be synthesized on one cluster.

SWNTs with different diameters grow at higher temperatures as discussed in Section 3.2.5. When the growth temperature is increased from 600 to ~700°C for layer 2 growth, the diameter distribution of SWNTs shifts to a large diameter, so that SWNTs grow with different diameters. This indicates that diameter and chirality control is possible only at low temperatures, if the shape and steps of the catalyst nano-particles are sufficiently well controlled.

Figure 3.12 summarizes the growth of layered SWNT mats under different conditions. No interfaces were observed if samples were not cooled after the first SWNT growth. Interfaces were formed only if the sample was cooled after the first growth. Although new caps were formed at the tips of the layer 2 SWNTs, SWNTs of both layers grown at the same temperature had same chirality distribution. The two SWNTs are attached by van der Waals attractions, so the layer 1 SWNTs can be easily peeled-off from the layer 2. If the growth temperature for the second growth increased, newly grown SWNTs had larger diameters, and different chiralities, probably due to reshaping of catalyst clusters at the higher temperature.

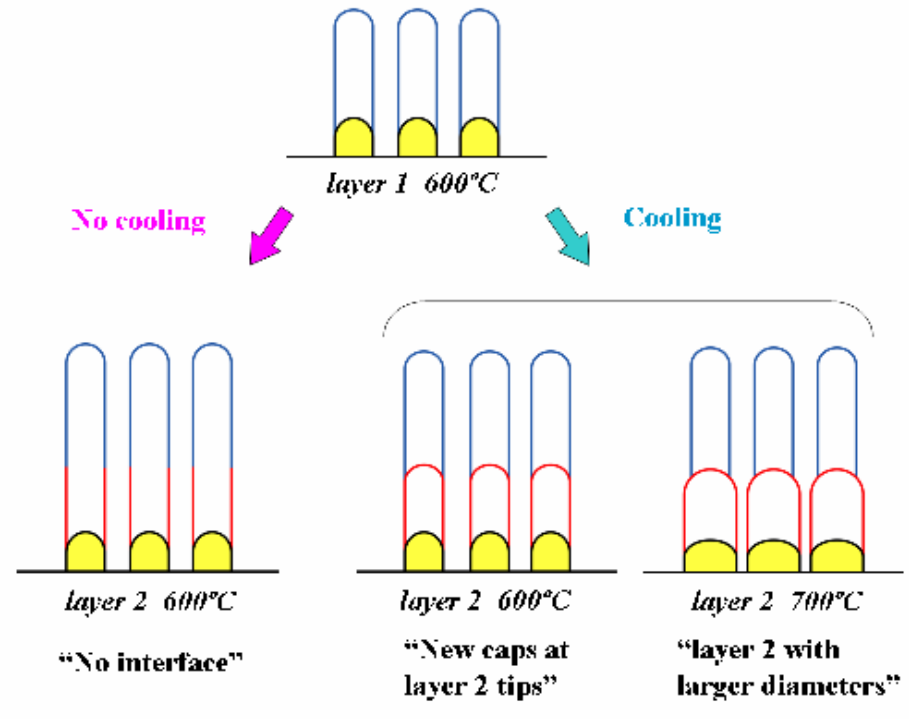

Figure 3.12 Layered growth of SWNT mats under different conditions.

It is interesting to consider the growth mechanism in more detail. How does the layer 2 SWNTs have the same chirality distribution as the layer 1? There are two possibilities as shown in Fig. 3.13. Figure 3.13(a) shows SWNTs with an identical chirality on a catalyst with a specific crystal phase. This is the principle of epitaxial control of nanotube growth [11, 12]. Thus, each particle could create two nanotubes of the same chirality. The catalyst is solid under our conditions, as recently demonstrated by in-situ studies [20, 21]. The nanotubes grow by a vapour-solid-solid (VSS) mechanism. It is known that the cap structure determines the chirality of a SWNT. The cap formation strongly depends on shape and crystallinity of the nanoparticle, probably in particular, a step-edge structure which acts as the cap nucleation site. When two SWNTs grow on the same step-edge of a nanoparticle, they should have the same chirality.

Another possibility is that SWNTs grow independently of the crystal phase of nano-particles as shown in Fig. 3.13(b). In this case, some SWNTs in layer 2 have different chirality from layer 1 and chirality is not continuous across the interface. However, the two layers should have same chirality distribution as their Raman RBM peaks show almost same relative intensities. In this case, it is speculated that the ratio of SWNTs with specific chiralities would be determined by growth environment such as temperature, pressure and feedstock. This occurs because tubes of different chiralities have only a small free energy difference.

The diameter of DWNTs is not easily evaluated as SWNTs because their outer wall diameters (4–5 nm) are below the range of normal RBM peaks. However, considering results of the TEM observations which were similar with SWNTs, it is expected that DWNTs in the layer 1 and 2 have same diameter distribution.

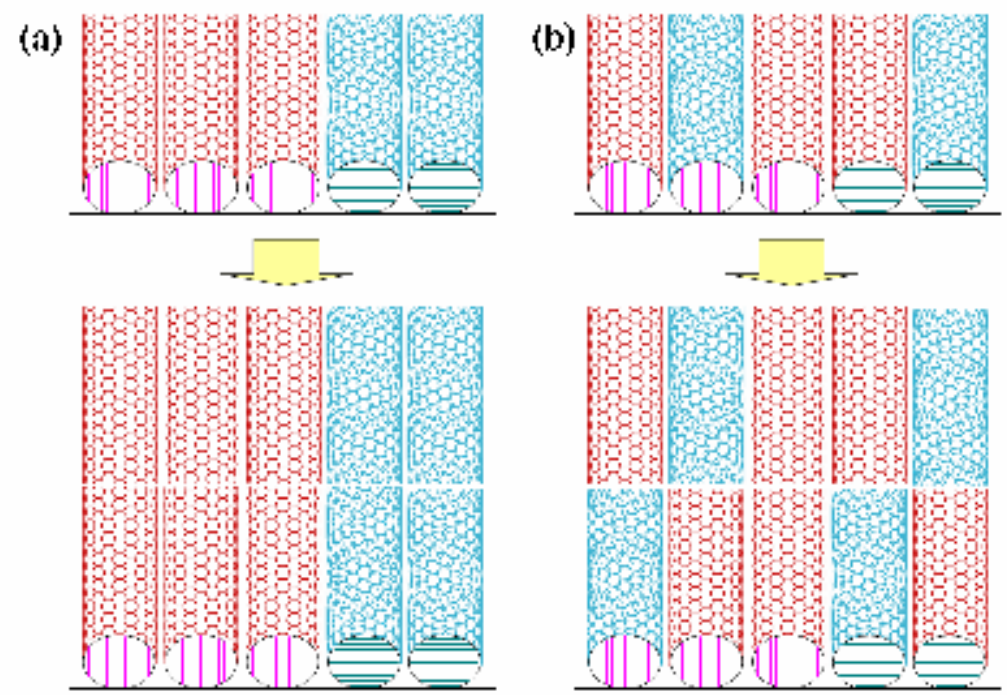

Figure 3.13 Possible combinations of nanotubes with different chiralities, but same diameter, and catalysts with different crystal phases in two layers. Catalysts with vertical or horizontal stripes have different crystal phases, but have same diameter. (a) Epitaxial growth of SWNTs. (b) SWNT growth independent with a catalyst crystal phase, but the ratio of specific chiralities is determined by the growth environment.

3.3.4. Surface structure of layer 2 SWNTs

The top surface of the 2nd layer has an interesting structure. Figure 3.14(a, b) show surfaces of the 1st layer before cutting and the 2nd obtained after cutting. It is well known that the top surface of CNTs with small diameters such as SWNTs and DWNTs are curved due to low density of CNTs in the initial growth stage [22]. On the other hand, as shown in Fig. 3.14(b), the top surface of the 2nd SWNTs shows a sharper structure, resulting form almost uniform length of the 2nd SWNTs. Larger space was observed between each structure. It is expected that this structure is suitable for fabrication of field emission devices because an applied electric field is concentrated at sharp edges of needle-shaped structures [23, 24].

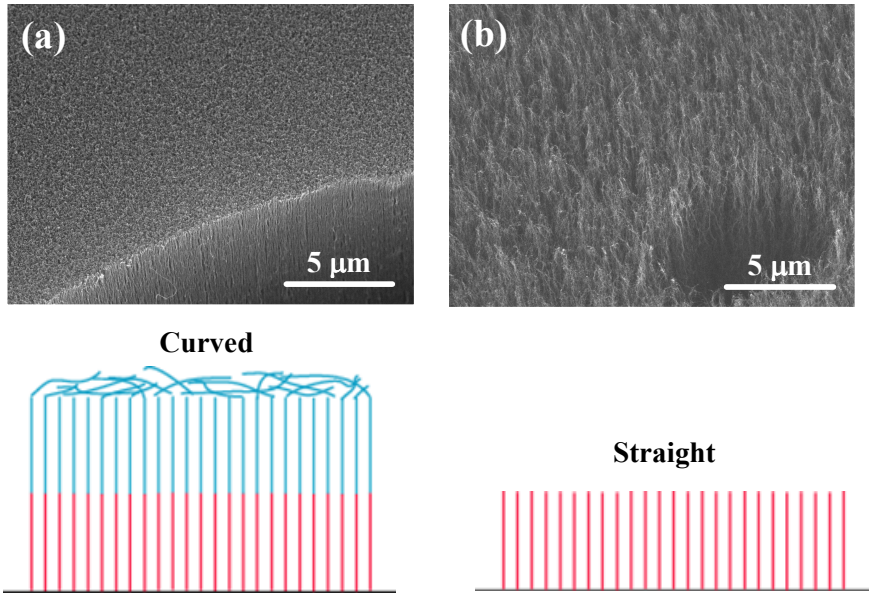

Figure 3.14 SEM images and schematic of the top surface of (a) the 1st SWNTs and (b) the 2nd SWNTs.

3.3.5. Success rate of cutting

The adhesion force between the 1st and 2nd CNTs is weak, but cutting over the entire substrate must be performed with circumspection because the adhesion force between the 2nd CNTs and catalyst particles is also weak. Moreover, once part of the 2nd layer is peeled off with the 1st layer, neighboring bundles, which interact with the peeled CNTs through van der Waals attraction, are also removed easily from the substrate. Thus, cutting must be performed slowly and in various directions to prevent significant detachment of the 2nd CNTs. Figure 3.15(a) shows a sample after cutting the 1st layer slowly and in two directions, denoted by green arrows. Successfully cut regions are light brown in color, and white parts observed at substrate edges indicate failure regions, where the 2nd SWNTs were also removed. The 2nd SWNTs were left on the substrate at most area about 95%. A dark brown linear region was formed at the boundary between the two cutting directions. By SEM observation at the boundary, SWNTs were formed to lean in the cutting direction and to be overlapped, resulting in the dark color. When cutting was performed from one direction at one time, the extent of failed regions increased markedly, as shown in Fig. 3.15(b). The extent of the successfully cut region decreased to 60%. Cutting in one direction stresses the sample in the same direction and the 2nd SWNTs would be more likely to be peeled off.

Although other methods of removing the 1st layer were tried, such as the use of Scotch tape and ultrasonication, only ultrasonication in alcohol at a very low power could remove part of the 1st layer. However, there was no reproducibility for ultrasonication and the 2nd layer was also removed for almost all substrates. The relationship between the SWNT length and the frequency of ultrasonication probably must be adjusted [25]. Not surprisingly, the 2nd SWNTs of the sample successfully cut by ultrasonication fell and formed a random network, losing vertical alignment. The optical-microscope and SEM images of a sample cut by the ultrasonication method are shown in Fig. 3.16.

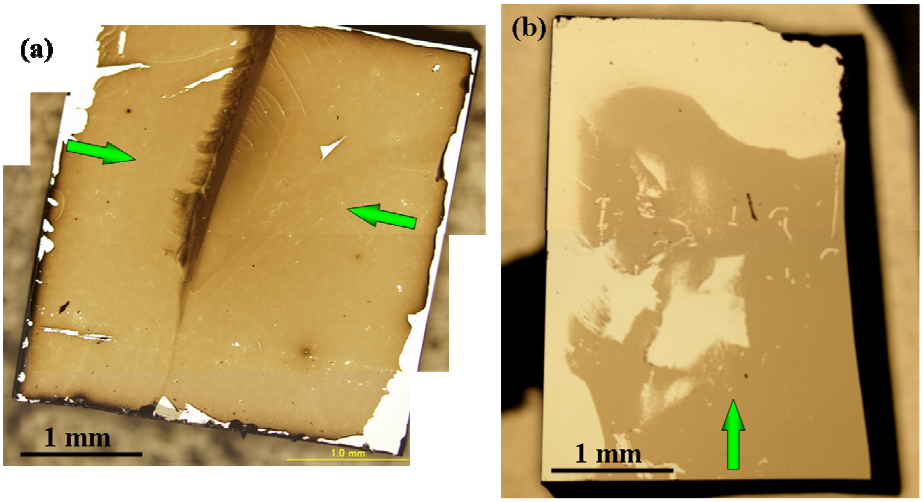

Figure 3.15 Optical microscope images after cutting the 1st layer. (a) Cutting was performed from the two directions very slowly. Almost all the 2nd SWNTs remained on the substrate. (b) Cutting was performed from one direction at one time. Half of the 2nd SWNTs were removed with the 1st SWNTs. The green arrows denote cutting directions.

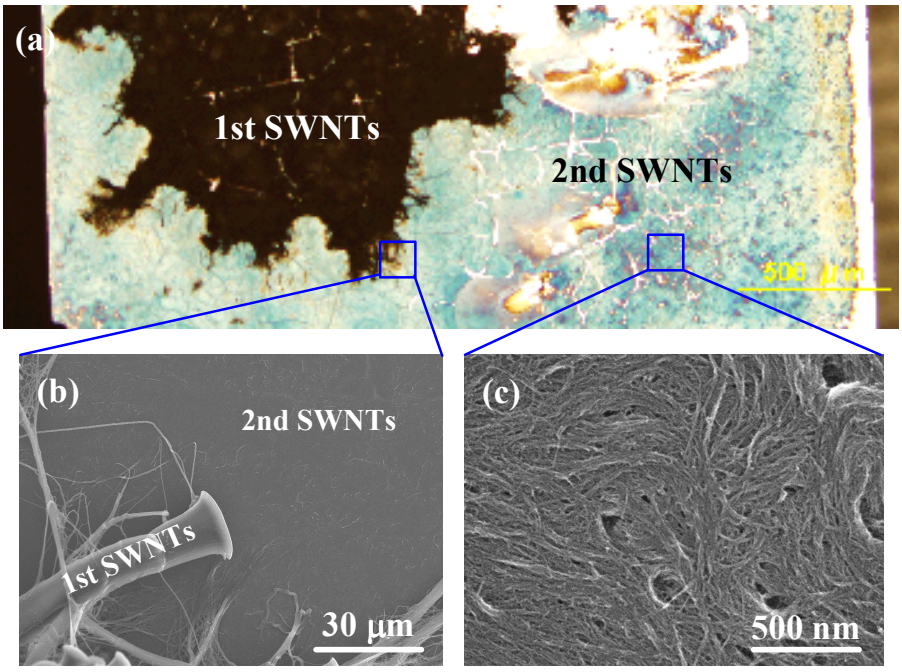

Figure 3.16 Sample cut by ultrasonication. (a) Optical-microscope image. The 1st SWNTs remain in black regions. Green parts show successfully cut regions. (b) SEM image of boundary between successful and failed regions. (c) Magnified SEM image of the 2nd SWNTs. The SWNTs of the 2nd layer fell and formed a random network.

3.3.6. Fabrication of short SWNT arrays

By decreasing the growth rate of SWNTs, 200–300-nm-long SWNTs can be obtained in the 2nd layer. Cutting the 1st layer resulted in the fabrication of short SWNT arrays, which have never been obtained from as-grown SWNTs because, as described in Section 3.3.3, the top surface of as-grown SWNTs is not straight and the curved length is often close to 1 μm. Short SWNTs (< 1 μm) are promising materials for one-dimensional building blocks and electronic-device applications, such as nanotweezers [26, 27] and FETs, which require precise placement of SWNTs in a well-defined electrode gap. Although previous studies have shown the preparation of short SWNTs (< 1 μm) using strong acids [28-31], gases [32, 33], or plasma etching [34], these methods often cause undesirable defects in SWNTs and a large weight loss of the used SWNTs, and furthermore, procedures using aggressive chemicals are very dangerous and unfavorable in industry. Moreover, short SWNTs obtained by such methods cannot be used for direct fabrication of devices because they are not aligned on a substrate. This section demonstrates the fabrication of short aligned SWNTs by the cutting of layered structures.

The growth rate resulting from the normal CVD conditions (CH_4 concentration: 10%) is too high obtaining short SWNTs. The growth rate is influenced by the input power, the chamber pressure, and the source gas concentration. In the remote-plasma CVD used in this study, the growth rate more strongly depends on the amount of CH_4 in the chamber than on the microwave power, and low chamber pressures below 10 Torr cause the microwave plasma to become unstable. Thus, the source gas concentration was adjusted to decrease the growth rate: H_2 / CH_4 = 198 sccm / 2 sccm. The CH_4 concentration was ~1%, one-tenth that of the 1st layer. The growth time of the 2nd layer was 60 s. The other CVD parameters were the same as in the growth of the 1st layer.

Figure 3.17(a, b) show short SWNTs 320 nm and 280 nm long formed below thick 1st layers, respectively. The 1st SWNTs in Fig. 3.17(a) are out of sight due to partial peel-off. The 1st layers above the short SWNTs could be removed by the razor blade method, and aligned short SWNTs on substrates were obtained, as shown in Fig. 3.17(c, d) although short SWNTs in Fig. 3.17(d) leaned in the cutting direction, from right to left in the figure. The SEM image, taken at a tilted angle, in Fig. 3.17(e) shows branches from each fiber structure. Therefore, it is clear that short SWNTs also form bundles. Figure 3.17(f) shows Raman spectrum of short SWNTs, measured using a 633 nm laser after cutting the 1st layer. A sharp G band and RBM peaks, a fingerprint of SWNTs, can be clearly observed, indicating that the low CH_4 concentration did not affect the CNT

quality. Short SWNT arrays can be used as a base substrate for the fabrication of CNT-AFM probes and nanotweezers. In addition, the fabrication of via-interconnects and vertical FETs without chemical mechanical polishing would be possible when the cutting is applied to SWNTs grown from dielectric holes. Although this section demonstrated short SWNTs with 300 nm length, it is expected that, in principle, much shorter SWNTs, even less than 100 nm, may be produced by the cutting method if more precise control of the growth rate of SWNTs can be achieved.

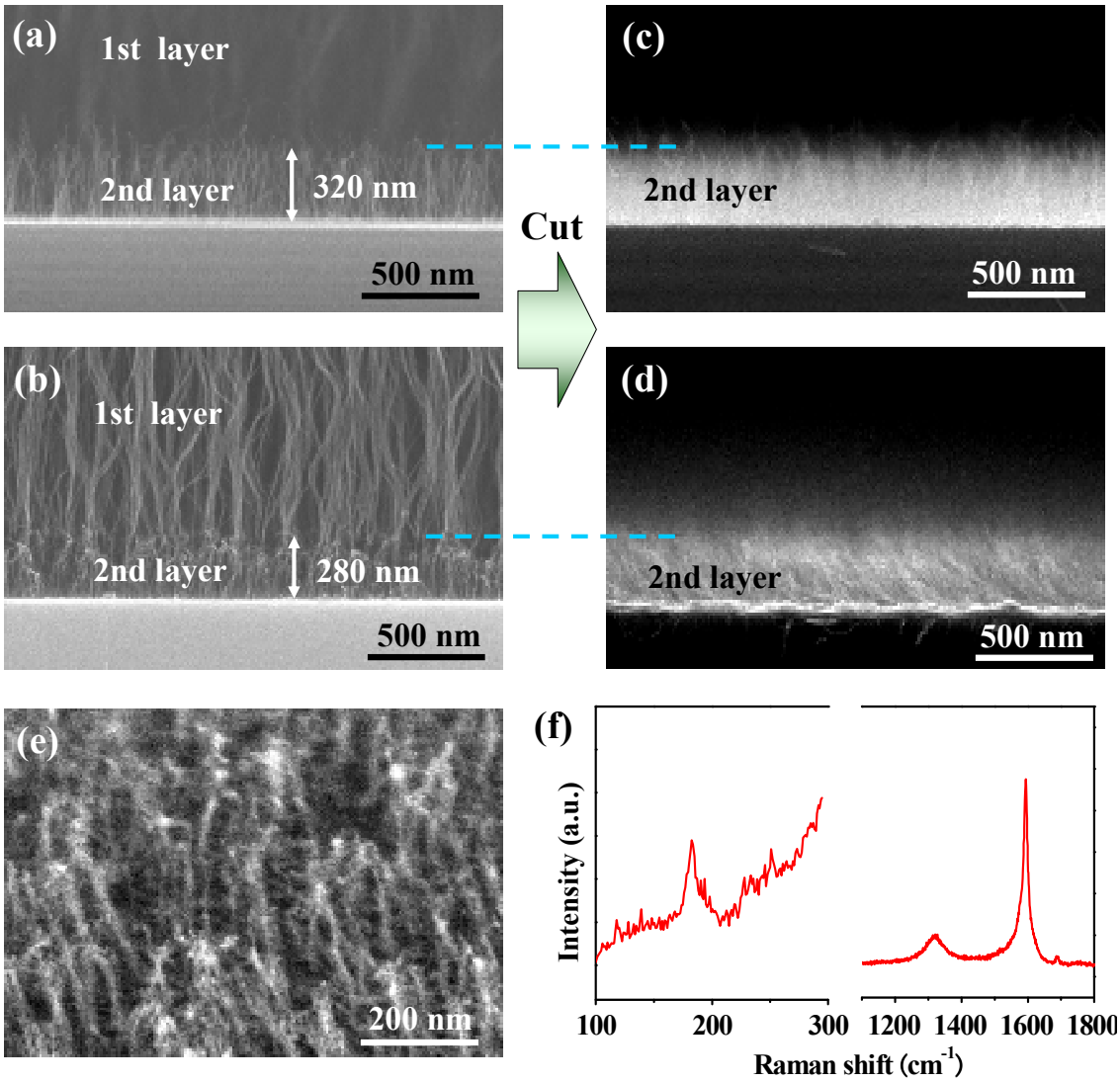

Figure 3.17 Fabrication of short SWNT arrays. SEM images (a, b) before and (c, d) after cutting of the 1st SWNTs. After cutting, SWNTs with short lengths of about 300 nm were aligned on the substrates. (e) Tilted view of short vertically aligned SWNTs. (f) Raman spectrumof short SWNTs.

3.4. Summary

To clarify the growth mode of the dense and vertically aligned SWNTs, a new method was proposed, which can be used to determine the growth mode of vertically aligned SWNTs without requiring complicated and time-consuming experiments. Therefore, this method can overcome the quantitative limitation of TEM observation. The root growth mode of a large quantity of vertically aligned SWNTs was determined successfully using a horizontal line between the two SWNT layers as a marker. The mechanism of layered SWNTs was investigated by cutting with a razor blade and found that new caps were formed when growth restarted. Raman spectra revealed that the two layers grown at the same temperature on the set of catalyst particles have almost the same chirality distribution. Re-growth at a higher temperature caused different diameters of layer 2 SWNTs. The diameter and chirality have been preserved in the layer 2 growth even after the first process has been terminated when the physical conditions were kept as same as before. Two possible modes are proposed. The first one is simply explained by epitaxial re-growth of SWNTs from an oriented and immobile catalyst particle. The second one is that physical conditions determine the distribution of chirality of SWNTs according to the subtle difference in free energy of chiralities. In this case, irrespective of orientation of catalyst particle, similar chirality distribution can be reproduced if the size of particles is fixed.

References

[1] V. I. Merkulov, A. V. Melechko, M. A. Guillorn, D. H. Lowndes, M. L. Simpson, Appl.Phys.Lett. 79, 2970, (2001).

[2] X. Cheng, R. Wang, J. Xu, D. Yu, Micron 35, 455, (2004).

[3] C. H. Hsu, C. H. Lin, H. J. Lai, C.T. Kuo, Thin Solid Films 471, 140, (2005).

[4] S. Huang, Chem.Phys.Lett 374, 157, (2003).

[5] I. K. Song, Y. S. Cho, G. S. Choi, D. J. Park, D. J. Kim, Diam. Relat. Mater. 13, 1210, (2004).

[6] L. Alvarez, A. Righi, T. Guillard, S. Rols, E. Anglaret, D. Laplaze, J. L. Sauvajol, Chem. Phys. Lett. 316, 186, (2000).

[7] S. Maruyama, R. Kojima, Y. Miyauchi, S. Chiashi, M. Kohno, Chem. Phys. Lett. 10, 229, (2002).

[8] Y. Wang, M. J. Kim, H. Shan, C. Kittrell, H. Fan, L. M. Ericson, W. F. Hwang, S. Arepalli, R. H. Hauge, R. E. Smalley, Nano Lett. 5, 997, (2005).

[9] R. E. Smalley, Y. Li, V. C. Moore, K. Price, R. Colorado, H. K. Schmidt, R. H. Hauge, A. R. Barron, J. M. Tour, J. Am. Chem. Soc. 128, 15824, (2006).

[10] G. Zhong, T. Iwasaki, J. Robertson, H. Kawarada, J. Phys. Chem. B 111, 1907, (2007).

[11] H. Zhu, K. Suenaga, A. Hashimoto, K. Urita, K. Hata, S. Iijima, Small 1, 1180, (2005).

[12] S. Reich, L. Li, J. Robertson, Chem. Phys. Lett. 421, 469, (2006).

[13] H. Telg, J. Maultzsch, S. Reich, F. Hennrich, C. Thomsen, Phys. Rev. Lett. 93, 177401, (2004).

[14] J. Maultzsch, H. Telg, S. Reich, C. Thomsen, Phys. Rev. B 72, 205438, (2005).

[15] F. Ding, K. Bolton, A. Rosen, J. Phys. Chem. B 108, 17369, (2004).

[16] H. Amara, C. Bichara, F. Ducastelle, Phys. Rev. B, 73, 113404, (2006).

[17] J. Y. Raty, F. Gygi, G. Galli, Phys. Rev. Lett. 95, 096103, (2005).

[18] V. V. Kovalevski, A. N. Safronov, Carbon 36, 963 (1998).

[19] X. Wang, W. Hu, Y. Liu, C. Long, Y. Xu, S. Zhou, D. Zhu, L. Dai, Carbon 39, 1533 (2001).

[20] S. Hofmann, R. Sharma, C. Ducati, G. Du, C. Mattevi, C. Cepek, M. Cantro, S. Pisana, A. Parvez, F. Cervantes-Sodi, A. C. Ferrari, A. R. Dunin-Borkowski, S. Lizzit, L. Petaccia, A. Goldini, J. Robertson, Nano. Lett. 7, 602, (2007).

[21] S. Helveg, C. Lopez-Cartes, J. Sehested, P. L. Hansen, B. S. Clausen, J. R. Rostrop-Nielsen, F. Abild-Pedersen, J. K. Norskov, Nature 427, 426, (2004).

[22] L. Zhang, Y. Tan, D. E. Resasco, Chem. Phys. Lett. 422, 198, (2006).

[23] L. Nilsson, O. Groening, C. Emmenegger, O. Kuettel, E. Schaller, L. Schiapbach, H. Kind, J-M. Bonard, K. Kern, Appl. Phys. Lett. 76, 2071, (2000).

[24] J. S. Suh, J. Seok, J. S. Lee, Appl. Phys. Lett. 80, 2392, (2002).

[25] S. H. Jeong, O. J. Lee, K. H. Lee, Chem. Mater. 14, 1859, (2002).

[26] P. Kim. C. M. Lieber, Science 286, 2148, (1999).

[27] S. Akita, Y. Nakayama, S. Mizooka, Y. Takano, T. Okawa, Y. Miyake, S. Yamanaka, M. Tsuji, T. Nosaka, Appl. Phys. Lett. 79, 1691, (2001).

[28] Y. Wang, L. Gao, J. Sun, Y. Liu, S. Zheng, H. Kajiura, Y. Li, K. Noda, Chem. Phys. Lett. 432, 205, (2006).

[29] X. Nan, Z. Gu, Z. J. Liu, Colloid Interface Sci. 245, 311, (2002).

[30] K. J. Ziegler, Z. Gu, H. Peng, E. L. Flor, ER. E. Hauge, R. E. Smalley, J. Am. Chem. Soc. 127, 1541, (2005).

[31] Z. Chen, K. Kobashi, U. Rauwald, R. Booker, H. Fan, W. F. Hwang, J. M. Tour, J. Am. Chem. Soc. 128, 10568, (2006).

[32] Z. Chen, K. J. Ziegler, J. Shaver, R. H. Hauge, R. E. Smalley, J. Phys. Chem. B 110, 11624, (2006).

[33] Z. Gu, H. Peng, R. H. Hauge, R. E. Smalley, J. L. Margrave, Nano. Lett. 2, 1009, (2002).

[34] S. R. Lustig, E. D. Boyes, R. H. French, T. D. Gierke, M. A. Harmer, P. B. Hietpas, A. Jagota, R. S. McLean, G. P. Mitchell, G. B. Onoa, K. D. Sams, Nano. Lett. 3, 1007, (2003).

Chapter 4

Highly Selective Growth of Vertically Aligned DWNTs by a Controlled Heating Method and their EDLC Properties

Parts of this chapter are discussed based on the following paper:

- T. Iwasaki, T. Maki, D. Yokoyama, H. Kumagai, Y. Hashimoto, T. Asari, and H. Kawarada, phys. stat. sol. (RRL) 2, 53 (2008).

4.1. Introduction

Capacitors are used in the wide fields ranging from electrical and electronic products to automobile, aircraft, space, medicine, and power supply circuits [1]. Electric double-layer capacitor (EDLC) is a new energy storage device having characteristics between those of a battery and a simple aluminum capacitor. EDLCs have superior rapid charge and discharge abilities, a wider endurance temperature range than batteries, and a semi-permanent charge/discharge cycle life.

Figure 4.1 shows the operating principle of EDLC. EDLC consists of two electrodes which are immersed in an electrolyte with a separator between them. The electrode consists of a current collector in contact with the active material (CNTs). In general, positive and negative electrical charges are arrayed in counter position with an extremely short distance at the contact interface between the difference phases (e.g. solid electrode and liquid). This charge distribution layer is called the electric double-layer. Therefore, the energy storage arises from the separation of electronic and ionic charges at the interface between high surface area electrode material and the electrolyte solution. The specific capacitance, C, accumulated in the electric double layer formed at the interface between the polarizable electrodes and electrolyte solution is defined by

$$C = \frac{1}{m}\int \frac{\varepsilon}{4\pi\sigma} dS \quad \text{(F/g)} \qquad (4.1)$$

where ε is the dielectric constant of the electrolyte, σ the distance from the electrode interface to the center of the ion, S the surface area of the electrode interface, m the mass of the active material [1]. The electrical energy density, W, stored in the polarized dielectric material is given by

$$W = \frac{1}{2} CV^2 \quad \text{(Wh/kg)} \qquad (4.2)$$

where V is the working voltage. Generally, higher capacitances are obtained in aqueous electrolytes than in nonaqueous electrolytes because the number of ions absorbed on activated materials can be larger for small ions. However, an organic solution is preferable for the fabrication of EDLCs with high energy densities because its working voltage (around 2.5 V) is higher than that of an aqueous solution (around 1.0 V). In this study, an organic solution of tetraethylammonium tetrafluoroborate ($TEABF_4$) in propylene carbonate (PC) was used for measurements of EDLC properties.

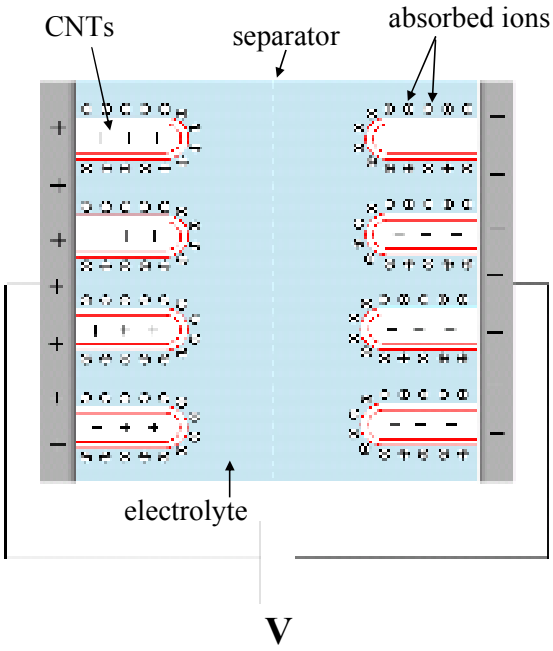

Figure 4.1 Schematic of the operating principle of EDLC.

Activated carbon (AC) is currently used for an active material. Although it has a high specific capacitance of ~200 F/g at relatively low discharge current densities [2], the capacitance decreased rapidly with an increase in discharge current density due to large ionic and electronic resistances. In contrast, vertically aligned CNTs show no distinct decrease in the capacitance because they have the easily accessible surface and high electrical conductivity [2]. Moreover, CNTs possess large surface area and structural stability. Therefore, CNTs have potential for use in EDLCs for energy storage. Recently, the EDLC characteristics of CNTs have been investigated. The EDLC properties of MWNTs and SWNTs in organic electrolytes have been demonstrated and their various specific capacitances were reported; 40–60 F/g for vertically aligned MWNTs [2], 45 F/g for HiPco SWNT bucky paper [3], and 80 F/g for vertically aligned SWNTs [4]. For vertically aligned SWNTs, a high energy density of 69.4 Wh/kg was also shown [4]. Although SWNTs have the smallest diameters in the CNT family, 2/3 of these nanotubes show semiconducting behavior [5]. Thus, metallic double-walled carbon nanotubes (DWNTs) with diameters of 3–5 nm are better candidates for EDLCs. However, there have been no previous reports of the EDLC characteristics of selectively grown DWNTs. DWNTs have received a lot of attention recently because they are likely to possess characteristics superior to those of SWNTs and MWNTs, in terms of, for example, mechanical properties, thermal conductivity, and structural stability [6].

DWNTs with more than 90% selectivity were prepared by chemical vapor deposition (CVD) using a purification technique [6] and an $FeSi_2$ catalyst [7]. Here, the word "selectivity" means a percentage of CNTs with the same wall number in the sample. However, resultant DWNTs were not aligned on a substrate. For EDLC applications, vertically aligned DWNTs are more interesting because ions can diffuse rapidly in vertically aligned CNTs compared with those of random-network CNTs and activated carbons. Although previous studies have shown the dominant growth of vertically aligned DWNTs with 80–88% selectivity by adjusting catalyst thicknesses [8–10], the EDLC characteristics of DWNT arrays have not been shown. In this chapter, vertically aligned DWNTs with a selectivity of 90% were synthesized, which is the highest value for vertically aligned DWNTs, by a controlled heating method without any purification; then their EDLC characteristics were evaluated and a specific capacitance of 83 F/g was obtained, which is one of the largest values for vertically aligned CNTs in a nonaqueous solution.

4.2. Selective growth of vertically aligned DWNTs

4.2.1. Morphology of vertically aligned DWNTs

For selective growth of DWNTs, a sandwich-like structure of 0.50 nm Al/0.45 nm Fe/5 nm Al was used as a catalyst. The films were deposited on Si substrates using a high-frequency magnetron sputtering system. The remote-plasma CVD system was used for the growth of DWNTs. To form catalyst particles appropriate for the DWNT growth, the substrate with the catalyst films was preheated at a temperature of 640°C for 5 min using a high-frequency induction heater, which is higher than the temperature of 600°C appropriate for SWNT growth shown in Chapter 2. Then, the microwave plasma ball was turned on at a power of 60 W in a gas mixture of 45-sccm H_2 and 5-sccm CH_4 at a pressure of 20 Torr to synthesize DWNTs for 30 min–3 h. Although the growth temperature was increased to 650°C by plasma, this temperature is lower than that in previous studies of DWNT growth [6–10]. CNTs directly grown on Si substrates were observed by FE-SEM. To identify the components of the CNT samples, TEM observations were performed.

Figures 4.2(a-c) show SEM images of selectively grown vertically aligned DWNTs with a uniform length of 280 μm on a Si substrate. A volume density of about 46 mg/cm^3 was obtained by measuring the weight, which is three times higher than that of a previously reported DWNT array [9]. Typical TEM images of DWNTs are shown in Fig. 4.2(d, e). By examining many TEM images, the percentage of DWNTs in the sample was found to be 90%, which is the highest value for vertically aligned DWNTs formed on substrates. The outer and inner diameters of DWNTs ranged from 3.37 to 4.87 nm (mean: 3.95 nm) and 2.47 to 4.00 nm (mean: 3.09 nm), respectively. The average interlayer spacing was about 0.43 nm.

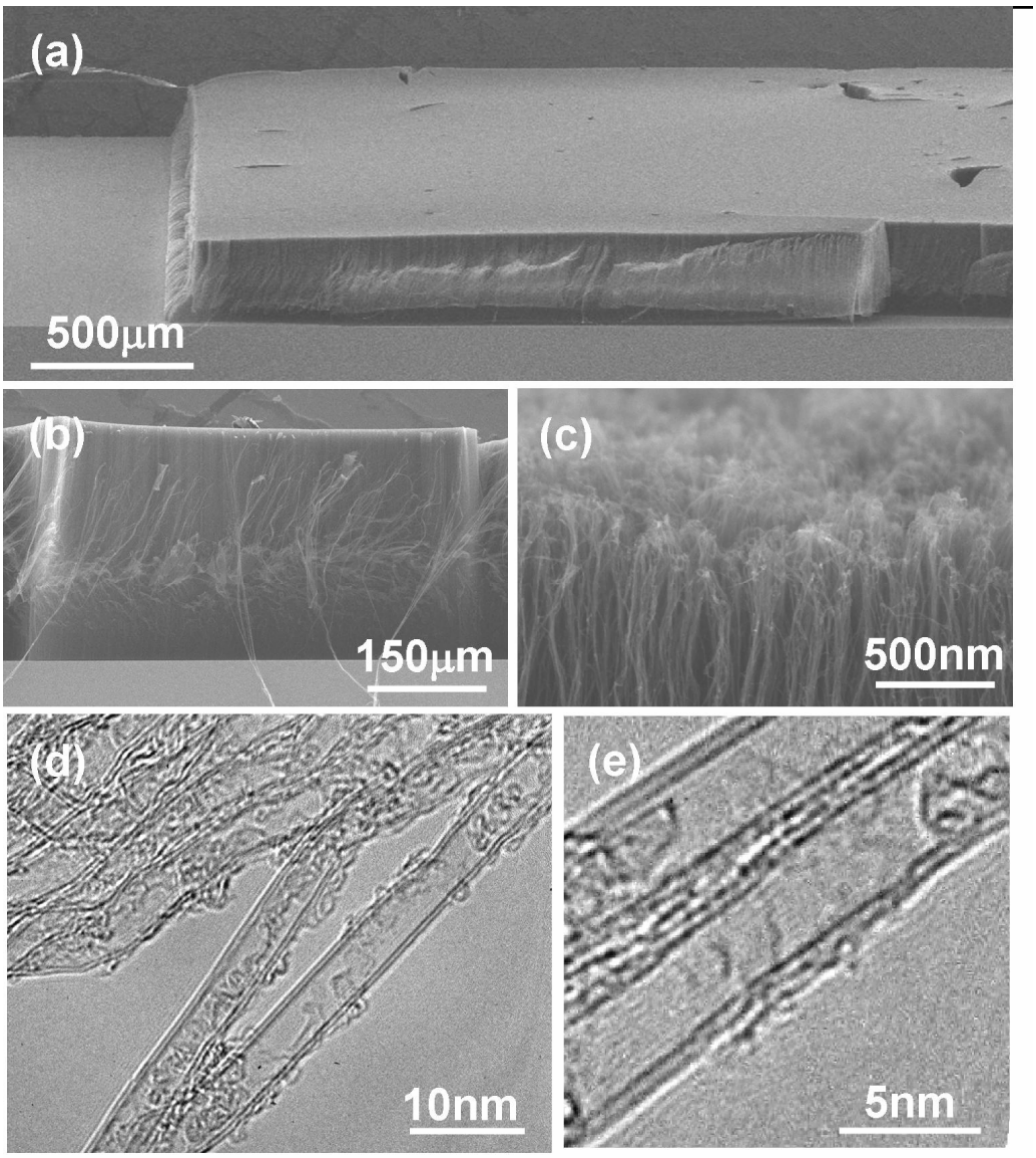

Figure 4.2 (a-c) SEM images of vertically aligned DWNTs on a Si substrate. (d, e) TEM images of selectively grown DWNTs.

4.2.2. Controlled heating method

The selectivity of 90% is the highest in vertically aligned DWNTs. Such a high selectivity was achieved by a controlled heating method during catalyst particle formation. To understand the effects of the preheating temperature, the wall number distributions of CNTs synthesized on particles formed at different preheating temperatures were investigated. The 5-min preheating temperature was controlled as follows: first, the temperature was raised to the target value for 2 min, and this temperature was maintained for the remaining time, 3 min. The temperature was measured with a pyrometer, calibrated using a thermocouple. Figure 4.3 shows wall number distributions and TEM images of CNTs grown under preheating temperatures of 600°C, 620°C, and 640°C. The wall number in 255 tubes was counted and the distributions were obtained. Although the difference in annealing temperature was not large, it was found that the percentage of DWNTs increased as the preheating temperature increased. A CNT array grown on catalysts formed at 640°C consists of 90% DWNTs. A few SWNTs and triple-walled CNTs were observed, but CNTs with larger wall numbers were not found in the sample. At 600°C, almost all CNTs were single-walled and there were few DWNTs. The number of DWNTs increased and the percentages of SWNTs and DWNTs became close at 620°C. Here, it was confirmed that the wall number of CNTs can be controlled by the preheating temperature during catalyst particle formation.

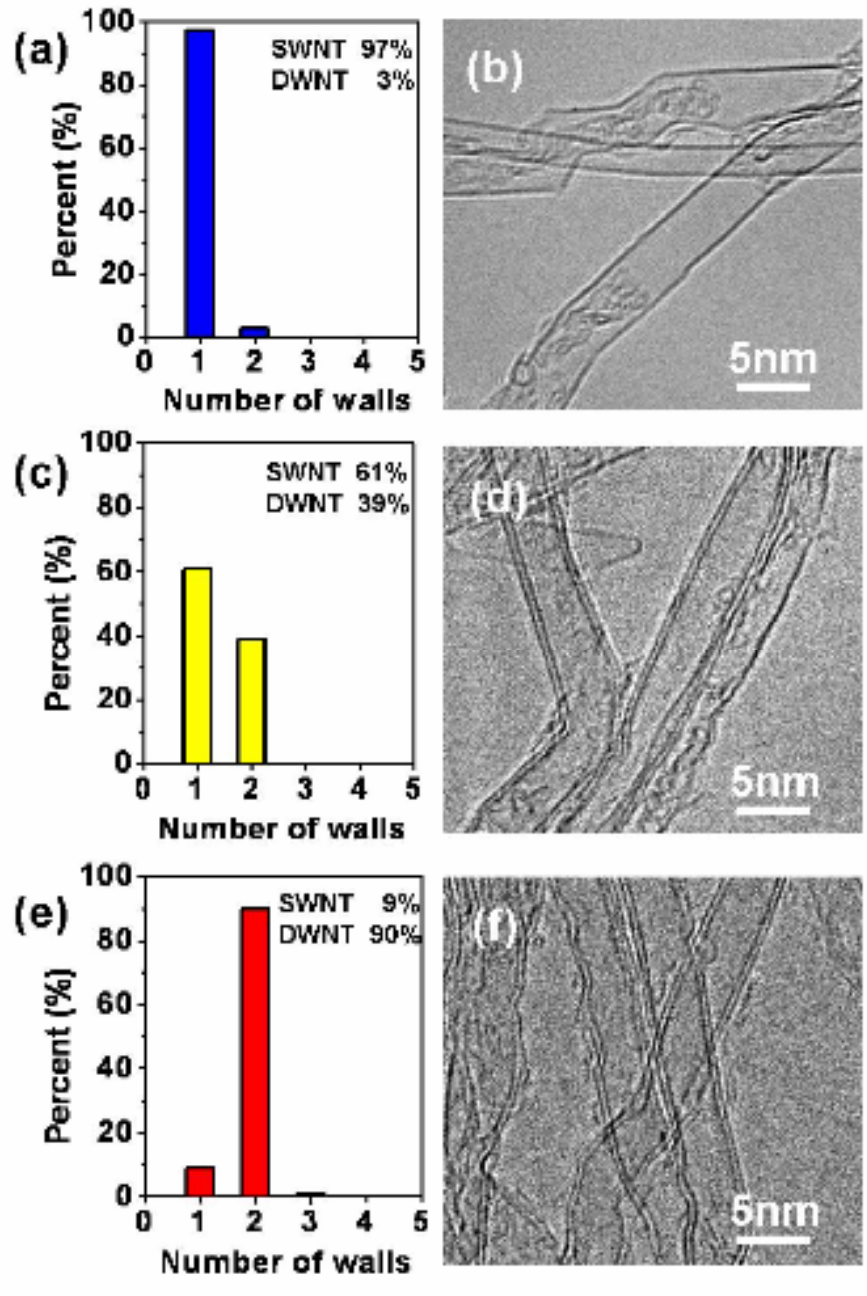

Figure 4.3 TEM images and wall number distributions of CNTs grown on catalyst particles formed at different preheating temperatures. (a, b) 600°C, (c, d) 620°C, and (e, f) 640°C.

4.2.3. Examination of catalyst particle size

To examine the catalyst particle size after preheating at different temperatures, catalyst particles were observed, because controlling the size of catalytic particles is important for selective growth of CNTs. The wall number of CNTs strongly depends on the size of catalyst particles. For growth of vertically aligned SWNTs by remote-plasma CVD, the substrate was annealed at 600°C to produce small particles [11-13]. The mobility of atoms on a substrate increases exponentially with temperature [14], indicating that high-temperature annealing results in the fabrication of larger nanoparticles. SEM images and diameter distributions of catalyst particles after annealing at 600°C and 640°C are shown in Fig. 4.4. The mean diameters of the catalyst particles were 4.1 nm for 600°C annealing and 5.3 nm for 640°C annealing, indicating that the higher temperature led to the formation of larger particles as expected. The mean diameters of CNTs grown at preheating temperatures of 600°C and 640°C were 3.08 nm and 3.97 nm, respectively. The difference of about 0.9 nm is in agreement with the particle size difference. Therefore, the approximately 1 nm larger particles have the optimal size for DWNT growth.

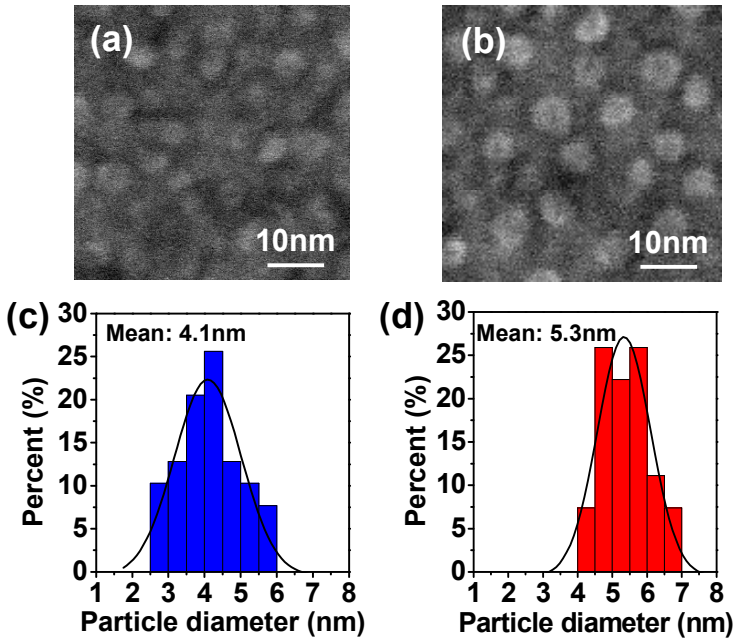

Figure 4.4 SEM images of catalyst particles annealed at (a) 600°C and (b) 640°C, and histograms of the diameters for (c) 600°C and (d) 640°C. The solid lines show Gaussian fitting curves of the histograms.

4.3. EDLC properties of vertically aligned DWNTs

4.3.1. Fabrication of CNT electrodes and conditions of EDLC measurements

The EDLC characteristics of electrodes based on as-grown vertically aligned DWNTs were investigated by cyclic voltammetry and chronopotentiometry. Figure 4.5 shows fabrication of an EDLC electrode and the measurement system. The measurements were performed using a three-electrode cell with the as-grown vertically aligned DWNTs as a working electrode, activated carbon as a counter electrode, and Ag/Ag^{+} as a reference electrode. A 0.7 M solution of $TEABF_4$ in PC was used to evaluate vertically aligned DWNTs. Note that under our CVD and substrate conditions, CNTs grow *via* the root growth mode, in which the catalyst particles are left on the substrate surface during the CVD process and the tips of CNTs are capped as discussed in Section 3.2 [13]. Thus, electric double layers were formed only on exterior walls of graphite sheets. EDLC electrodes with as-grown vertically aligned DWNTs were fabricated on p-type Si substrates. A p-type Si substrate was coated with a catalyst of 7.5×5.5 mm^2 area by sputtering with a mask. Then, a DWNT array was synthesized by remote-plasma CVD. After drying in vacuum, the sample was immersed in an electrolyte for EDLC measurements.

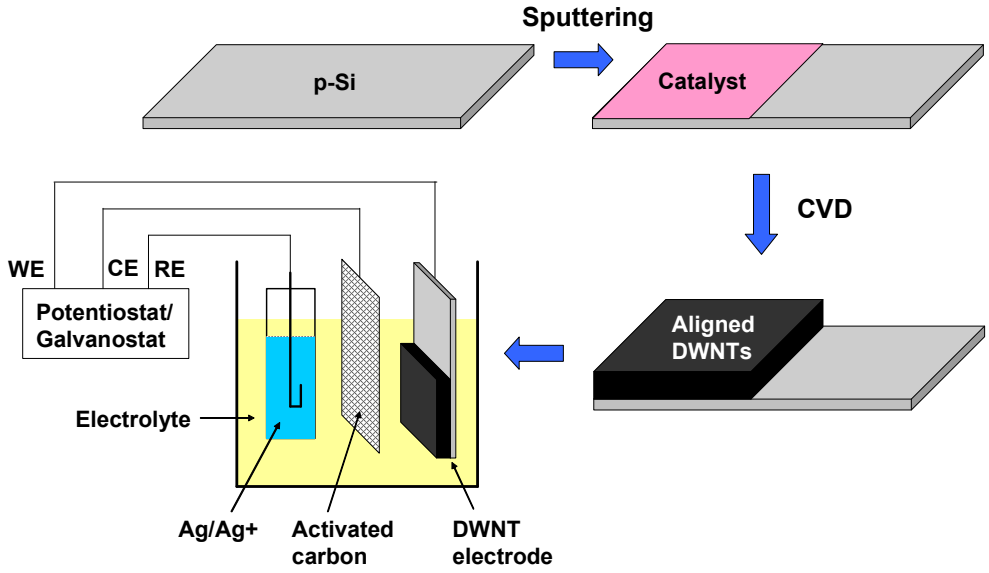

Figure 4.5 Illustration of the preparation process for the CNT electrode, and the measurement system.

To investigate the effects of the wall number distribution of CNTs on the EDLC characteristics, CNTs were also synthesized on thicker Fe catalysts of 0.75 nm and 1.50 nm thickness. The thicker Fe films resulted in larger wall numbers and broad distributions as shown in Fig. 4.6. The dominant components were double- and triple-walled CNTs (mean outer diameter: 4.23 nm) from the 0.75-nm Fe film, and triple- and four-walled CNTs (mean outer diameter: 5.44 nm) from the 1.50 nm Fe film.

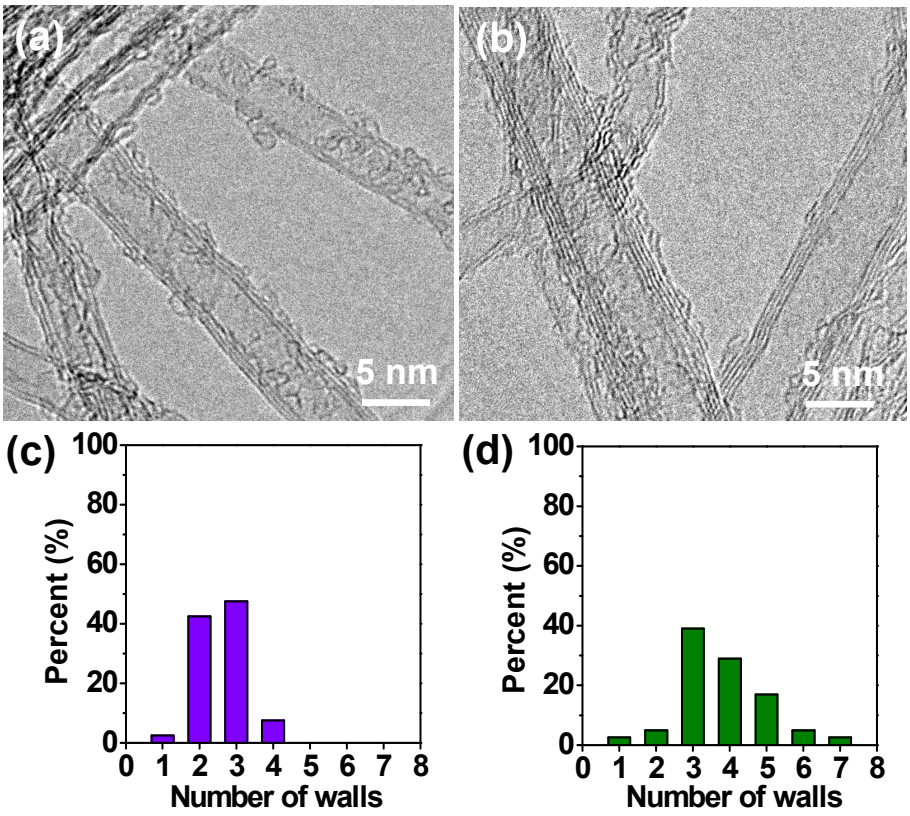

Figure 4.6 TEM images and wall number distributions of CNTs grown on different Fe thickness; (a, c) 0.75 nm and (b, d) 1.50 nm.

4.3.2. EDLC properties of vertically aligned DWNTs

Cyclic voltammograms of as-grown vertically aligned CNTs at a scan rate of 28 mV/s are shown in Fig. 4.7(a). The measured current data were normalized to the mass of CNTs on the substrates. Higher currents were obtained from the sample containing 90% DWNTs than from the other two samples. Figure 4.7(b) shows the specific capacitances of the CNT samples estimated from charge-discharge curves measured by chronopotentiometry, as a function of the mean wall number of CNTs. The DWNT sample had the largest specific capacitance of 83 F/g. For fabrication of high-performance EDLCs, it is essential to have a large electrode surface area. Although CNTs grown on thicker Fe films had large outer diameters, they showed lower specific capacitances of 38 and 58 F/g (Fig. 4.7 (b)), which is in agreement with the 40-60 F/g reported for vertically aligned MWNTs with diameters of 5-15 nm [2]. The specific capacitance decreased with increasing wall number in the CNT sample because the inner walls do not contribute to the adsorption of ions for the formation of the electric double layer on the CNT surface, and the effective surface area against the CNT sample weight decreased. It is expected that a large specific capacitance will be obtained from small-diameter CNTs with low wall numbers. Interestingly, the specific capacitance of 83 F/g for vertically aligned DWNTs is almost the same as that for vertically aligned SWNTs (80 F/g) reported by Futaba *et al*. [4] and is much higher than that of HiPco SWNT bucky paper (45 F/g) reported by Shiraishi *et al.* [3] as shown in Fig. 4.7(b). The specific capacitance is expected to be higher in the SWNTs than in the DWNTs because of the lack of inner walls in the former. However, two-thirds of the SWNTs, especially those with small diameters, behave as semiconductors with lower contribution to the capacitor characteristics. Therefore, it is speculated that the specific capacitance of vertically aligned DWNTs is equivalent to that of vertically aligned SWNTs (mean diameter: 2.8 nm) despite the inner CNTs. The electrical energy density was estimated using Eq (4.2). For vertically aligned DWNTs, an energy density of 72 Wh/kg was obtained, which is almost equal to that of vertically aligned SWNTs (69 Wh/kg). At the same specific capacitance and energy density, DWNTs are more promising candidates for practical capacitors than SWNTs because of their superior characteristics, such as their being structurally robust and less bundled.

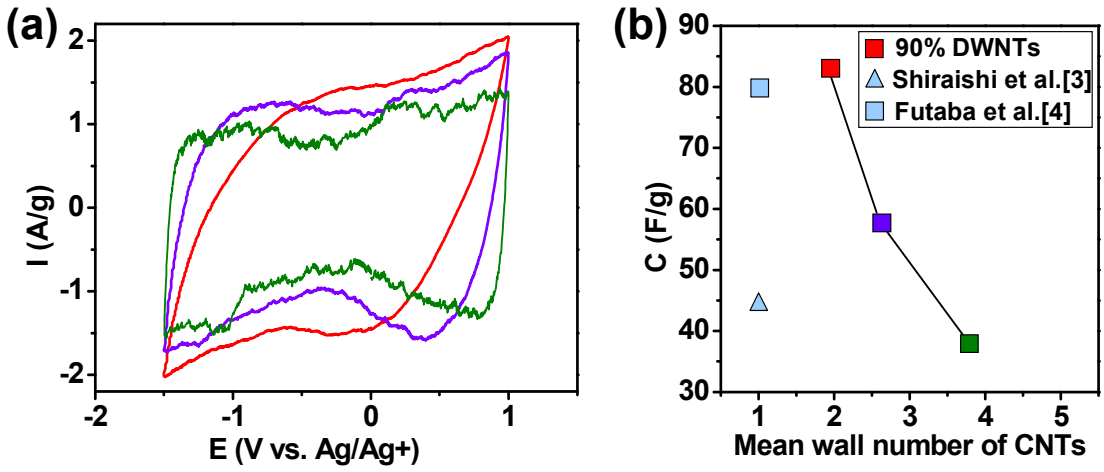

Figure 4.7 (a) Cyclic voltammograms. (b) Specific capacitances, measured by chronopotentiometry, of vertically aligned CNTs with different catalyst thicknesses: 0.45 nm (red), 0.75 nm (purple), and 1.50 nm (green). The squares and the triangle denote the capacitances of vertically aligned and non-aligned CNTs, respectively.

4.4. Summary

DWNT arrays with a high selectivity of 90% were synthesized on Si substrates at a low temperature of 650°C and obtained a high specific capacitance of 83 F/g in a nonaqueous solution, as determined by chronopotentiometry. The size of the catalyst particles was optimized for DWNT growth at an annealing temperature of 640°C, which is higher than the temperature of 600°C appropriate for SWNTs. CNTs with larger wall numbers grown on thick catalyst films showed lower specific capacitances. These results indicate that DWNT arrays are suitable for use as electrodes of EDLCs.

References

[1] A. Nishino, J. Power. Sources, 60, 137 (1996).

[2] Y. Honda, T. Haramoto, M. Takeshige, H. Shiozaki, T. Kitamura, and M. Ishikawa, Electrochem. Solid-State Lett., 10, A106 (2007).

[3] S. Shiraishi, H. Kurihara, K. Okabe, D. Hulicova, and A. Oya, Electrochem. Commun., 4, 593 (2002).

[4] D. N. Futaba, K. Hata, T. Yamada, T. Hiraoka, Y. Hayamizu, Y. Kakudate, O. Tanaike, H. Hatori, M. Yumura, and S. Iijima, Nature. Mater., 5, 987 (2006).

[5] R. Saito, M. Fujita, G. Dresselhaus, and M. S. Dresselhaus, Appl. Phys. Lett., 60, 2204 (1992).

[6] M. Endo, H. Muramatsu, T. Hayashi, Y. A. Kim, M. Terrones, and M. S. Dresselhaus, Nature, 433, 476 (2005).

[7] H. Qi, C. Qian, and J. Liu, Nano Lett., 7, 2417 (2007).

[8] T. Yamada, T. Namai, K. Hata, D. N. Futaba, K. Mizuno, J. Fan, M. Yudasaka, M. Yumura, and S. Iijima, Nature Nanotechnol., 1, 131 (2006).

[9] L. Ci R. Vajtai, and P. M. Ajayan, J. Phys. Chem. C, 111, 9077 (2007).

[10] V. K. Katastha, S. Wu, J. Moscatello, and T. K. Yap, J. Phys. Chem. C, 111, 10158 (2007).

[11] G. Zhong, T. Iwasaki, K. Honda, Y. Furukawa, I. Ohdomari, and H. Kawarada, Jpn. J. Appl. Phys., 44, 1558 (2005).

[12] G. Zhong, T. Iwasaki, K. Honda, Y. Furukawa, I. Ohdomari, and H. Kawarada, Chem. Vapor. Dep., 11, 127 (2005).

[13] T. Iwasaki, G. Zhong, T. Aikawa, T. Yoshida, and H. Kawarada, J. Phys. Chem. B, 109, 19556 (2005).

[14] A. Javey, and H. Dai, J. Am. Chem. Soc., 127, 11942 (2005).

Chapter 5

CNT Interconnection in LSI

Parts of this chapter are discussed based on the following papers:

- T. Iwasaki, R. Morikane, G. Zhong, T. Edura, K. Tsutsui, Y. Wada, H. Kawarada, NSTI Nanotech 2006 proceedings (2006).
- T. Iwasaki, R. Morikane, T. Edura, M. Tokuda, K. Tsutsui, Y. Wada, H. Kawarada, Carbon, 45, 2351 (2007).
- T. Iwasaki, S. Mejima, T. Koide, R. Morikane, H. Nakayama, T. Shinada, I. Ohdamari, H. Kawarada, Diam. Relat. Mater, in press (2008).
- D. Yokoyama, T. Iwasaki, T. Yoshida, S. Sato, T. Hyakushima, M. Nihei. Y. Awano, H. Kawarada, Appl. Phys. Lett., 91, 263101 (2007).

5.1. Research background

The scaling of lateral dimensions in silicon technology influences not only the transistors but also their interconnection. Scaling the width of the interconnection increases the resistance, not only because of the reduced cross section, but also due to increased scattering from the surface and the grain boundaries in interconnection materials [1]. The International Technology Roadmap for Semiconductors (ITRS) 2005 states [2] that the current density required for wiring materials will exceed that of Cu (10^7 A/cm^2) by 2014, as shown in Fig. 5.1. These problems cannot be addressed by using another bulk metal because the only metal with better bulk conductivity than copper is silver with a 10% improvement. If, however, wires could be made without intrinsic defects and with perfect surfaces, additional scattering might be avoided.

CNTs may fulfill these requirements. They offer unparalleled translational symmetry in one dimension with an intrinsically perfect surface. For metallic CNTs, the electron density is high and the conduction is easy along the tube axis due to the π-electron system. Moreover, it has been shown [3] that electron transport along the tubes is ballistic within the electron-phonon scattering length, which is of the order of micrometers at room temperature [4, 5]. The absence of scattering also allows for much higher current densities (>10^9 A/cm^2) than in Cu (10^7 A/cm^2).

In this chapter, for application of CNTs for multilayer interconnection, the development of processes including catalyst preparation, CNT growth and via fabrication, and the evaluation of electrical properties of CNT vias are reported.

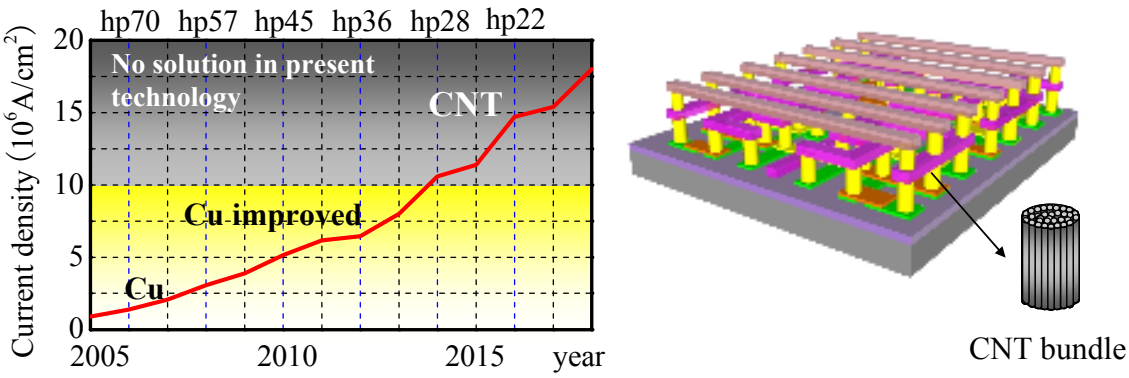

Figure 5.1 Expected current density required for multilayer interconnection.

5.2. Electrical properties of CNTs grown at low temperatures

5.2.1. Introduction

For multilayer interconnect applications, it is essential to synthesize densely packed CNT bundles at temperatures below 400°C, the allowable temperature in Si LSI [6]. The growth temperatures used in previous studies of the CNT-via process were above 450°C [7-10]. There have been reports regarding the low-temperature growth of CNTs at about 400°C by both thermal [11-13] and plasma-enhanced CVD (PE-CVD) [14-18]. However, the electrical properties of CNTs were not measured. This section demonstrates the electrical properties of MWNTs grown in via-holes at 390°C by remote-plasma CVD and the results of comparing resistances of MWNT-vias with and without planarization by chemical mechanical polishing (CMP) [19]. In addition, changes in the via resistance upon annealing at 400°C in hydrogen atmosphere are demonstrated.

5.2.2. Size-classified Co particles deposited by impactor

To grow vertically aligned CNTs, size-classified Co catalyst particles with an average diameter of 3.8 nm were deposited on a 5-nm-thick TiN layer using an impactor [20] (Fig. 5.2), which enabled the deposition of Co particles at the bottom of 40-nm –deep via-holes. Figure 5.2 shows schematic of the impactor apparatus and an SEM image of deposited Co particles, and diameter distribution of the particles estimated by AFM and SEM.

The impactor is a system in which the particles' inertia is used in their classification. Classification is achieved in the instrument by turning the gas flow and capturing the particles with sufficient inertia to cross gas streamlines. Particles with less inertia will remain in the gas flow. The impactor used in this study in Fig. 5.2(a) consists of a nozzle and a downstream impaction plate. First Co particles were generated by laser ablation of a Co target. The particles were then brought to the impaction plate by a carrier gas (He) for size classification. Particles with large inertia cannot avoid colliding with the impaction plate and are collected. As a result, particles with smaller inertia are brought to a substrate. The particle size can be controlled by adjusting the carrier gas flow rate, gas pressure and the scan rate of the impaction plate. The substrate is moved for uniform deposition of the size-classified particles. The particle density is governed by the deposition time.

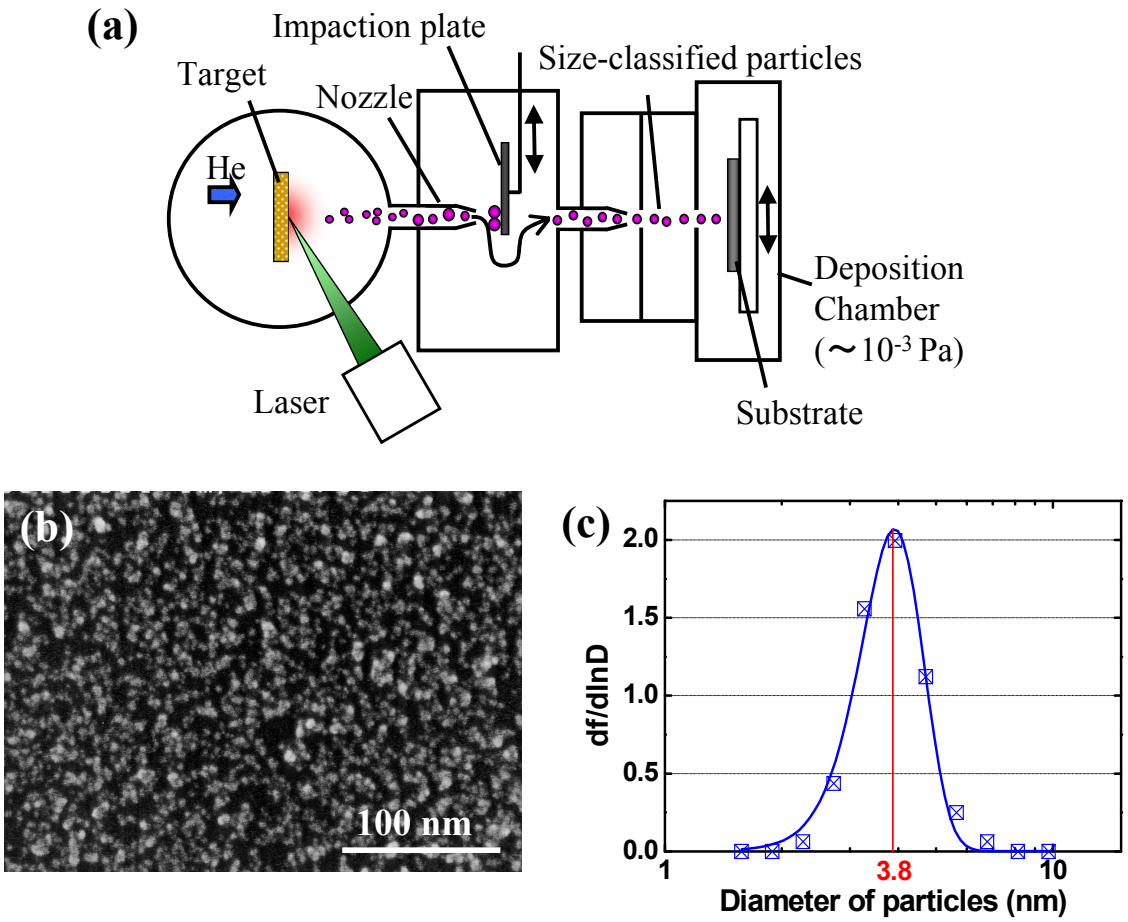

Figure 5.2 Fabrication of size-classified particles. (a) Schematic of Impactor system. (b) SEM image of Co particles deposited on TiN layer. (c) Diameter distribution of Co particles.

5.2.3. Growth of vertically aligned CNTs below 400˚C

Figure 5.3 shows CNTs grown at various temperatures. The other conditions were same as SWNT growth discussed in Chapter 2. All CNTs are vertically aligned, even at 350°C. However, the growth rate decreases as the growth temperature decreases because the catalyst activity is very sensitive to temperature. Figure 5.4(a) shows a tilted view of vertically aligned CNTs at 390°C, which have a uniform length on the substrate. Uniformity is very important for practical applications. A TEM image of CNT is shown in Fig. 5.4(b). Important points are whether CNTs maintain a hollow structure and have straight graphite layers, because it is thought that defects and deformation cause high

resistance during the measurement of electric properties. Regardless of the growth at low temperature under 400°C, CNTs have hollow structures and continuous graphite layers.

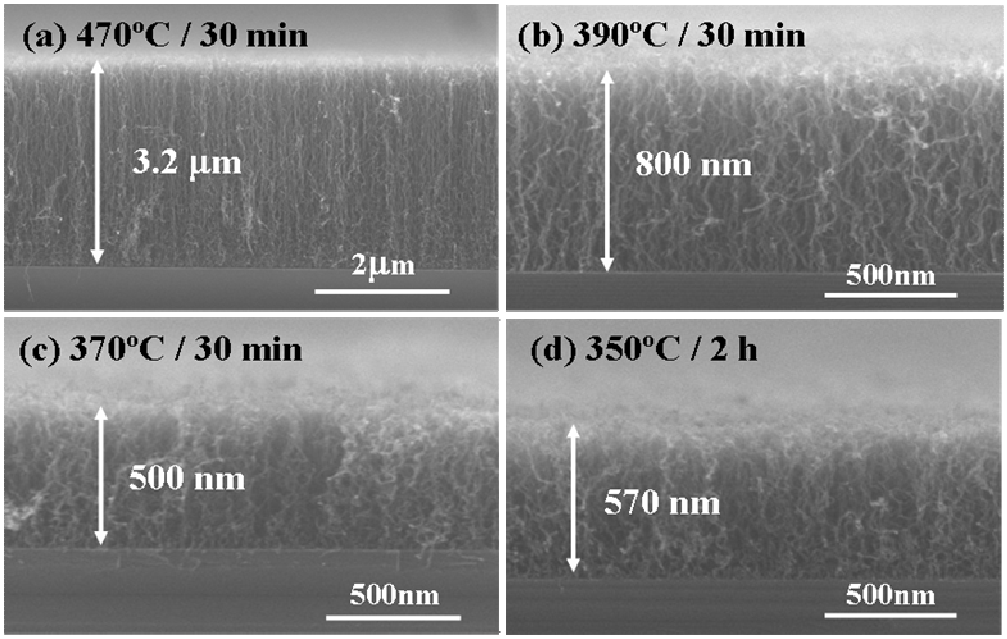

Figure 5.3 Growth of vertically aligned CNTs at low temperatures.

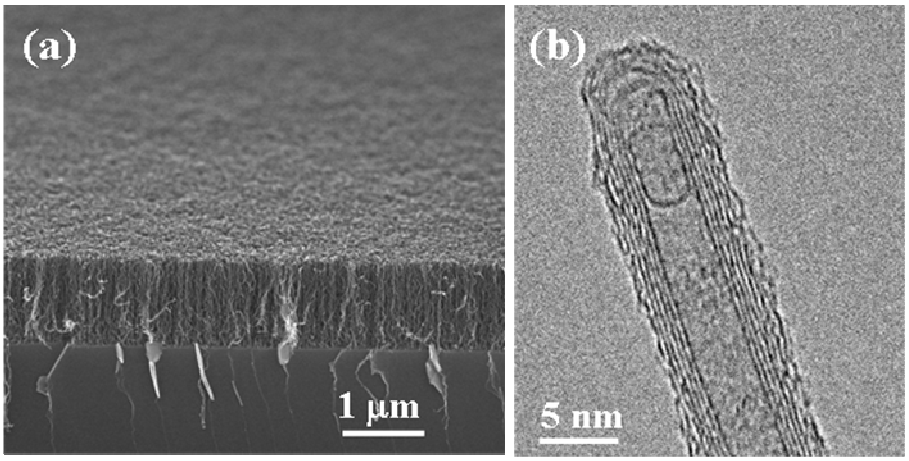

Figure 5.4 CNTs grown at 390°C. (a) SEM image. (b) TEM image.

5.2.4. Process of via fabrication

CNT-vias were fabricated using two processes with and without planarization of CNTs by CMP. In the first process without planarization shown in Fig. 5.5(a), the bottom electrodes composed of Cu wiring (100 nm) covered by a Ta diffusion barrier layer (15 nm) were formed by sputtering. A TiN contact layer (5 nm) was deposited on the bottom electrodes by sputtering. After depositing a tetraethylorthosilicate (TEOS) dielectric layer (250 nm), via-holes ranging in size from 2–11 μm were made using conventional photolithography and buffered hydrofluoric (BHF) wet etching. Then, Co catalyst particles were deposited over the whole substrate and CNTs were grown selectively from via-holes because CNTs were not grown from Co catalyst particles on SiO_2 dielectric. It is speculated that the bottom TiN layer plays a key role to the catalytic reaction of the Co particles at the low temperature. Positive ions were not provided to the substrate and the SiO_2 dielectric layer was covered with Co particles during CNT growth, indicating that there would be no plasma damage to the SiO_2 layer. To measure the electrical properties, the Ti contact layer (10 nm) and Cu wiring (300 nm) were deposited as top electrodes on CNTs by sputtering. Cu wiring was covered with a Ta barrier layer (15 nm) to prevent oxidation and erosion. Co particles on the SiO_2 layer were removed when the top layers were patterned by etching.

In the second process including CMP, shown in Fig. 5.5(b) [9], a TiN layer and Co catalyst particles were formed over the whole substrate after fabrication of via holes and CNTs were grown from full wafers by CVD. No plasma damage to the SiO_2 dielectric layer would occur because they were protected by the TiN layer during CNT growth. CNTs were held by Spin-on-Glass (SOG) and polished by CMP with silica slurry under a low pressure of 2 psi (13.8 kPa). Top electrodes were deposited on the planarized CNTs in the same way as in the first process. The via resistances were measured with a four-point probe method at room temperature. After measuring the electrical properties of CNTs, the CNT-vias were annealed at 400°C for 30 min in a hydrogen atmosphere. The changes in the resistance of CNT-vias by annealing were evaluated.

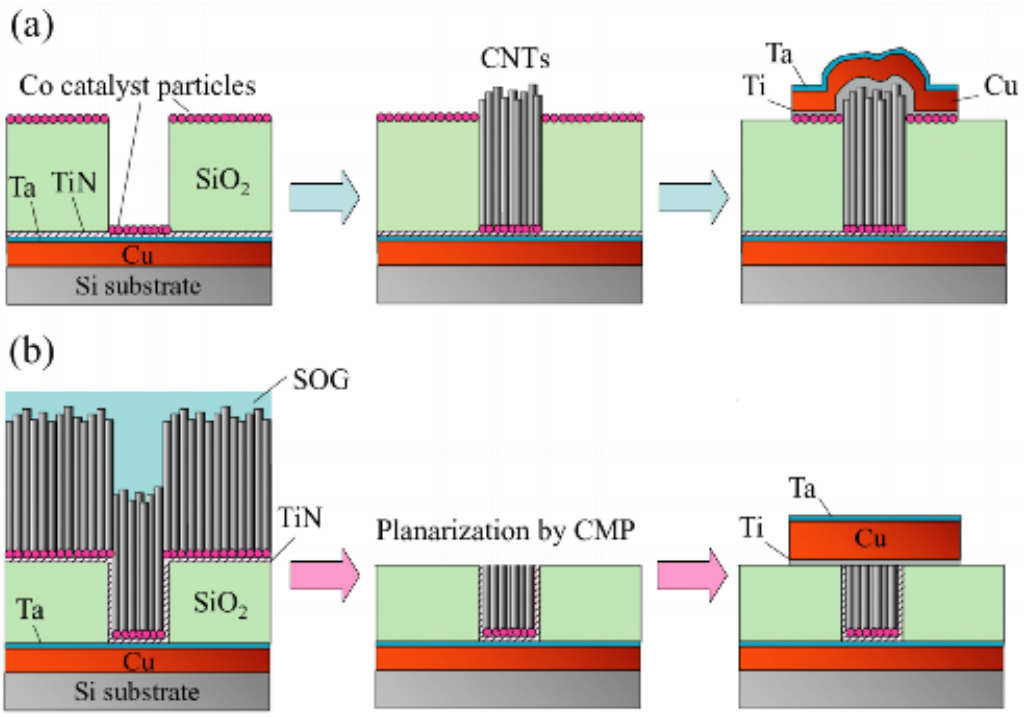

Figure 5.5 Processing of CNT-via for electrical properties. (a) First process without CMP. CNTs were grown selectively from via-holes using remote-plasma CVD. The Ti contact layer and top electrodes were then deposited by sputtering. (b) Second process with CMP. The TiN contact layer and Co catalyst particles were deposited over the whole substrate and CNTs were grown from full wafers. Then, CNTs were held by SOG and polished using CMP. Finally, top electrodes were deposited on planarized CNTs.

5.2.5. Morphology of CNTs grown in dielectric holes

Figure 5.6(a, b) show SEM images of vertically aligned CNTs grown at 390°C for 30 min in via-holes 2 μm in diameter. CNTs grew selectively in all holes with good reproducibility. The diameter of grown CNTs ranged from 5 to 10 nm (avg. 7 nm) and the density of CNTs was 1.6×10^{11} cm^{-2} corresponding to one-tenth of the close-packed density of 7 nm CNT. The density was estimated from tiled SEM images of the roots of CNTs by counting the number of CNTs. Before CMP, the main path for carrier conduction is the outermost graphite sheets of CNTs because the tips of CNTs are capped as shown in Fig. 5.4(b) and the electrodes only make contact with the outside sheets of CNTs. Figure 5.6(c-e) show SEM images of planar CNT-vias after CMP. CNT-vias were planarized and CNTs grown on the SiO_2 were removed completely. White dots in Fig. 5.6(e) are tips of CNTs polished after CMP. After applying CMP, the caps of CNTs would be opened and the inner sheets would also act as channel for carrier conduction, which is suggested by results of electrical measurements of CNTs described in Section 5.2.6.

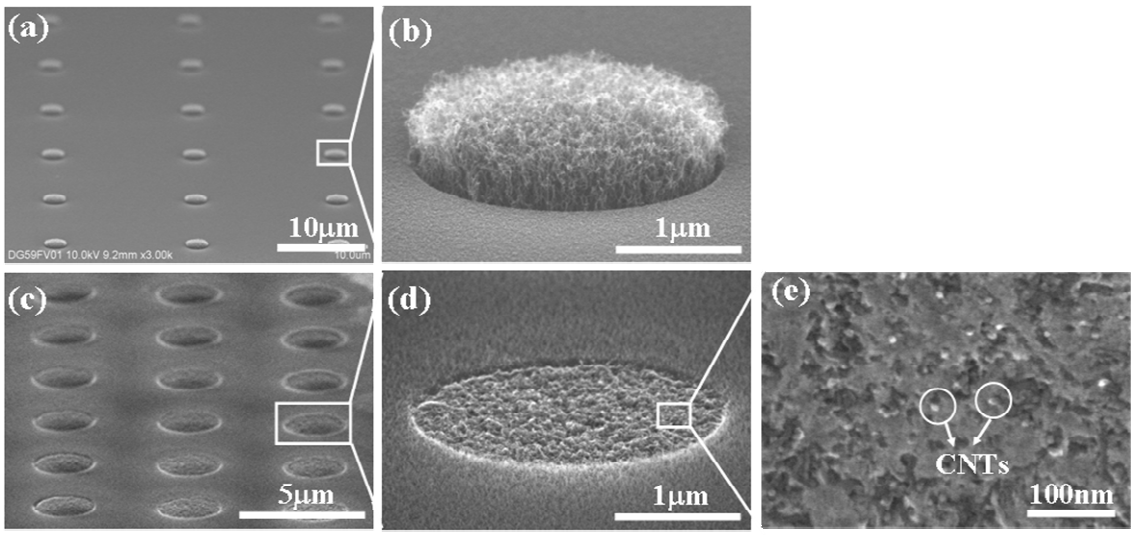

Figure 5.6 (a, b) SEM images of CNTs grown at 390°C in via-holes. Before CMP. (c-e) SEM images of planar CNT-vias after CMP.

5.2.6. Electrical properties of CNTs

Figure 5.7(a) shows that good ohmic behavior was obtained in both processes with and without CMP and the resistance of vias 2.1 μm in diameter decreased from 36 to 0.9 Ω after CMP. However, Fig. 5.7(b) shows that the resistance of CNT-via without CMP is inversely proportional to the via diameter (r) and not the via area. From the density of CNTs, the number of CNTs in the via area 2.1 μm in diameter was ~6700 and that along the via circumference was 82. The measured via resistance of 36 Ω was lower than the calculated resistance of 79 Ω for the outermost 82 CNTs of CNT-via using quantum resistance (6.45 kΩ/tube) [5]. Thus, good contact was formed not only on CNTs along the via circumference, but also slightly on CNTs around the center in the via area. This tendency has an undesirable effect on current density tolerance of the CNT-via and on reduction of the total via resistance because the number of active carrier paths in the via area is insufficient. In contrast, Figure 5.7(b) also shows that the resistances of CNTs with CMP are an order of magnitude lower than those of CNTs without CMP. As shown in Fig. 5.7(c), the main carrier paths were the outermost graphite shells of outer CNTs along the via circumference without CMP because the tips of CNTs were capped and the via resistance had 1/r dependence caused by the nonuniformity of CNT-via contacts. The 1/r dependence was improved due to the planarization with CMP. Then, the ohmic contacts were formed not only on the outermost CNTs but also on most of the inner CNTs in the via area after CMP. Moreover, the inner shells of CNTs were used as contributing paths for carrier conduction by opening caps of CNTs using CMP. Consequently, the number of graphite shells of CNTs having contact with the top electrode was increased by applying CMP.

Figure 5.7(d) shows that the resistance of almost all vias with CMP was reduced after annealing of the substrates at 400°C in the hydrogen environment. The resistance of vias with CMP 2.1 μm in diameter also decreased from 0.9 to 0.6 Ω after annealing. Significantly, the improved via resistance with CMP of 0.6 Ω was lower than the calculated resistance of ~1 Ω for outermost graphite shells of all 6700 CNTs in the via expected from quantum resistance of 6.45 kΩ/tube. This observation confirmed that the inner shells of CNTs are also involved in carrier conduction after CMP, as shown in Fig. 5.7(c). Although the caps of CNTs were opened by CMP, it is thought that not all of the inner shells were used as carrier paths. These nonactive inner shells were thought to make contact with the top electrodes due to the annealing and the total via resistance was improved. Note that the 400°C annealing contributed mainly to the contacts between CNTs and the top electrodes because the bottom electrodes and CNTs were

already heated at 390°C when CNTs grew from via-holes.

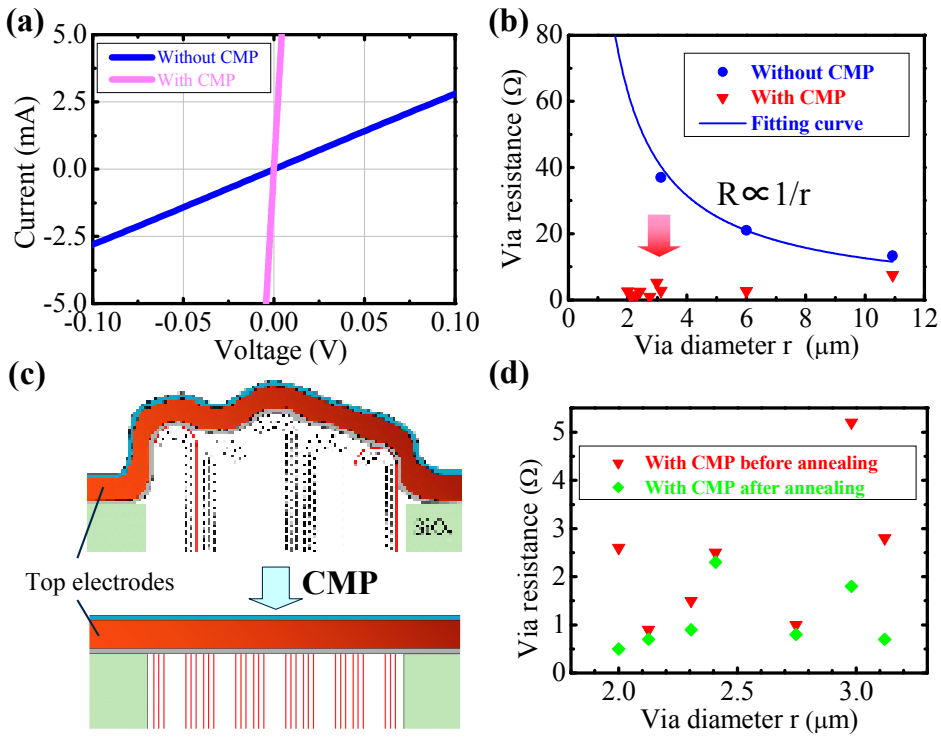

Figure 5.7 Electrical properties of CNT-vias with or without CMP. (a) Current-voltage characteristics of CNT-vias 2.1 μm in diameter. (b) Comparison of the via resistances between CNTs with and without CMP. (c) Cross-sectional image of CNT-vias and increase in carrier paths by CMP. The red solid lines and black dotted lines show the graphite shells of CNTs which do and do not act as carrier paths, respectively. (d) The improvement of via resistance of CNT-via with CMP by annealing.

In order to compare the resistances for different via diameters, we normalized the via resistance by via surface area. The resistivity ρ of the CNT-via is given by

$$\rho = \frac{R_{via} \cdot S}{H} \ (\Omega \cdot cm) \qquad (5.1)$$

where R_{via} is the resistance of CNTs in the via-holes, H is the height and S is the surface area. The height of all vias used in this study was fixed at 270 nm. Therefore, the via resistances were normalized as

$$R_S = R_{via} \cdot S \ (\Omega \cdot \mu m^2) \qquad (5.2)$$

R_S is the resistance to current through a unit area of 1 μm^2 and can be used as normalized value among different via diameters. The normalized resistance has the same unit as the contact resistance, Ω·μm^2. Figure 5.8 shows the lowest measured resistances (R_{total}) at each via diameter, which are normalized by via surface area; it includes the contact resistance between the electrodes and CNTs. R_{total} is given by

$$R_{total} = R_{via} \cdot S + R_c = R_s + R_c \left(\Omega \cdot \mu m^2\right) \qquad (5.3)$$

where R_c is the contact resistances between CNTs and two electrodes (Fig. 5.8). R_{total} can be compared among different via diameters. The ideal via resistance was calculated using the quantum resistance of 6.45 kΩ as the resistance of one graphite shell and the CNT density of 1.6 × 10^{11} cm^{-2} estimated from SEM images. If it is assumed that only the outermost layer contributes to carrier conduction, the normalized resistance would be 4 Ω·μm^2, as indicated by the solid horizontal line in Fig. 5.8. If it is assumed that all 7 layers act as carrier conduction paths, the normalized resisatnce would be 0.57 Ω·μm^2, as shown by the dotted line in Fig. 5.8. The measured via resistances were lower than the ideal resistance calculated using only one outermost sheet of CNT shown as the solid line in Fig. 5.8. However, the improved resistance of 1.7 Ω·μm^2 at 2 μm diameter was still higher than the ideal resistance of 0.57 Ω·μm^2 calculated with all 7 graphite shells in the via. There are two reasons: (1) not all 7 layers are in contact with the electrode, (2) the defects in graphene sheets causes the electron scattering and the length of the electron mean free path of ballistic transport would be shorter than the via height in the real system. First, although the contact between CNT tips and the top electrode was improved by annealing, it is speculated that not all inner layers are in contact with the electrode, resulting in resistances higher than the ideal one. Second, although CNTs show ballistic transport, the electron mean free path of CNTs grown at low temperatures should be very short. The electron mean free path of CNT-vias grown at 450°C by thermal CVD was estimated to be 80 nm [10]. Thus, the electron mean free path of CNTs grown by remote-plasma CVD would be near 80 nm, which is shorter than the height of via-holes (270 nm). This factor made the measured resistance higher than the ideal.

Although the resistances of CNTs improved upon CMP and annealing, they were still several times higher than those of a tungsten plug (0.3-0.6 Ω·μm^2). The resistance is expected to be reduced by improving the factors discussed above, but the most important factor is the CNT density. At the present time, our growth method has a

problem of the aggregation of Co catalyst particles during preheating. The density of 1.6 × 10^{11} cm^{-2} would be improved by preventing this aggregation and optimizing remote-plasma CVD conditions such that CNTs grow from smaller catalyst particles at the low temperatures.

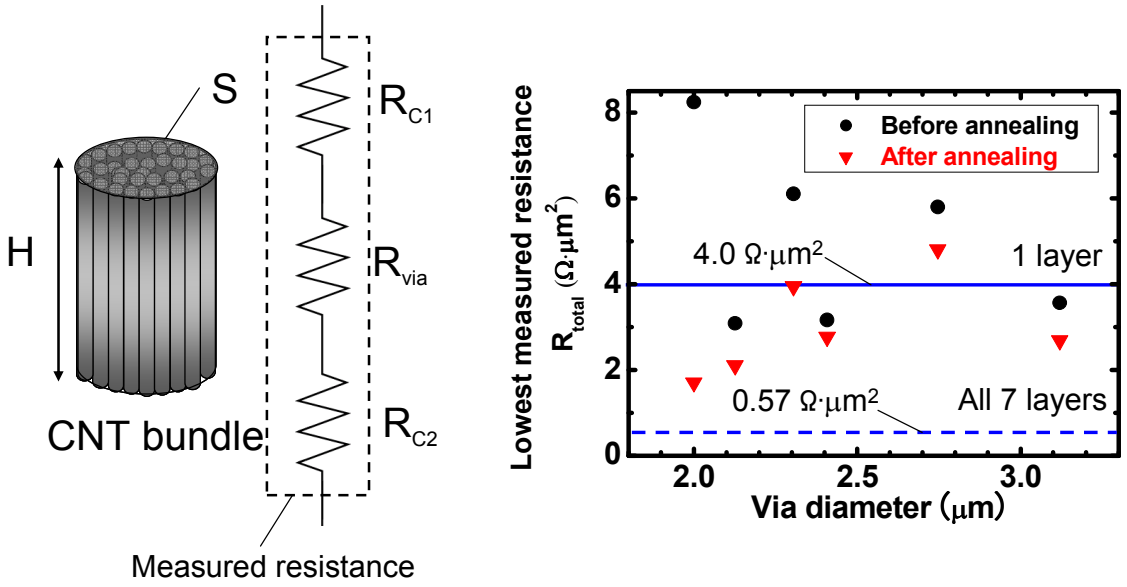

Figure 5.8 Lowest measured resistance normalized by surface via area at each via diameter; it includes the contact resistances between CNTs and electrodes. The solid line (only outermost layer) and dotted line (7 layers including all inner layers) indicate ideal resistances calculated using the quantum resistance as the resistance of one graphene sheet = 6.45 kΩ.

5.2.7. Summary

CNT-based vias were fabricated using MWNTs grown at a low temperature of 390°C using remote-plasma CVD and the electrical properties of CNTs were measured by achieving ohmic contacts. The resistances of planar CNTs with CMP were improved by about one order magnitude as compared to CNTs without CMP. The resistances decreased further after annealing at 400°C in a hydrogen environment and the resultant resistance was 0.6 Ω for 2-μm vias. This growth method will be useful for future multi-layer interconnects of LSI because it can reduce thermal damage to LSI.

5.3. Growth of dense SWNTs in nano-sized SiO_2 holes

5.3.1. Introduction

Although CNT-vias have been successfully fabricated, as described in Section 5.2, large-diameter (>5 nm) CNTs are undesirable for achieving low resistance because the total number of the graphite shells, including inner shells in MWNTs, in a via hole can be larger for small diameter CNTs. Based on a previously reported calculation [6], the resistance of close-packed SWNTs with a diameter of less than 2 nm can be lower than that of Cu used for LSI interconnects. However, a reliable method for the growth of dense SWNTs in nano-sized holes has not been reported. In addition to multilayer interconnects, vertically aligned SWNTs are promising candidates for use in fabricating vertical FETs with a round-gate [21]. SWNTs can also be used as channels in a transistor because they show semiconducting as well as metallic behaviour as discussed in Section 1.2 [22]. This section reports the growth of dense SWNTs in nano-sized SiO_2 holes by the vertically aligned SWNT growth method developed in Chapter 2.

5.3.2. Process of via fabrication

Two methods have been proposed for growth of CNTs in SiO_2 holes. One method involves the fabrication of holes of SiO_2 in which CNTs are then grown [19, 23], while the other method involves synthesis of freestanding CNTs on patterned catalysts followed by deposition of SiO_2 [7]. The second process is possible for large-diameter MWNTs by plasma CVD in which a bias voltage is applied between an upper and a lower electrodes. This results in a high electric field at the substrate and promotes the vertical alignment of CNTs. Although our method uses plasma, there is no high electric field at the substrate because the plasma is kept at a distance and there are no ions around the substrate as discussed in Section 2.2. In addition, SWNTs have extremely small diameters and are very flexible. Although SWNTs grown by remote-plasma CVD have a very high density, it is difficult to fabricate freestanding nano-sized patterned SWNTs with a high aspect ratio. Therefore, the process in which SWNTs were grown after fabrication of SiO_2 holes was used.

As a catalyst, a sandwich-like catalyst structure of Al (0.5 nm)/Fe (0.5 nm)/Al (>5 nm) was used. Two processes were used, in which a catalyst layer was deposited using sputtering with different timings. In the first and second processes, the Fe catalyst was deposited after and before the fabrication of SiO_2 holes, respectively.

5.3.2.1. Process 1: Catalyst deposition after opening holes

In the first process shown in Fig. 5.9, (a) layers of Al 50 nm thick and SiO_2 240-380 nm thick were deposited on Si wafers by sputtering and TEOS-CVD, respectively. (b) Nano-sized resist patterns were formed by electron beam (EB) lithography using a chemically amplified negative resist. (c) A layer of Ni 50 nm thick was deposited as a metal mask for the next SiO_2 etching process. Then, the patterned resists were removed by lift-off. (d) For fabrication of holes, SiO_2 was etched using an inductively coupled plasma (ICP) system with fluoride gas. (e) A catalyst layer with a top part of sandwich-like structure of Al/Fe was deposited. (f) A coating of photo-resist was applied for the next polishing. (g) The resist and the catalyst were polished by CMP. (h) The Ni metal mask and the resist in the holes were etched by chemicals. (i) SWNTs were grown using the remote-plasma CVD apparatus.

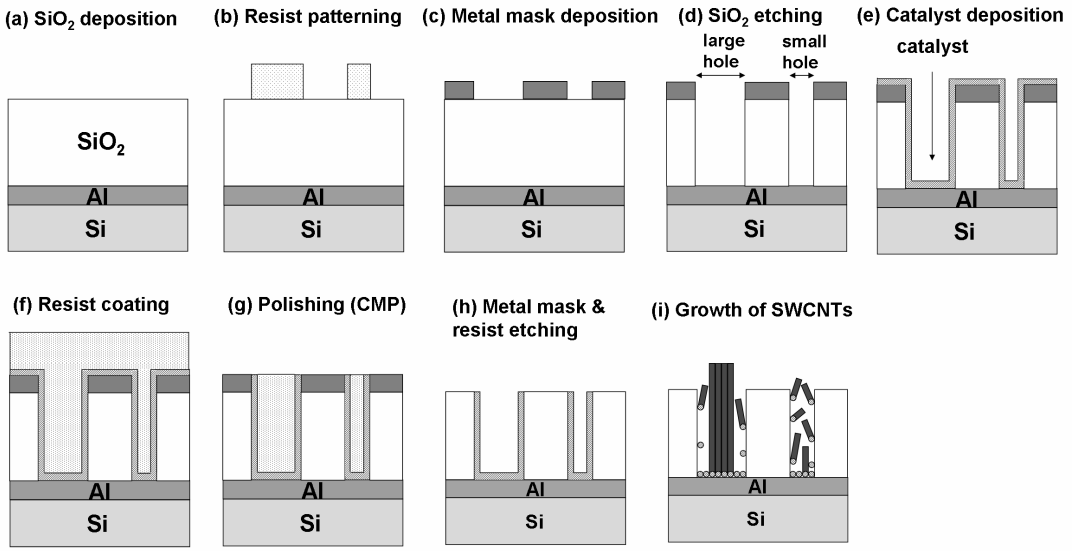

Figure 5.9 Schematic of the first process, in which the catalyst layer was deposited after fabrication of the holes.

5.3.2.2. Process 2: Catalyst deposition before opening holes

In the second process shown in Fig. 5.10, (a) a catalyst layer with a sandwich-like structure of Al/Fe/Al was deposited on Si wafers. (b) A SiO_2 layer 240 nm thick was formed on the catalyst by TEOS-CVD. (c) SiO_2 holes were fabricated using the same methods as shown in Fig. 5.9(b–d). (f) SWNTs were synthesised by remote-plasma CVD.

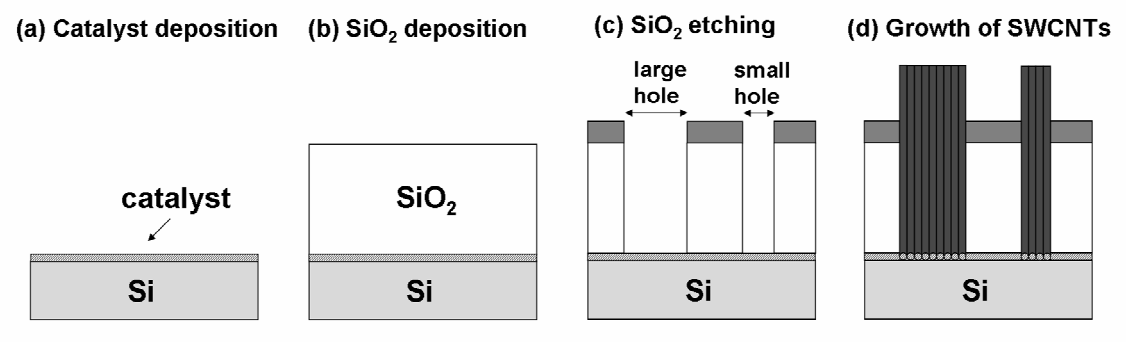

Figure 5.10 Schematic of the second process, in which the catalyst layer was deposited before fabrication of the holes.

5.3.3. Morphology of SWNTs grown from nano-sized holes

As shown in Fig. 5.11, CNTs were grown in the holes with diameters of 200 nm–650 nm using the first process in Fig. 5.9. However, as the hole size decreased to less than 300 nm, most of the CNTs grew from catalysts at the sidewalls of the holes, because sputtering led to isotropic catalyst deposition in the holes. CNTs were grown at the upper parts of the holes in the case smaller than 300 nm, indicating that it would be difficult to grow CNTs at the bottom even with use of a thinner SiO_2 layer.

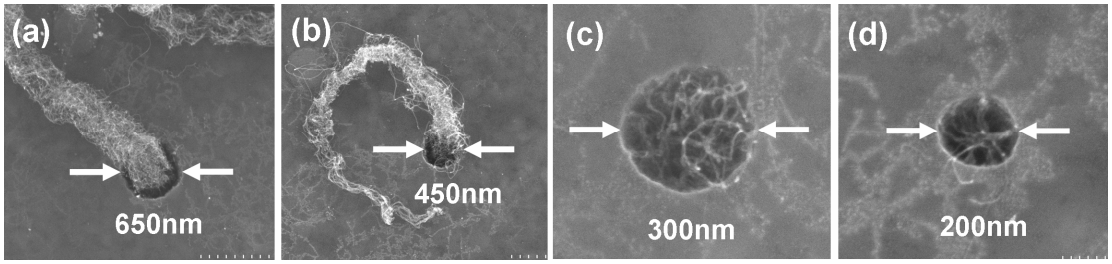

Figure 5.11 CNTs grown in holes using the first process. Holes with diameters of (a) 650 nm, (b) 450 nm, (c) 300 nm and (d) 200 nm. The growth time was 30 min.

In contrast, as shown in Fig. 5.12, CNTs were synthesised successfully in nano-sized holes smaller than 300 nm using the second process in Fig. 5.10. CNTs were grown in holes of various sizes and shapes. Figure 5.12(a) shows a 3-μm pitch array of CNTs in holes with a diameter of 250 nm. It can be seen that CNTs were outside the holes. SEM images of a 550-nm hole at high magnification, as shown in Fig. 5.12(b, c), indicated that the grown CNTs had a high density. As shown in Fig. 5.12(d–h), CNTs were synthesised successfully in small holes with diameters of 350 nm, 250 nm, 150 nm, 130 nm and 100 nm. Dense CNTs could also be synthesised in square and triangular holes, as shown in Fig. 5.12(i, j). As expected, nano-sized patterned CNTs curved and were not aligned vertically as their length increased. In this study, the minimum hole size was 100 nm. The hole size was limited by the patterning of the EB resist. Small resist patterns could be easily pushed down or swept out during the development process. Note that no CNTs were observed on the Ni mask. Under the CVD conditions used in the present study, it was difficult for the thick Ni film to become small particles or the process was affected by fluoride gas during SiO_2 etching.

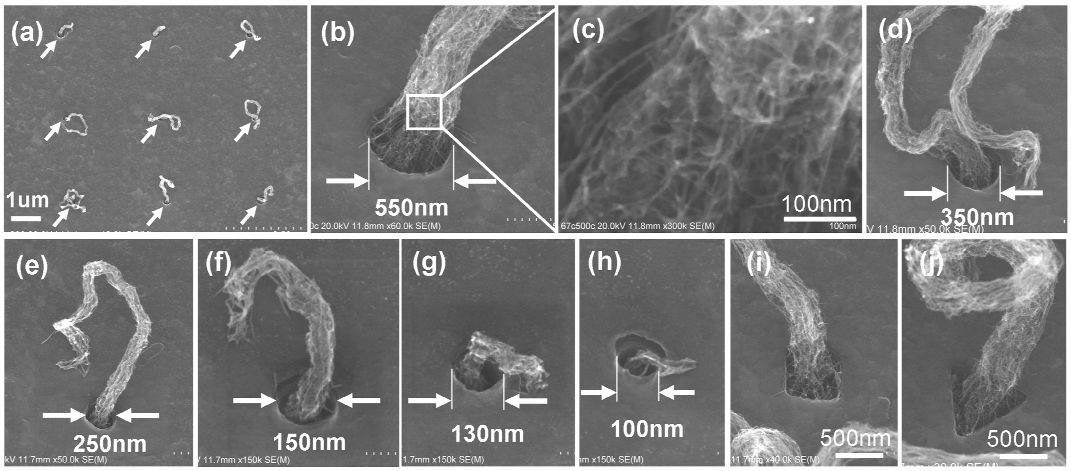

Figure 5.12 CNTs grown in holes of various sizes and shapes using the second process. (a) 3-μm pitch array of CNTs in holes with a diameter of 250 nm. Circlar holes with diameters of (b, c) 550 nm, (d) 350 nm, (e) 250 nm, (f) 150 nm, (g) 130 nm and (h) 100 nm. (i) Square hole. (j) Triangular hole. The growth time was 30 min.

Figure 5.13 shows CNTs observed from a different angle to see the orientation of CNTs. Although small-diameter rod-shaped CNTs were curved, the root parts near the holes were vertically aligned, suggesting that CNTs in the vias were also straight. The CNT density in the vias is an important factor for interconnect application. In the case of large-diameter MWNTs, the density can be estimated by counting the number of CNTs at the root. However, this method could not be used here because small-diameter CNTs form bundles. We have estimated the density of homogeneously grown SWNTs on a substrate by measuring the weight gain after CVD and the SWNT diameter, and have obtained a value of $10^{12}/cm^2$ as discussed in Section 2.3.7. Taking into account the possibility of formation of MWNTs in the bundles as discussed below (Section 5.3.5), the CNT density of the vias would be in the order of $10^{11}/cm^2$.

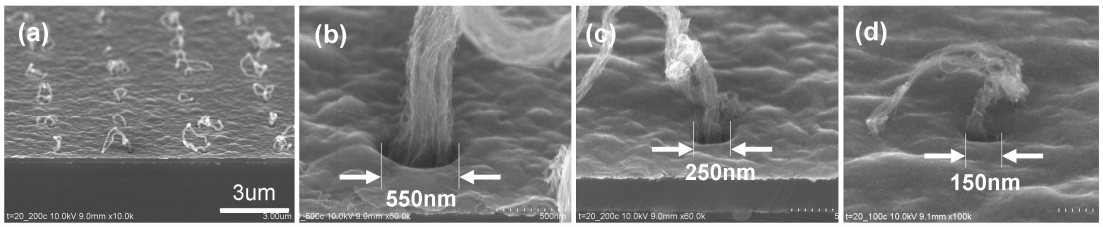

Figure 5.13 Side-view SEM images of CNTs grown using the second process. (a) An array of 250 nm holes. Holes with diameters of (b) 550 nm, (c) 250 nm and (d) 150 nm.

5.3.4. Growth rate of SWNTs in nano-sized holes

The CNTs became shorter in length in the smaller holes. As shown in Fig. 5.14, the growth rate of CNTs in the holes decreased as the size of the holes became smaller. For comparison, the growth rate of SWNTs grown homogeneously on a Si substrate is 200–300 μm/h. All the patterns were formed on the same substrate, and so the growth conditions, such as growth time and temperature, were the same. Moreover, the etching rate of SiO_2 was the same for holes of different sizes. Therefore, the difference in growth rate was caused by the amount of carbon radicals diffusing to the catalyst particles at the bottom of the holes. It was speculated that the possibility of carbon radicals arriving at smaller holes was reduced, resulting in a decrease in the growth rate. Another possibility is an effect of sidewall interactions. The outermost CNTs along the circumference in vias interact with the sidewalls of the SiO_2 dielectric layer. The ratio of CNTs with this interaction increases as the hole size is reduced. This sidewall interaction effect could suppress the growth of CNTs in the vias and result in the lower growth rate in the smaller vias.

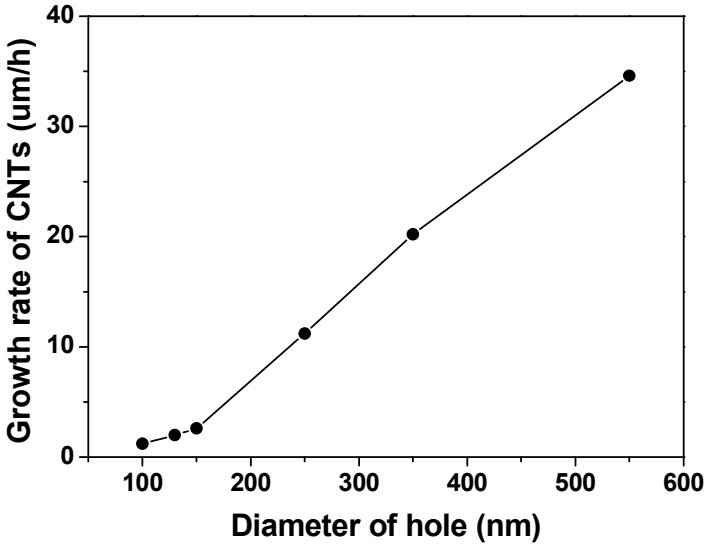

Figure 5.14 Variation in growth rate of CNTs with hole size. The growth time was 30 min and all the holes were on the same substrate.

5.3.5. Characterization of as-grown CNTs by Raman spectroscopy

Characterization of as-grown CNTs in the holes was performed by micro-Raman spectroscopy using a laser with an excitation wavelength of 633 nm. Figure 5.15 shows Raman spectra of CNTs grown in holes of various sizes and grown homogeneously on a Si substrate. In Fig. 5.15(b), radial breathing mode (RBM) peaks can be seen for all holes, indicating the existence of SWNTs. The diameter of SWNTs shown in the superior axis in Fig. 5.15(b) was estimated using the correlation [24], $d = 248/\nu$, where d is the diameter of SWNT in nm and ν is the Raman shift in cm^{-1}. However, Raman data in the high frequency region in Fig. 5.15(a) show that CNTs in the holes have higher D bands than SWNTs grown homogeneously. In the process of fabrication of the holes, it is difficult to stop the etching of the SiO_2 layer just above the sandwich-like structure of Al/Fe/Al. The thin Al layer above the Fe film (top Al layer) is very important for the growth of vertically aligned SWNTs. This layer interrupts diffusion of Fe particles during the preheating period, so that a high density of Fe catalytic particles can be obtained. As a result, densely packed vertically aligned SWNTs can be synthesized. It is speculated that parts of the top Al and the Fe films were removed in the process of SiO_2 etching and that the region without the top Al layer resulted in a mixture of SWNTs and MWNTs, which caused the higher D-bands than homogeneous growth.

In addition to aggregation of Fe particles, sidewall interactions, discussed in Section 5.3.4, could also cause the observed increase in the D-band signal. The sidewall interaction effect hinders the growth of CNTs in the vias, resulting in formation of more defective graphite layers. To clarify the state of CNTs in vias, many characterizations, such as cross-sectional SEM and TEM observations, are required. Electrical properties should also be measured in future studies to explore the applicability of the obtained CNTs for interconnects and vertical FETs.

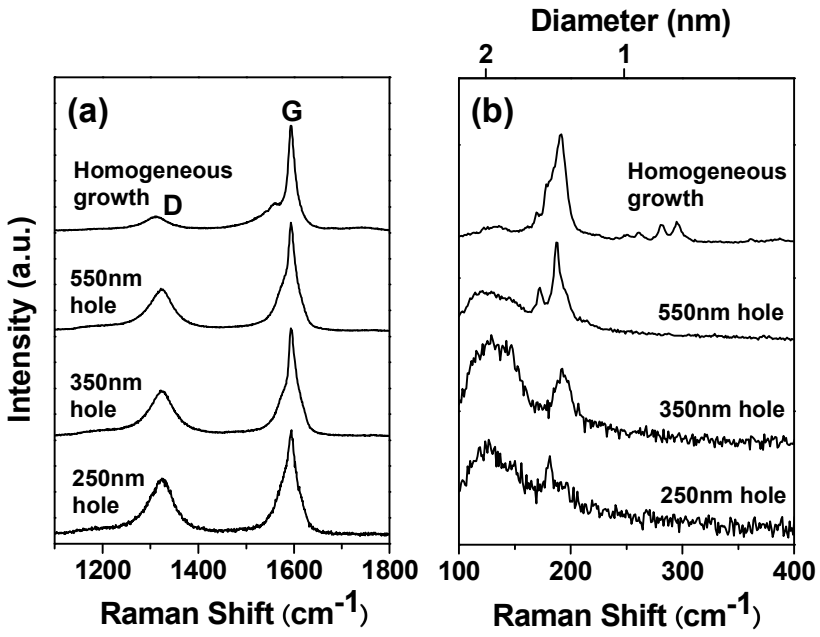

Figure 5.15 Raman spectra of CNTs grown in nano-sized holes with diameters of 550 nm, 350 nm and 250 nm and grown homogeneously on a Si substrate, measured using a 633 nm laser. (a) Raman data for G- and D-bands. (b) Raman data for RBM.

5.3.6. Summary

Dense SWNTs were synthesised in nano-sized SiO_2 holes fabricated using EB lithography and plasma etching. To grow SWNTs in holes smaller than 300 nm, the catalyst layer was deposited on Si wafers before opening holes. The growth rate of SWNTs in the holes decreased as the size of the holes became smaller. Moreover, the smaller the size of the hole, the higher the D-band became on Raman spectroscopy. The nano-sized SWNT pattern could be applied for three-dimensional microelectronics, such as vertical FETs with a round-gate and multi-layer interconnects.

5.4. CNT growth from Ni nanoparticles prepared by ion implantation

5.4.1. Introduction

To use CNTs in multilayer interconnection and vertical FET applications, catalysts for CNT growth should be prepared in nano-sized dielectric holes. However, it is difficult to prepare catalysts in a controlled amount at the bottom of high-aspect-ratio via holes. In Section 5.3, SWNTs were grown in nano-sized via holes, but the predeposited thin catalyst film is easily etched and removed during the opening of holes by the etching process. For the impactor method described in Section 5.2, the etching process does not affect the catalyst quality. The particles can be deposited after opening holes because this method is highly isotropic. However, there is another problem for the impactor: throughput for the LSI process. It takes a long time to deposit the particles on a substrate because size-classified particles are deposited one by one. Therefore, another appropriate method should be considered for the practical LSI process.

Ion implantation is a very interesting method for this purpose. Ion implantation can be applied easily in LSI processes and catalysts can be implanted at the bottom of via holes in precisely controlled amounts (Fig. 5.16). Recently, growth of carbon nanofibers, MWNTs and SWNTs has been demonstrated by Ni and Fe ion implantation [25–29]. Adhikari [27] obtained catalyst particles with a density of 1.6×10^{11} cm^{-2}. However, the resultant CNTs were not aligned. Although vertically aligned CNTs were shown at a dose in the order of 10^{16} ions/cm^2, catalyst particles and grown CNTs had very low densities [29]. The microelectronic applications described above require a high-density of vertically aligned CNTs. Thus, high-density catalyst particles must be prepared by ion implantation.

In this section, a focused-ion-beam (FIB) system was used to investigate formation of high-density nanoparticles in high doses up to 5.0×10^{17} ions/cm^2. The particle diameter and density were studied with different doses and post-implantation annealing temperatures. Finally, vertically aligned and dense CNTs from implanted Ni catalysts were successfully synthesized.

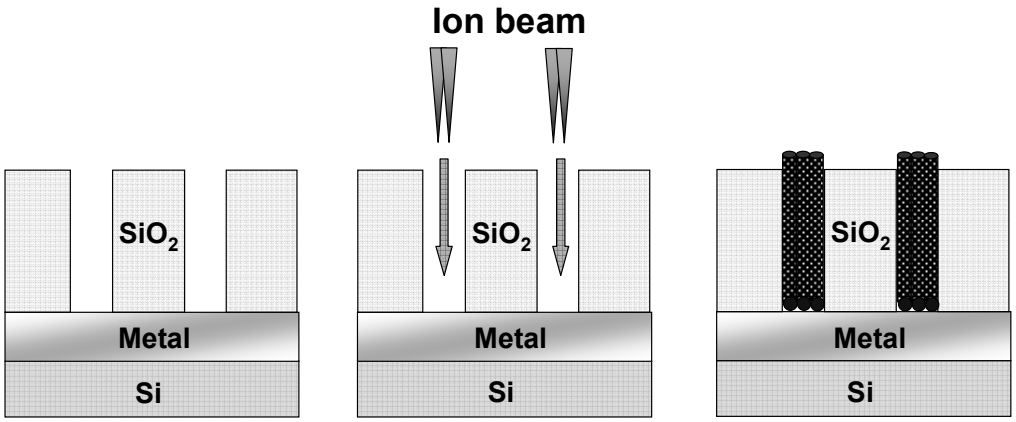

Fig. 5.16 Concept of catalyst preparation at the bottom of via holes by ion implantation.

5.4.2. CNT growth on SiO_2 substrates

5.4.2.1. Ion implantation conditions and process

The growth process of vertically aligned CNTs by implanted catalysts is shown in Fig. 5.17. (a) First, Ni ions were separated from Ni-P-Pt liquid metal ion sources (LMIS) using a mass separator, and then Ni^+ ions were implanted into a SiO_2 layer 500 nm thick on a Si substrate at an acceleration voltage of 30 kV with doses of $1.0–5.0\times10^{17}$ ions/cm^2 using FIB. Implantation was performed at room temperature and the implanted region was 30×30 μm–100×100 μm. The implanted Ni was analyzed using secondary ion mass spectrometry (SIMS). (b) After Ni implantation, the substrate was annealed at 460–700°C for 30 min in H_2 gas to control the density and the diameter of Ni particles on the surface. The SiO_2 was not etched after ion implantation and Ni catalysts formed on the substrate surface were used. (c) The substrates were then introduced into the remote-plasma CVD apparatus for CNT growth. CNTs were grown at 600˚C in a mixture of H_2 (45 sccm) and CH_4 (5 sccm) at 60 Torr for 2 h.

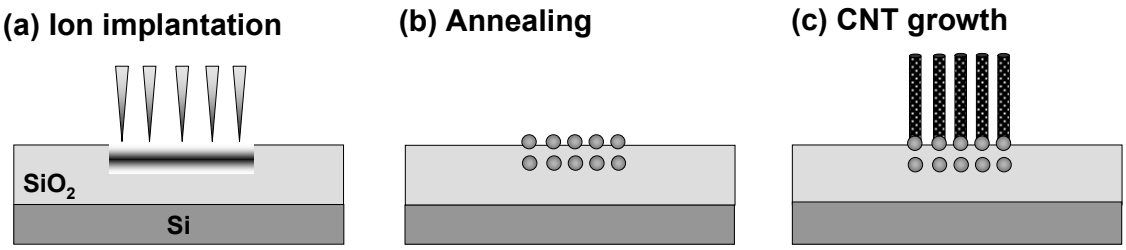

Figure 5.17 Schematic of the growth process of vertically aligned CNTs on catalysts prepared by ion implantation.

SIMS techniques were used to measure Ni concentrations as a function of depth from the surface (Fig. 5.18). Although it is difficult to evaluate the Ni concentration quantitatively by SIMS at the high doses used in this study, the tendencies of shifts in peak positions can be determined. The position of the peak Ni concentration shifted close to the surface as the dose increased. It is well known that the higher the dose, the larger the sputtered depth [30]. Sputtered depths measured by atomic force microscopy (AFM) after ion implantation were in agreement with this tendency. As a result, the Ni concentration at the surface increased with increasing the dose.

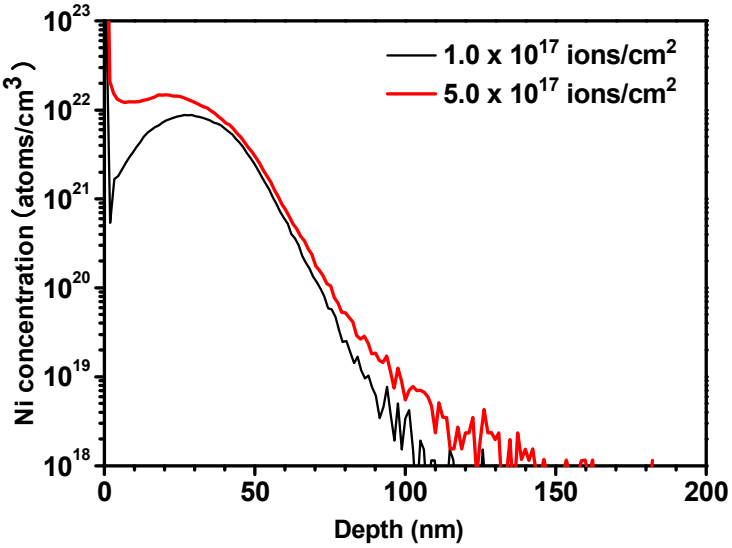

Figure 5.18 Ni concentrations at doses of 1.0×10^{17} and 5.0×10^{17} ions/cm^2 from SIMS.

5.4.2.2. Formation of Ni nanoparticles

Ni nanoparticles were formed on the SiO_2 surface after ion implantation without annealing the substrates. The density was 8.6×10^{11} and 5.4×10^{11} cm^{-2} at doses of 2.5×10^{17} and 5.0×10^{17} ions/cm^2, respectively (Fig. 5.19(a)). The particle density and diameter were controlled by post-implantation annealing. Figs. 5.19(b-d) show Ni particles on the surface at a dose of 5.0×10^{17} ions/cm^2 after annealing at 460–700°C. The particle density and the mean diameter variation with annealing temperature are shown in Fig. 5.19(e). The plots at room temperature indicate as-implanted states. Although the density increased to 9.2×10^{11} cm^{-2} after annealing at 460°C, it decreased at higher temperatures and was 3.0×10^{11} cm^{-2} with annealing at 700°C, which was lower than that of as-implanted (5.4×10^{11} cm^{-2}). The diameter showed the opposite tendency. This phenomenon occurred due to Ostwald ripening [31]. Ni atoms or clusters below the substrate surface diffused and participated in the formation of larger particles. Here, it was confirmed that formation of dense nanoparticles, approximately 10^{12} cm^{-2}, was possible by ion implantation.

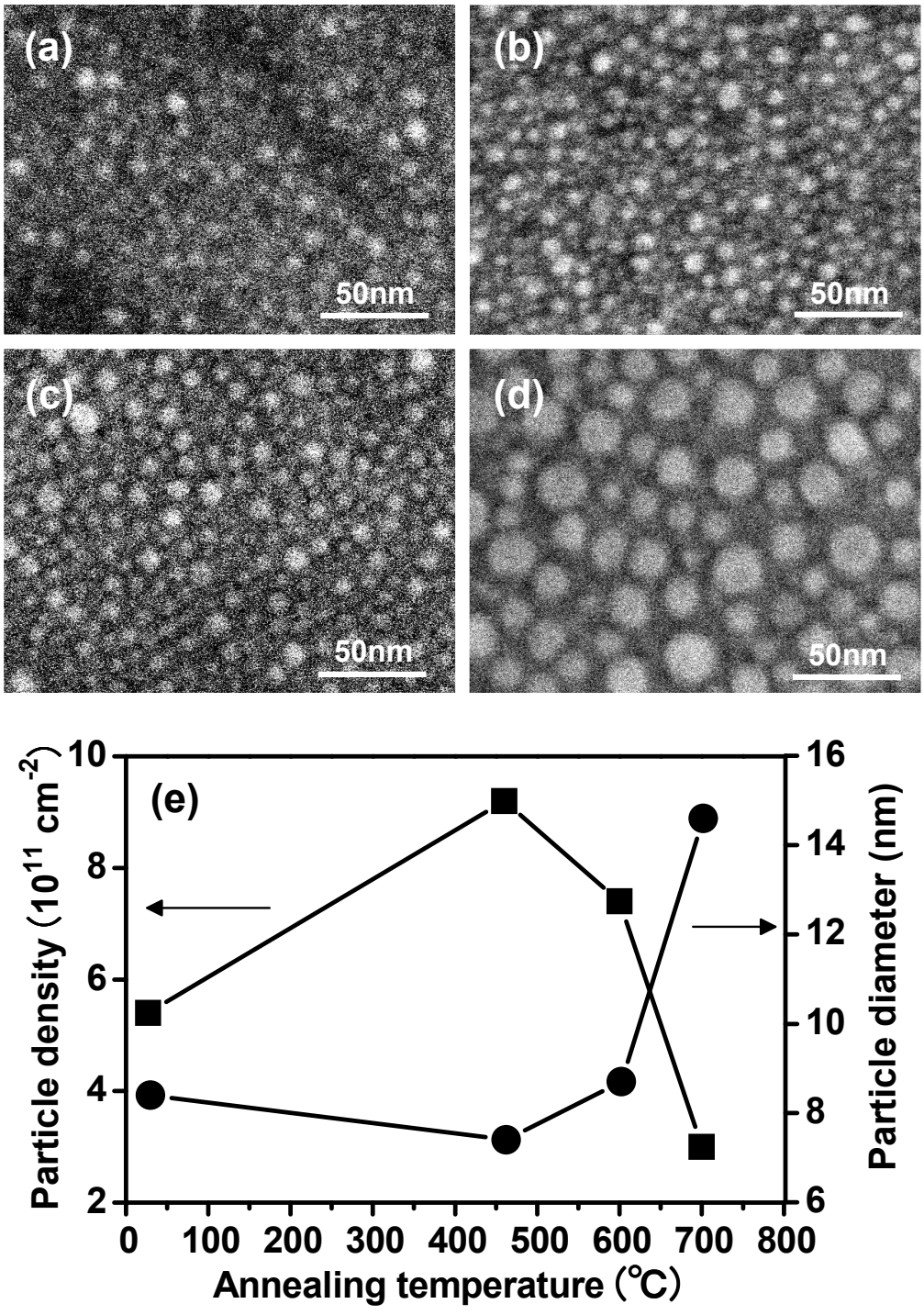

Figure 5.19 SEM images of Ni nanoparticles at a dose of 5.0×10^{17} ions/cm^2 (a) without annealing, after annealing at (b) 460°C, (c) 600°C and (d) 700°C. (e) Particle density and mean diameter variation with annealing temperature at a dose of 5.0×10^{17} ions/cm^2.

5.4.2.3. Effects of ion dose on CNT growth

First, the effects of an ion dose on CNT growth were investigated using the particles with the highest densities formed with annealing at 460°C. As shown in Fig. 5.20, a very small number of CNTs were observed at a dose of 1.0×10^{17} ions/cm^2, and CNT yield increased with increasing dose although the particles at a dose of 2.5×10^{17} ions /cm^2 were denser (1.3×10^{12} cm^{-2}) than that at a dose of 5.0×10^{17} ions/cm^2 (9.2×10^{11} cm^{-2}). Particle sizes should be considered for clarifying this phenomenon. The mean particle diameter at 2.5×10^{17} ions /cm^2 was smaller (5.7 nm) than that at 5.0×10^{17} ions/cm^2 (7.4 nm). Therefore, it was speculated that CNTs grew preferentially from large particles under these CVD conditions and for the combination of the Ni catalysts and the SiO_2 substrate. Thus, a key point to improving the CNT yield and forming CNT arrays is not only the particle density but also the control of particle size.

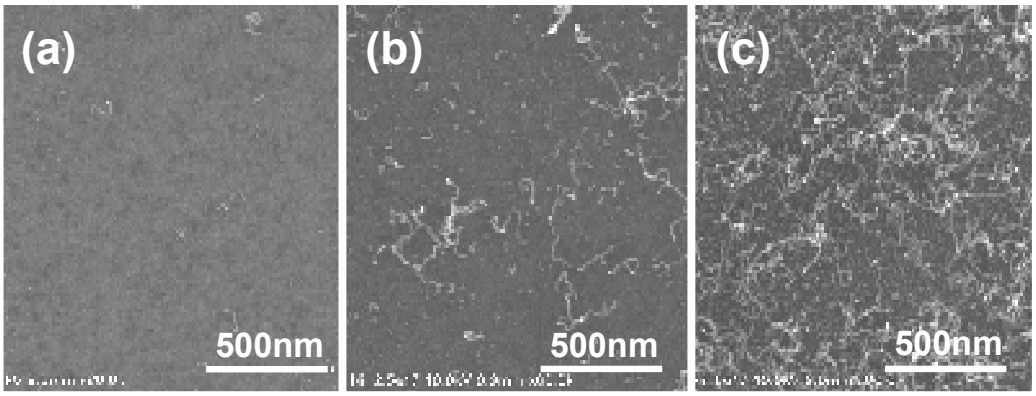

Figure 5.20 Top-view SEM images of CNTs grown from particles at doses of (a) 1.0×10^{17} ions/cm^2, (b) 2.5×10^{17} ions/cm^2 and 5.0×10^{17} ions/cm^2. The annealing temperature was 460°C.

5.4.2.4. Effects of post-implantation annealing temperature on CNT growth

Second, CNTs were synthesized from Ni particles formed at different post-implantation annealing temperatures at a dose of 5.0×10^{17} ions/cm^2. As shown in Figs. 5.21(a-c), there were no marked changes in CNT yield from particles without annealing and those annealed at 460°C and 600°C annealing. The particles formed under the three conditions had similar mean diameters, approximately 8 nm, as shown in Fig. 5.19(e). In contrast, much denser CNTs were synthesized on the particles with annealing at 700°C (Fig. 5.21(d)). Although annealing at 700°C led to the lowest particle density of 3.0 x 10^{11} cm^{-2}, the particles had an average diameter of 14.6 nm, which was roughly twice as large as the others. This particle size is probably appropriate for nucleation of CNTs under these conditions. This result is coincident with the first experiment described in Section 5.4.2.

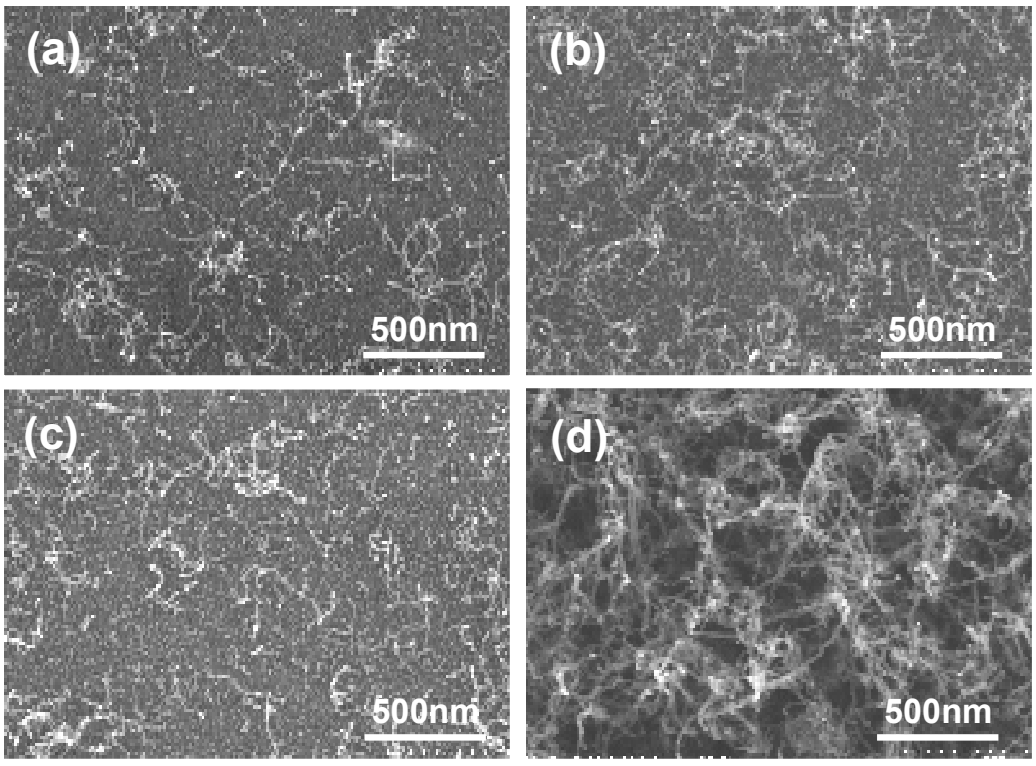

Figure 5.21 Top-view SEM images of CNTs grown from particles at a dose of 5.0×10^{17} ions/cm^2 formed (a) without annealing, and with annealing at (b) 460°C, (c) 600°C and (d) 700°C.

5.4.2.5. Vertically aligned CNTs on buried catalysts

To see the alignment of CNTs grown from the particles annealed at 700°C in Fig. 5.21(d), CNTs were observed from the side of the implanted region as shown in Fig. 5.22(a, b). CNTs 4 μm in length were vertically aligned at the ion implanted region. Figure 5.22(c) shows a cross-sectional SEM image of the SiO_2 surface. Interestingly, catalysts were not spherical but longer along the vertical axis like a rugby ball and the lower half of the Ni particle was buried in SiO_2. Figure 5.22(d) is a schematic of the buried Ni particle. This phenomenon is unique to catalysts prepared by ion implantation. The frequency of the Ni particle and CNT diameters are shown in Fig. 5.22(e). The Ni particle diameter is the horizontal width. Seventy percent of CNTs have diameters of 10–15 nm. The mean diameters of the Ni particles and CNTs were 14.6 nm and 13.0 nm, respectively. Therefore, the CNT diameters were determined by the width of the Ni particles in the same way as catalyst particles prepared by sputtering or electron-beam methods [32].

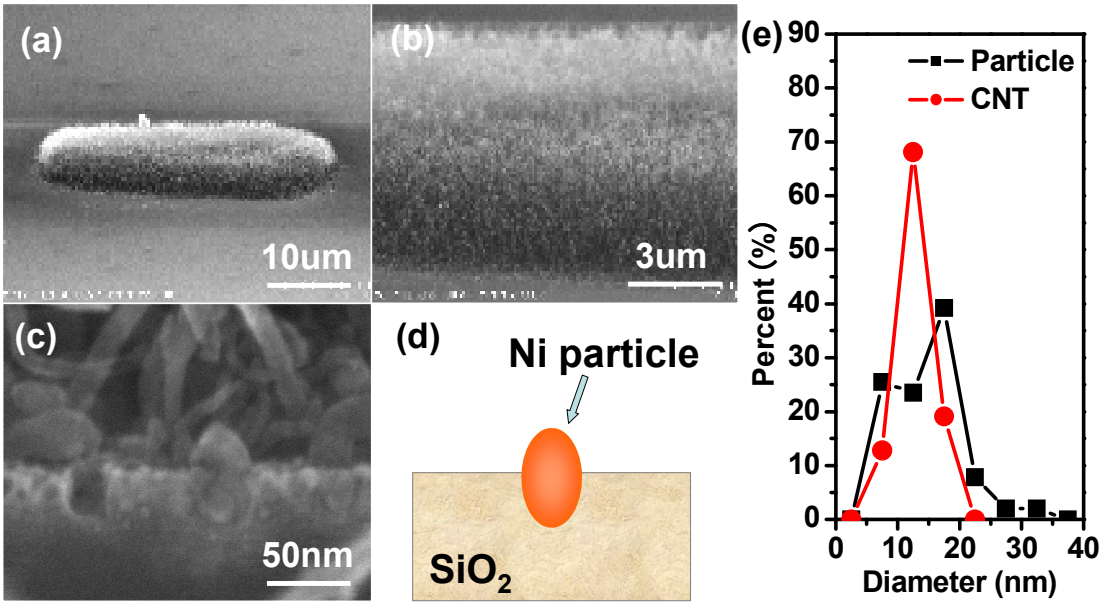

Figure 5.22 (a, b) Side-view SEM images of vertically aligned CNTs from the particles annealed at 700°C. (c) Ni catalyst particle, the lower half of which was buried in SiO_2. (d) Schematic of the buried Ni particle in (c). (e) Diameter histogram of the Ni particles annealed at 700°C and vertically aligned CNTs.

5.4.2.6. Summary

In summary, the formation of dense Ni nanoparticles of the order of 10^{11}–10^{12} cm^{-2} was achieved by ion implantation using FIB. Vertically aligned CNTs were synthesized from particles annealed at 700°C although the highest particle density was obtained after post-implantation annealing at 460°C. CNTs were grown preferentially from particles larger than 10 nm under these CVD conditions and in the Ni/SiO_2 system. Growth of vertically aligned CNTs from catalyst particles prepared by ion implantation is a very useful technique for microelectronics applications.

5.5. Summary

This chapter demonstrated the process developments for CNT-based LSI interconnections.

In Section 5.2, the growth of uniform vertically aligned MWNTs at 390°C by remote-plasma CVD below the allowable temperature in Si LSI was described and their electric properties were examined. The resistances of CNTs planarized by CMP became lower than in the case without CMP as a result of the increase in the number of carrier paths in inner graphite shells of MWNTs.

In Section 5.3, the synthesis of SWNT arrays in SiO_2 holes 100-550 nm in diameter was described. To grow SWNTs in holes smaller than 300 nm, a catalyst layer was deposited on Si wafers before the formation of SiO_2. It was found that the growth rate of SWNTs in the holes decreased as the hole size became smaller. In addition, the smaller the size of the hole, the higher the D-band became in the Raman spectrum, probably because of the mixture of MWNTs or the formation of defective graphite layers through sidewall interactions.

In Section 5.4, the preparation of catalyst particles by ion implantation was described. On the SiO_2 surface, Ni catalyst particles with a density of 10^{11}–10^{12} cm^{-2} were formed. The catalyst particle size and density could be controlled by post-implantation annealing, and vertically aligned CNTs were synthesized from particles annealed at 700°C.

References

[1] W. Steinhogl, M. Engelhardt, G. Schindler and G. Steinlesberger, Phys. Rev. B 66, 075414 (2002).

[2] International Technology Roadmap for Semiconductors (ITRS) 2005, http://public.itrs.net.

[3] S. Frank, P. Poncharal, Z. L. Wang and W. A. de Heer, Science 280, 1744 (1998).

[4] J. Appenzeller, R. Martel, P. Avouris, H. Stahl, and B. Lengeler, Appl. Phys. Lett. 78, 3313 (2001).

[5] C. L. Kane, E. J. Mele, R. S. Lee, J. E. Fischer, P. Petit, H. Dai, A. Thess, R. E. Smalley, A. R. M. Vershueren, S. J. Tans and C. Dekker, Europhysics Letters 41, 683 (1998).

[6] M. Nihei, M. Horibe, A. Kawabata and Y. Awano, Jpn. J. Appl. Phys. 43, 1856 (2004).

[7] J. Li, Q. Ye, A. Cassell, H. T. Ng, R. Stevens, J. Han and M. Meyyappan, Appl. Phys. Lett. 82, 2491 (2003).

[8] Y. Choi, S. Lee, H. Yoon, M. Lee, H. Kim, I. Han, Y. Son, I. Yeo, U, Proc. Chung and J. Moon, Proc. IEEE-NANO 2006. Conf. 262 (2006).

[9] F. Kreupl, A. P. Graham, G. S. Duesberg, W. Steinhoegl, M. Liebau, E. Unger and W. Hoenlein, Microelectron. Eng. 64, 399 (2002).

[10] M. Nihei, T. Hyakushima, S. Sato, T. Nozue, M. Norimatsu. M. Mishima, T. Murakami, D. Kondo, A. Kawabata, M. Ohfuti and Y. Awano: Proc. IEEE Int. Interconnect. Technol. Conf. 2007. 204 (2007).

[11] A. H. Mahan, J. L. Alleman, M. J. Heben, P. A. Parilla, K. M. Jones, and A. C. Dillon, Appl. Phys. Lett. 81, 4061 (2002).

[12] M. Cantoro, S. Hofmann, S. Pisana, V. Scardaci, A. Parvez, C. Ducati, A. C. Ferrari, A. M. Blackburn, K-Y. Wang, and J. Robertson, Nano Lett. 6, 1107 (2006).

[13] G. Yu, J. Gong, D. Zhu, S. He and Z. Zhu, Carbon, 43, 3015 (2005).

[14] S. Kyung, Y. Lee, C. Kim, J. Lee and G. Yeom, Thin Solid Films, 506, 268 (2006).

[15] G. Y. Chen, C. H. P. Poa, S. J. Henley, V. Stolojan, S. R. P. Silva, S. Haq, Appl. Phys. Lett. 87, 253115 (2005).

[16] Y-S. Min, E. J. Bae, B. S. Oh, D. Kang and W. Park, J. Am. Chem. Soc. 127, 12498 (2005).

[17] J-M.Ting and K-H. Liao, Chem. Phys. Lett. 396, 469 (2004).

[18] S. Hofmann, C. Ducati, J. Robertson and B. Kleinsorge, Appl. Phys. Lett. 83, 135 (2003).

[19] M. Horibe, M. Nihei, D. Kondo, A. Kawabata and Y. Aawano, Jpn. J. Appl. Phys. 43, 6499 (2004).

[20] S. Sato, M. Nihei, A. Mimura, A. Kawabata, D. Kondo, H. Shioya, T. Iwai, M. Mishima, M. Ohfuti and Y. Awano, Proc. IEEE Int. Interconnect Technol. Conf. 2006. 230 (2006).

[21] P. Graham, G. S. Duesberg, R. V. Seidel, M. Liebau, E. Unger, W. Pamler, F. Kreupl, W. Hoenlein. small 1, 382, (2005).

[22] S. J. Tans, A. R. M. Verschueren, C. Dekker. Nature 393, 49, (1998).

[23] G. S. Duesberg, A. P. Graham, F. Kreupl, M. Liebau, R. Seidel, E. Unger, W. Hoenlein. Diam. Relat. Mater. 13, 354 (2004).

[24] Jorio, R. Saito, J. H. Hafner, C. M. Lieber, M. Hunter, T. McClure, G. Dresselhaus, M. S. Dresselhaus. Phys. Rev. Lett. 86, 1118 (2001).

[25] D. Ferrer, T. Shinada, T. Tanii, J. Kurosawa, G. Zhong, Y. Kubo, S. Okamoto, H. Kawarada, I. Ohdomari, Appl. Surf. Sci. 234, 72 (2004).

[26] J. M. Mao, L. F. Sun, L. X. Qian, Z. W. Pan, B. H. Chang, W. Y. Zhou, G. Wang, and S. S. Xie, Appl. Phys. Lett. 72, 3297 (1998).

[27] R. Adhikari, M. B. Huang, D. Wu, and K. Dovidenko, Appl. Phys. Lett. 86, 053104 (2005).

[28] Y. Choi, J. S. Oakley, and A. Ural, Appl. Phys. Lett. 89, 153130 (2006).

[29] X. Z. Ding, L. Huang, X. T. Zeng, S. P. Lau, B. K. Tay, W. Y. Cheung, and S. P.

Wong, Carbon 42, 3003 (2004).

[30] *Ion Implantation and Synthesis of Materials*, by M. Nastai and J. W. Mayer (Springer, Berlin, 2006).

[31] E. Cattaruzza, F. Gonella, G. Mattei, P. Mazzolde, D. Gatteschi, S. Sangregorio, M. Falconieri, G. Salvetti, and G. Battaglin, Appl. Phys. Lett. 73, 1176 (1998).

[32] M. Chhowalla, K. B. K. Teo, C. Ducati, N. L. Rupesinghe, G. A. J. Amaratunga, A. C. Ferrari, D. Roy, J. Robertson, and W. I. Milne, J. Appl. Phys. 90, 5308 (2001).

Chapter 6

Summary

The findings and conclusions obtained in this study are summarized as follows.

Chapter 2

- Vertically aligned SWNTs with a high surface density of 10^{12} /cm^2 were synthesized at a low temperature of 600°C by microwave remote-plasma CVD.

- A sandwich-like catalyst structure of Al_2O_3 / Fe / Al_2O_3 played a key role in the synthesis of vertically aligned SWNTs. The top Al_2O_3 layer increases the surface diffusion barrier of catalytic atoms during preheating, resulting in the formation of dense Fe catalyst particles.

- The decrease in the growth rate of homogeneously grown SWNTs is mainly caused by the limited diffusion of carbon radicals. By patterned growth of the wall structure, linear growth was achieved and 5-mm-long vertically aligned SWNTs were obtained.

- It was found that the growth rate was dependent on the growth temperature. The maximum growth rate was obtained at 680–690°C. Long-time deposition at this temperature resulted in 7.4-mm-long vertically aligned SWNTs on nonpatterned catalysts.

Chapter 3

- The root growth mode of vertically aligned SWNTs was clarified by a new method, marker growth, which involves interrupting the nanotube growth by lowering the substrate temperature and turning off the plasma, and observing the layering of the resulting stack.

- The growth mechanism of marker growth was investigated by cutting the layers. New caps were formed at the re-growth. Therefore, the new layers re-grew exactly like the fresh layers.

- Selected-area Raman spectra revealed that the chirality distribution of the layers was the same across the interface. The diameter and chirality distribution were preserved during re-growth when the growth conditions were kept the same as those of the 1st growth.

Chapter 4

- Vertically aligned DWNTs with a high selectivity of 90% were synthesized by a controlled heating method. It was found that preheating at 640°C can produce catalyst particles appropriate for the DWNT growth.

- A high specific capacitance of 83 F/g was obtained for the DWNT arrays in an organic solution. This value was almost equivalent to that of SWNT arrays. At the same specific capacitance, DWNTs, which have superior structural properties, are more promising for practical capacitors than SWNTs.

Chapter 5

- CNT vias were fabricated using CNTs grown at 390°C and their electrical properties were measured. The resistances of CNTs planarized by CMP were improved by one order of magnitude because of the increase in the number of carrier paths using the inner graphite shells.

- Using remote-plasma CVD, dense vertically aligned SWNTs were grown in SiO_2 via holes 100–550 nm in diameter. The growth rate of SWNTs in the holes decreased as the size of the holes became smaller due to the reduced amount of carbon radicals diffusing into the holes.

- Ni catalytic nanoparticles were formed by ion implantation. The particle density and diameter were controlled by post-implantation annealing. Vertically aligned CNTs were synthesized from catalytic particles prepared by ion implantation.

The author hopes that the findings and the developed processes presented in this thesis will contribute to further fundamental studies on CNTs and the development of applications of CNTs.

ACKNOWLEDGMENTS

I would like to express my sincere gratitude to my supervisor, Prof. Hiroshi Kawarada for his thoughtful and helpful direction, continued advice and encouragement throughout the course of my research. I would also like to thank Prof. Iwao Ohdomari, Prof. Yoshiji Horikoshi, Prof. Shuichi Shoji, and Assistant Prof. Takanobu Watanebe at Waseda University for their careful reading of the thesis and fruitful advices. I would like to express my sincere gratitude to Prof. John Robertson and Dr. Goufang Zhong at Cambridge University for their continuous direction and support.

I would also like to express my gratitude to Prof. Yukio Furukawa and Dr. Kotaro Honda at Waseda University for the collaboration on the measurements of Raman spectra of vertically aligned SWNTs, and Prof. Yukio Honda and Dr. Minekazu Fujiwara at Waseda University for repeated assistances in TEM operations. For the field emission measurements of vertically aligned SWNTs, I would like to Mr. Hiroyuki Kurachi at Noritake Company Ltd in Section 2.3.8.

I would like to thank Mr, Takuma Asari, Mr. Hironori Kumagai, and Mr. Yasuhiro Hashimoto at Matsushita Electric Industrial Co. Ltd for the precious collaboration on the application of CNTs to EDLCs in Chapter 4, from which I fortunately could learn many things.

I would like to express my gratitude to Selete members, especially Dr. Yuji Awano, Dr. Mizuhisa Nihei, Dr. Shintaro Sato, and Dr. Takashi Hyakushima for their collaboration and many helps and discussions regarding preparation of size-classified catalyst particles and LSI via processes in Section 5.2. I would also like to acknowledge Dr. Tomohiko Edura (Tokyo Electron at the present time), Dr. Ken Tsutsui and Prof. Yasuo Wada (Toyo University at the present time) for his useful advices about the fabrication process of SWNT-vias in Section 5.3. I would like to thank Prof. Iwao Ohdomari, Dr. Takahiro Shinada, and Mr. Hideki Nakayama for the collaboration and repeated assistances on the fabrication of LMIS for ion implantation of catalysts in Section 5.4.

I am grateful to all my current and former lab members for their considerate advices and precious contributions.

This work was supported in part by a Grant-in Aid for Center of Excellence (COE) and Scientific Research from the Ministry of Education, Science and Culture, and in part by Ambient SoC Global COE Program of Waseda University of the Ministry of Education, Culture,

Sports, Science and Technology. This work was also supported in part by the MIRAI Project from NEDO.

Finally, I want to express my gratitude to my parents, Katsumi and Mitsue, my brother, Hiroyuki for their kind support and encouragement throughout my research.

Takayuki Iwasaki

LIST OF PUBLICATIONS

Papers

Publications in Journals

1. **T. Iwasaki**, J. Robertson, H. Kawarada, "Mechanism Analysis of Interrupted Growth of Single-Walled Carbon Nanotube Arrays", Nano. Lett, in press 2008.

2. **T. Iwasaki**, S. Mejima, T. Koide, R. Morikane, H. Nakayama, T. Shinada, I. Ohdamari, H. Kawarada, "Vertically Aligned Carbon Nanotube Growth from Ni Nanoparticles Prepared by Ion Implantation", Diam. Relat. Mater, in press 2008.

3. **T. Iwasaki**, T. Maki, D. Yokoyama, H. Kumagai, Y. Hashimoto, T. Asari, H. Kawarada, "Highly Selective Synthesis of Vertically Aligned Double-Walled Carbon Nanotubes by a Controlled Heating Method and Their Electric Double-Layer Capacitor Properties", phys. stat. sol. (RRL) 2, 53, 2008.

4. D. Yokoyama, **T. Iwasaki**, T. Yoshida, S. Sato, T. Hyakushima, M. Nihei. Y. Awano, H. Kawarada, "Low Temperature Grown Carbon Nanotube Interconnects Using Inner Shells by Chemical Mechanical Polishing", Appl. Phys. Lett, 91, 263101, 2007.

5. **T. Iwasaki**, R. Morikane, T. Edura, M. Tokuda, K. Tsutsui, Y. Wada, H. Kawarada, "Growth of Dense Single-walled Carbon Nanotubes in Nano-sized Silicon Dioxide Holes for Future Microelectronics", Carbon, 45, 2351-2355, 2007.

6. G. Zhong, **T. Iwasaki**, J. Robertson, H. Kawarada, "Growth Kinetics of 0.5 cm Vertically Aligned Single-Walled Carbon Nanotubes", J. Phys. Chem. B, 111, 1907-1910, 2007.

7. **T. Iwasaki**, G. Zhong, H. Kawarada, "Low-Temperature Growth of Vertically Aligned Single-Walled Carbon Nanotubes by Radical CVD", New. Diam. Front. C. Tec, 16, 177-184, 2006.

8. G. Zhong, **T. Iwasaki**, H. Kawarada, "Semi-Quantitative Study on the Fabrication of Densely Packed and Vertically Aligned Single-Walled Carbon Nanotubes", Carbon, 44, 2009-2014, 2006.

9. **T. Iwasaki**, G. Zhong, T. Aikawa, T. Yoshida, H. Kawarada, "Direct Evidence for Root Growth of Vertically Aligned Single-Walled Carbon Nanotubes by Microwave Plasma Chemical Vapor Deposition", J. Phys. Chem. B, 109, 19556-19559, 2005.

10. **岩崎孝之**, 鐘国倣, 川原田洋, "先端放電型マイクロ波プラズマCVDによる単層カーボンナノチューブ配向成長", プラズマ・核融合学会誌, 81, 665-668, 2005.
    T. Iwasaki, G. Zhong, H. Kawarada, "Vertically Aligned Single-Walled Carbon Nanotubes by Point-Arc Microwave Plasma CVD", Journal of Plasma and Fusion Research, 81, 665-668, 2005.

11. G. Zhong, **T. Iwasaki**, K. Honda, Y. Furukawa, I. Ohdomari, H. Kawarada, "Very High Yield Growth of Vertically Aligned Single-Walled Carbon Nanotubes by Point-Arc Microwave Plasma CVD", Chem. Vap. Deposition, 11, 127-130, 2006.

12. G. Zhong, **T. Iwasaki**, K. Honda, Y. Furukawa, I. Ohdomari, H. Kawarada, "Low Temperature Synthesis of Extremely Dense and Vertically Aligned Single-Walled Carbon Nanotubes", Jpn. J. Appl. Phys, 44, 1558-1561, 2005.

13. G. Zhong, **T. Iwasaki**, H. Kawarada, I. Ohdomari, "Synthesis of Highly Oriented and Dense Conical Carbon Nanofibers by a DC Bias-Enhanced Microwave Plasma CVD Method", Thin solid films, 464-465, 315-318, 2004.

Publication in International Conference Proceedings

1. **T. Iwasaki**, R. Morikane, G. Zhong, T. Edura, K. Tsutsui, Y. Wada, H. Kawarada, "Fabrication of Nano-sized Single-Walled Carbon Nanotube Vias for Electronic Device Applications", NSTI Nanotech 2006 proceedings, 2006.

Presentations

1. **T. Iwasaki**, J. Robertson and H. Kawarada, “Cutting of Layered Single-Walled Carbon Nanotubes: Investigation of Interface Structure and Fabrication of Short Single-walled Carbon Nanotube Arrays”, 2007 MRS Fall Meeting, Boston, USA, November 2007.

2. **T. Iwasaki**, T. Maki and H. Kawarada, “Growth of Half-Centimeter Long Single- and Double-Walled Carbon Nanotubes by Radical CVD”, Fifth International Symposium on Control of Semiconductor Interfaces, Tokyo, Japan, November 2007.

3. **T. Iwasaki**, T. Koide, R. Morikane, S. Mejima, H. Nakayama, T. Shinada, I. Ohdomari, and H. Kawarada, "Vertically Aligned Carbon Nanotubes from Ni Catalysts Implanted by Focused-Ion-Beam", 18th European Conference on Diamond, Diamond-Like Materials, Carbon Nanotubes, and Nitrides, Berlin, Germany, September 2007.

4. **T. Iwasaki**, D. Yokoyama, T. Yoshida, S. Sato, M. Nihei, Y. Awano, H. Kawarada, “Low Temperature Radical Chemical Vapor Deposition of Vertically Aligned CNTs using Size-classified Co Particles for LSI Multi-layer Interconnects”, 1st International Conference on New Diamond and Nano Carbons, Osaka, Japan, May 2007.

5. **T. Iwasaki**, T. Koide, R. Morikane, S. Mejima, H. Nakayama, T. Shinada, I. Ohdomari, H. Kawarada, “Synthesis of Carbon Nanotubes from Focused Ion Beam Implanted Ni Catalysts”, 1st International Conference on New Diamond and Nano Carbons, Osaka, Japan, May 2007.

6. **T. Iwasaki**, G. Zhong, H. Kawarada, "Enhanced Growth of Millimeter Long Vertically Aligned Single-Walled Carbon Nanotubes by Edge Growth", Nanotube 2006, Nagano, Japan, June 2006.

7. **T. Iwasaki**, G. Zhong, T. Yoshida, T. Aikawa, R. Morikane, H. Kawarada, "Millimeter Long Vertically Aligned Single-Walled Carbon Nanotubes by an ultra long lifetime of catalysts", NSTI Nanotech 2006, Boston, U.S.A., May 2006.

8. **T. Iwasaki**, T. Yoshida, T. Aikawa, G. F. Zhong, I. Ohdomari, H. Kawarada, "Synthesis of Millimeter Long Vertically Aligned Single-Walled Carbon Nanotubes by Point-Arc Microwave Plasma CVD", 2005 AIChE Annual Meeting, Cincinnati, USA, October 2005.

9. **T. Iwasaki**, Y. Yoshida, T. Aikawa, R. Hosaka, K. Honda, G. Zhong, Y. Furukawa, I. Ohdomari, H. Kawarada, "Low Temperature Synthesis of Vertically Aligned and Very Dense Single-Walled Carbon Nanotubes by Antenna-Edge Microwave Plasma Chemical Vapor Deposition", 2004 MRS Fall Meeting, Boston, USA, November 2004.

10. **T. Iwasaki**, G. Zhong, I. Ohdomari, H. Kawarada, "Structural Investigation of Conical Carbon Nanofibers", The 9th International Conference on New Diamond Science and Technology, Tokyo, Japan, March 2004.

Patent

1. **T. Iwasaki** and H. Kawarada, “Growth Method of Single-Walled Carbon Nanotubes: Fabrication Process of LSI Interconnects”, Japan patent, Registered number: 2007-152632